Aus dem Max-Delbrück-Centrum für Molekulare Medizin

DISSERTATION

Role of the oligodendrocytic connexin47 in CNS myelination

zur Erlangung des akademischen Grades
Doctor of Philosophy in Medical Neurosciences
(PhD in Medical Neuroscience)

vorgelegt der Medizinischen Fakultät
Charité – Universitätsmedizin Berlin

von

Marta Maglione

aus Genoa, Italien

Gutachter: 1. Prof. Dr. H. Kettenmann
2. Prof. Dr. K.-A. Nave
3. Prof. Dr. med. R. Dermietzel

Datum der Promotion: 18.10.2010

Acknowledgments

I sincerely thank Prof. Dr. H. Kettenmann for giving me the opportunity to work at this project and for his supervision, in particular for making me grow as a scientist; Prof. Dr. K. Willecke for his precious contribution to a project which was originally born from an idea of Dr. B. Uhlenberg; and my special friend and previous collegue Dr. B. Haas for her unique supervision when I moved my first steps in the lab, for her help along the past years and for her friendship; last but not least for carefully proof reading this thesis. I thank my great collaborator Oliver Tress, who generated the Cx47M282T mutant mice, for all the motivating scientific (and not) discussions along the way. Thanks also to him the connexins world became clearer and clearer every day of the last four years. I thank Prof. Dr. J. Trotter and Dr. K. Karram for providing me the NG2-EYFP mice; Prof. Dr. D. Rowitch for the Olig2 antibody; Jun. Prof. Dr. J. Meier for advices on immunohistochemistry and life, with him I became more and more self confident as a scientist. Thanks to Dr. R. Jüttner for his patience and advices with electrophysiology, but in particular for proof reading up to the smallest detail my thesis. I would like to thanks Dr. C. Nolte for her help when I was lost in oligodendrocytic markers immunohistochemistry (one can really get lost!) and for the german translation of the summary text; Dr. C. Eichhorn for her help with statistic. Many thanks go to Karin Heufelder and Simone Röthkegel for their efficient help in genotyping all the mouse lines used in this study. I am grateful for financial and academic support to the *International Graduate Program Medical Neuroscience* at the Charité Universitätsmedizin Berlin and to the *Graduiertenkollegs GRK 1258 Neuroinflammation*; for helpful administrative assistance to our super-special Birgit Jarchow, without her the lab would not run so smoothly. I am thankful for all my former and present colleagues, in particular to Stefanie Seifert and Gretje Tessmann for supporting me during the bad and good times.

A special thank to Andreas Lutter for walking by my side during such a stressful time, without forgetting his help with the AxioVision software.

Finally, this thesis is for my sister and my mother, for their love and constant support along the way.

This work was financed by a grant of the DFG: SFB 665 to H.K. and SFB 645 (B2) to K.W.

Table of Contents

List of Figures

List of Tables

List of Abbreviations

Artificial cerebrospinal fluid (aCSF),

Access resistance (R_a)

Adenosine triphosphate (ATP)

Basic helix-loop-helix (bHLH)

β-galactosidase (β-gal)

Bovine serum albumine (BSA)

5-bromo-4-chloro-3-indolyl- beta-D-galactopyranoside (X-gal)

Central nervous system (CNS)

Central medial thalamic nucleus CM)

Charcot-Marie-Tooth (CMT)

2',3'-Cyclic nucleotide 3'-phosphohydrolase (CNPase)

Cytoplasmatic loop (cl)

Connexin (Cx)

Decaying time constant (τ)

Diaminobenzidine (DAB)

Dimethylsulfoxide (DMSO)

Double knock out (dKO)

Ethylene glycol tetraacetic acid (EGTA)

Enhanced green fluorescent protein (EGFP)

Enhanced yellow fluorescent protein (EYFP)

Extracellular loop (el)

Extracellular potassium concentration ($[K^+]_o$)

Fast capacitative transient (C_f)

Frameshift mutation (fs)

Galactosylceramidase (Gal C)

Gap junction protein γ2 (GJC2)

Gap junction protein β1 (GJB1)

Glial fibrillary acidic protein (GFAP)

Hereditary spastic paraplegia (HSP)

Hereditary neuropathy with liability to pressure palsies (HNPP)

Hippocampus (Hip)

Human glial fibrillary acidic protein (hGFAP)

Input resistance (R_{in})

Juxtaparanode (JXP)

Knock out (KO)

β-galactosidase encoding gene (LacZ)

Lateral ventricle (LV)

Lucifer Yellow (LY)

Maximum current (I_{max})

Mediodorsal thalamic nucleus, central (MDC)

Membrane capacitance (C_m)

Myelin associated glycoprotein (MAG)

Myelin basic protein (MBP)

Myelin/oligodendrocyte glycoprotein (MOG)

Membrane potential (V_m)

Normal goat serum (NGS)

NG2 chondroitin sulphate proteoglycan (NG2)

Offset current (I_{off})

Oligodendrocyte precursor cells (OPC)

Oligodendrocyte lineage genes (Olig1/2)

Oligodendrocyte-type-2 astrocyte (O-2A)

Pelizaeus-Merzbacher disease (PMD)

Pelizaeus-Merzbacher-like-disease (PMLD)

Peripheral nervous system (PNS)

Peripheral myelin protein 22 (PMP22)

Pipette resistance (R_p)

Platelet-derived neurotrophic factor receptor α (PDGFRα)

Polimerase chain reaction (PCR)

Polysialylated neuronal cell adhesion molecule (PSA-NCAM)

Postnatal day (p)

Pro-oligodendroblast antigen (POA)

Proteolipid protein 1 (PLP1)

Receptor tyrosine-protein kinase erbB-2 (ErbB2)

Septate-like junction (SpJ)

Series resistance (R_s)

Slow capacitative transient (C_s)

Subventricular zone (SVZ)

Transjunctional voltage (V_j)

Transmembrane domain (m)

Tris buffered saline (TBS)

Tris-HCl buffer (TB)

Triton X-100 (TX-100)

Ventrolateral thalamic nucleus (VL)

Voltage (U)

Wildtype (WT)

X-linked Charcot-Marie-Tooth type 1 (CMT1X)

Zonula occludens 1 (ZO-1)

ZO-1-associated nucleic acid-binding protein (ZONAB)

1 Introduction

1.1 Organization of the Brain

The vertebrate Central Nervous System (CNS) can be divided in two anatomical areas: the gray matter, where information is processed, and the white matter, constituted by fiber tracts connecting different brain regions. The major constituents of the gray matter are neuronal somata, unmyelinated local axons and glia cells (Hildebrand et al. 1992). The CNS white matter consists of neuronal fibers wrapped by myelin provided by oligodendrocytes, as well as oligodendrocyte precursors, astrocytes and a small number of microglia (see description of glial cells in paragraph *1.2*.; Raff et al. 1983a; Barres et al. 1988). In placental mammals the major white matter tract is the corpus callosum, which allows inter-hemispheric conduction for axonal fibers. The callosal regions connecting primary and secondary sensory and motor areas are characterized by a large proportion of fast-conducting, large-diameter fibers, while regions connecting the so-called association and prefrontal areas bear a high density of slow-conducting, lightly myelinated and thin fibers (fig. 1.1, Aboitiz et al. 1992).

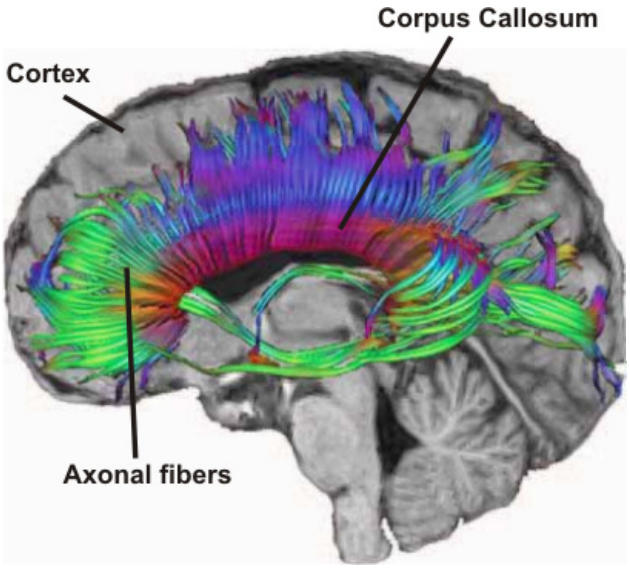

Figure 1.1: Corpus callosum connects the left and right cerebral hemispheres. Image illustrating fiber tracts (colors) coursing through the corpus callosum of a human brain (modified from news.byu.edu/archive08-MAR-concussion.aspx)

High speed conduction, fidelity of signaling transfer on long distances and space economy are the three main advantages conferred to the vertebrate CNS by myelin. For example myelin reduces the time needed for action potential to propagate between the right and left side of the human cortex from 300 ms (in unmyelinated fibers) to 5 ms (Bakiri et al. 2009). In contrast, in the invertebrate nervous system rapid conduction can only be achieved by increasing axonal diameter. In fact myelin unique composition and structure (see paragraph *1.2.1.2*) is essential for the saltatory conduction of nerve impulses and allow the myelin sheaths to support fast nerve conduction of relatively thin fibers (for review see Baumann and Pham-Dinh 2001). The importance of myelin in human development became evident from several neurological diseases such as multiple sclerosis and leukodystrophies affecting the CNS, or peripheral neuropathies in the PNS, as discussed in paragraph *1.3*.

1.2 Glia Cells

In 1846 Virchow described for the first time cells morphologically different from neurons, which he called “nervenkitt” (nerve glue), i.e. neuroglia, since he supposed they were part of the connective tissue of the brain. Although the original concept changed during centuries, the name survived. As an overview, the glia to neuron ratio in the brain grows during evolution: in Drosophila glia cells account for 25% of total cells, in rodents for 65% and in humans for 90% (Pfrieger and Barres 1995). In the beginning of the last century, using the first morphological techniques, Ramon y Cajal and Rio Hortega characterized the major glia cell types: the macroglial cells astrocytes and oligodendrocytes, and the microglia (fig. 1.2; for review see Kettenmann and Verkhratsky 2008). Microglia cells are the immunocompetent cells

of the CNS and they are viewed as sensors for pathological events (Barres 2008; Kettenmann 1999; Kettenmann and Verkhratsky 2008).

Astrocytes are a functionally and morphologically heterologous population of glia cells with different physiological properties and they express various receptors and transporters, according to brain region. They constitute a neurovascular unit and thus control the blood flow on one side and provide metabolic support to neurons on the other (Magistretti 2006; Mulligan and MacVicar 2004). Astroglial cells can sense synaptic activity by expression of neurotransmitter receptors and, moreover, they can also actively participate in synaptic transmission and plasticity by release of

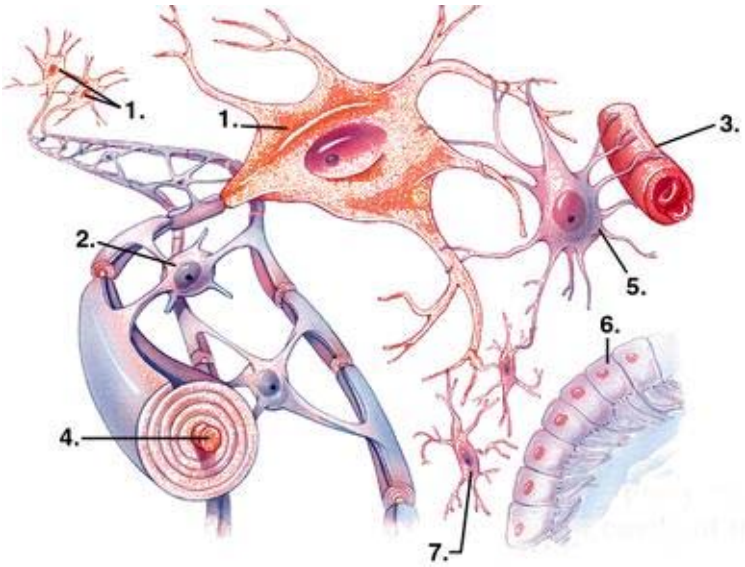

Figure 1.2: Different types of glia cells in the central nervous system: (1.) Neuron; (2.) Oligodendrocytes; (3.) Capillary; (4.) Axon; (5.) Astrocytes; (6) Ependimal cells; (7.) Microglia. Oligodendrocytes myelinate axons to speed up neuronal transmission. Astrocytes ensheath blood vessels and synapses with their extended processes. Microglia keep the brain under surveillance for damage or infection (from legacy.owensboro.kctcs.edu/.../Image426.gif).

so-called gliotransmitters or by neurotransmitter uptake (Araque et al. 1999; Volterra and Meldolesi 2005). Several studies demonstrated that astrocytes have intrinsic signaling systems mediated by raise of intracellular Ca^{2+} concentration. Calcium signals can propagate to neighboring astrocytes through gap junctions, or by means of extracellular transmitters like ATP, thus integrating glial activity. Therefore Glial

Ca^{2+} signaling can be regarded as a form of glial excitability even if they are not electrically excitable in the classical way like neurons (for reviews see Barres 2008; Kettenmann 1999; Verkhratsky et al. 1998).

Oligodendrocytes and Schwann cells, the myelinating cells in the CNS and the PNS, respectively, provide for electrical insulation of axons, thus allowing the saltatory propagation of action potentials (see paragraph *1.2.1*). Recently a new class of macroglia cells, the NG2 cells, has been characterized. NG2 cells or synantocytes (for review see Butt et al. 2005) do receive synaptic contacts and share some physiological features with neurons. They might also play an important role in gliogenesis and myelination, in particular in the adult brain, and in modulating synaptic transmission (for review see Nishiyama 2007). Nowadays it has become increasingly evident that glia cells play a critical role in every major aspect of brain development, function and disease as they control synapse formation, function and blood flow (for review see Barres 2008).

1.2.1. Oligodendrocytes and Myelin

Oligodendrocytes are the myelinating cells of the CNS (fig. 1.3). Myelin is a lipid-protein membrane structure contained in the central and peripheral nervous system of vertebrates that acts primarily as an electrical insulator (see paragraph *1.2.1.2*; for review see Baumann and Pham-Dinh 2001; Morell 1984). Oligodendrocytes ensheat and wrap axons with their processes at a number of discontinuous points or internodes, forming the nonconductive counterpart to the Node of Ranvier and thus allowing the rapid saltatory conductance along the axon (myelin structure described in paragraph *1.2.1.2*; (Deber and Reynolds 1991). On the same axon adjacent myelin segments belong to several oligodendrocytes and a single oligodendrocyte can myelinate up to 15 axons (Peters et al. 1991). In addition to provide insulation

and trophic support to neurons, oligodendrocytes lead structural and electrical properties of axons by controlling their diameter, as well as spacing and clustering of ion channels at the Nodes of Ranvier (Barres 2008).

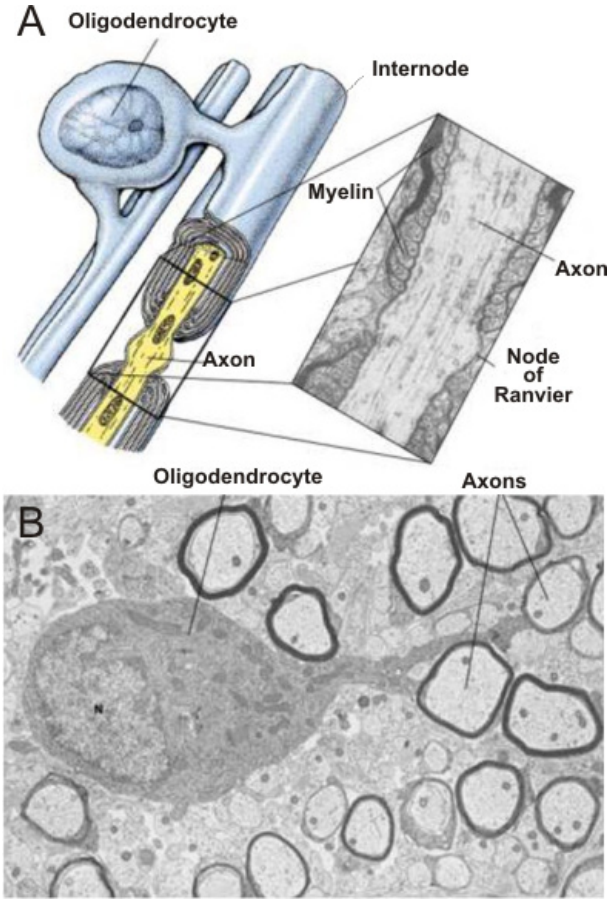

Figure 1.3: Oligodendrocytes, the myelinating glial cells in the central nervous system. (A) Diagram depicts an oligodendrocyte and its myelin sheathes formed by the oligodendrocytic membrane enwrapped several times around the axon. Myelin covers the axon at intervals (internodes), leaving bare gaps — the nodes of Ranvier (inset shows an electron microscopic image of a myelinated axon at the node of Ranvier). Oligodendrocytes can myelinate different axons and several internodes per axon. (B) Electron micrograph displaying an oligodendrocyte myelinating several nearby axons (obtained from www.psy.jhu.edu).

1.2.1.1 Oligodendrocyte Development

Oligodendrocytes are generated postnatally by oligodendrocyte precursor cells (OPC) in the telencefalic subventricular zone (SVZ), a germinal matrix of multipotential and lineage restricted precursors. The majority of these cells are glia precursors that migrate in white matter and cortex, giving rise to astrocytes or oligodendrocytes, rarely to neurons (Levison and Goldman 1993). During embryonic life OPC originate from neuroepithelial cells of the ventral spinal cord and then migrate dorsally during development. Between postnatal day 5 and 20, oligodendrogenesis occurs at the dorsal regions both intrinsically and through the

ventral to dorsal migration of oligodendrocyte precursors (for review see Barres et al. 1988; Baumann and Pham-Dinh 2001). Determination of neuronal versus glia cell fate depends on the two oligodendrocyte lineage genes Olig1 and Olig2, encoding basic helix-loop-helix (bHLH) transcription factors (Lu et al. 2000; Zhou et al. 2000). Both Olig1 and Olig2 are sufficient for formation of oligodendrocytes or early OPC, although Olig2 plays a prominent role in the developing spinal cord while Olig1 promotes oligodendrocytes formation and maturation in the brain (Ligon et al. 2006). From precursor cells to mature myelinating oligodendrocytes, through progenitors, preoligodendrocytes (or pro-oligodendroblasts) and immature nonmyelinating oligodendrocytes, each developmental stage of cells belonging to the oligodendrocytic lineage is characterized by sequential expression of different biochemical and molecular markers (fig. 1.4, Hardy and Reynolds 1993; Pfeiffer et al. 1993). Migrating oligodendrocyte precursors, or “pre-progenitors”, express the polysialylated embryonic form of neuronal cell adhesion molecule PSA-NCAM (Ben-Hur et al. 1998; Wang et al. 1994), the alpha subunit of the platelet-derived growth factor receptor (PDGFRα; Hart et al. 1989), a potent mitogen, survival and differentiation factor for oligodendrocytes (Grinspan and Franceschini 1995), and the internal filaments vimentin (Behar et al. 1988) and nestin, specifically expressed by neuroepithelial stem cells but also by glial precursors such as radial glia (Hockfield and McKay 1985; Lendahl et al. 1990). PSA-NCAM has been shown to be essential for OPC migration in response to PDGF (Zhang et al. 2004). Oligodendrocyte precursors were identified using the A2B5 antibody that recognizes several gangliosides yet uncharacterized (Fredman et al. 1984; Raff et al. 1985). While these cells constitutively differentiate into oligodendrocytes, under the influence of different environmental signals *in vitro*, they have the potential to express neuronal antigenic determinants or the glial fibrillary acidic protein (GFAP), a major astrocytic filament

protein (Raff et al. 1983b). This bipotential nature led Raff and coworkers to term these cells oligodendrocyte-type-2 astrocyte (O-2A). Slightly after the appearance of the PDGFRα, another OPC marker detected is the chondroitin sulfate proteoglycan NG2, a type 1-transmembrane (Nishiyama et al. 1996). NG2-positive cells are numerous and ubiquitous both in gray and white matter of the developing and adult CNS (Chang et al. 2000; Nishiyama et al. 1999). Although NG2-expressing cells have been principally viewed as oligodendrocyte precursors, nowadays they are also considered as a fourth glial class (Peters 2004), with specific electrophysiological properties (Bergles et al. 2000; Karadottir et al. 2005). As rodent OPC start to differentiate they express the pro-oligodendroblast antigen (POA; Bansal et al. 1992), a cellular surface sulfatide yet unidentified that is recognized by the monoclonal antibody O4 (Sommer and Schachner 1981). In comparison to OPCs, the pro-oligodendroblast developmental stage is characterized by continued proliferation but altered response to mitogens (Gard and Pfeiffer 1990).

From the pro-oligodendroblast to myelinating oligodendrocytes, the real differentiation of OPC to mature oligodendrocytes is characterized by loss of precursor antigens such A2B5 (Raff et al. 1983b; Raff et al. 1984) and gain of expression of early myelin components like galactosylceramidase (GalC), a galactocerebroside (Raff et al. 1978), while the O4 antibody continues to recognize mature oligodendrocytes (Bansal et al. 1992). This differentiation is accompanied by a decrease in proliferation and an increase in structural and morphological complexity (Hardy and Reynolds 1993). While premyelinating oligodendrocytes posses radial processes that bifurcate into slender longitudinal extensions, mature oligodendrocytes are characterized by parallel longitudinal processes, which are the individual myelin segments (Butt and Ransom 1993).

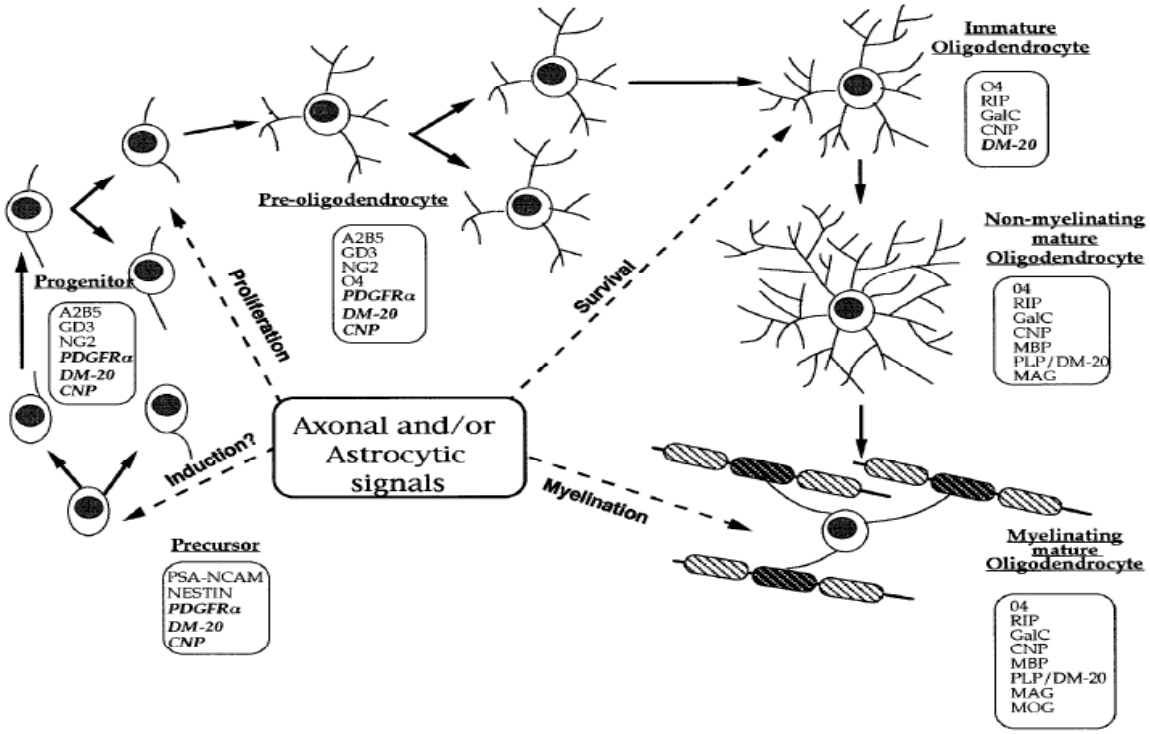

Figure 1.4: Schematic representation of the developmental stages of cells of the oligodendrocyte lineage. Image shows the morphological and antigenic progression from precursor cells to myelinating mature oligodendrocytes, through progenitors, preoligodendrocytes, and immature nonmyelinating oligodendrocytes (italic text refers to mRNA expression; from Baumann and Pham-Dinh, 2001).

The earliest myelin specific protein to be synthesized is 2',3'-cyclic nucleotide 3'-phosphohydrolase (CNPase; Reynolds and Wilkin 1988), a myelin membrane associated protein mediating process extension and membrane expansion during myelination (Gravel et al. 1996). Expressed sequentially after CNPase, the most abundant myelin proteins are the integral membrane proteins myelin basic protein (MBP), the proteolipid protein (PLP) in the CNS. PLP and its spliced isoform DM20 constitute 50% of the protein mass of myelin while MBP and its multiple isoforms 30%-40% (fig. 1.5, for review see Baumann and Pham-Dinh 2001). PLP plays a critical role in differentiation, since mutations in its gene result in severe dysmyelination and oligodendrocyte death (Schneider et al. 1992), while MBP has a major role in myelin compaction; also mutations in this protein are associated to myelinopathies (Grinspan et al. 1998). Other minor membrane proteins of myelin are the myelin associated glycoprotein (MAG), expressed following MBP and involved in

the interaction with neurons, and the myelin/oligodendrocyte glycoprotein (MOG), whose expression occurs relatively late during myelination (fig. 1.5, Filbin 1996).

1.2.1.2 Myelin Composition and Morphological Structure

Myelin is the essential constituent of the white matter in the CNS; it is a poorly hydrated structure and its dry weight consists of 70% lipids and 30% proteins, a peculiar ratio of the myelin membrane. The lipids contained in oligodendrocytes and myelin are cholesterol, phospholipids and glycolipids, with cholesterol in a greater molar ratio. One of the main characteristic of myelin lipids composition is their richness in glycosphingolipids, in particular galactocerebrosides: galactosylceramides (GalC) and the sulfated derivatives sulfogalactosylceramides, or sulfatides. Myelin richness in lipids, low water content and structure allow its insulating properties, favoring rapid nerve conduction velocity (for review see Morell and Ousley 1994).

Compact myelin is characterized by a periodicity of lamellae, concentric electron dense layers, and light layers. The dark layer called major dense line forms as cytoplasmatic surfaces of the myelinating processes appose to each other, thus extruding the cytoplasm (fig. 1.5). The extracellular apposition of two outer leaflets forms the intraperiodic lines. Cytoplasmatic faces of the myelin sheath that did not compact to form the major dense line constitute pockets of uncompacted glial cytoplasm, the Schmidt-Lanterman incisures.

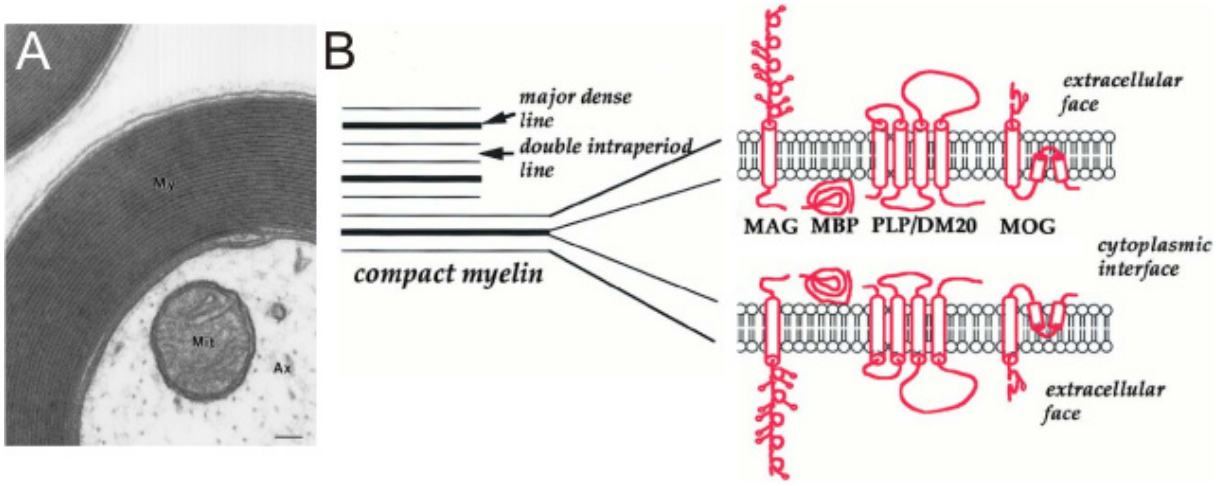

Figure 1.5: Compact myelin structure and composition in the in the CNS. (A) Electron micrograph showing the compact myelin composed by apposed external faces of the oligodendrocytic membrane, which constitute the "double intraperiodic line". Apposition of the internal faces followed by cytoplasm extrusion forms the "major dense line." The myelin proteins are schematically described (adapted from Baumann and Phaum Dinh, 2001; electron micrograph from starklab.slu.edu/neuro/myelin.jpg)

They extend across the entire thickness of the sheath, thus providing a pathway between the cytoplasm on the outside and the inside of the sheath. The Schmidt-Lanterman incisures are common in the PNS, but rare in the CNS. The myelin sheath and the axonal membrane are separated by a narrow extracellular cleft called periaxonal space. Myelinated fibers show distinct membrane morphologies corresponding to different anatomical domains: the internode, the paranodal region and the node of Ranvier (fig. 1.6).

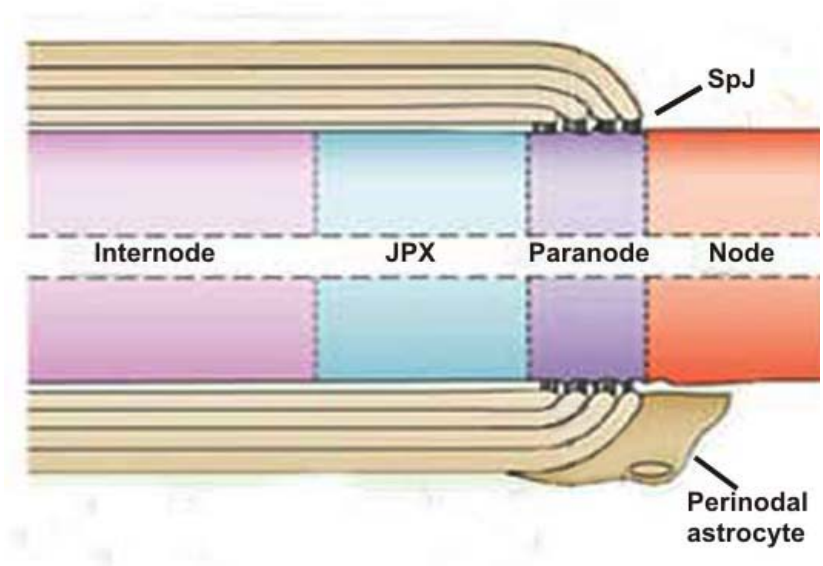

Fig 1.6: Schematic representation of myelinated fiber around the node of Ranvier. The node, paranode, juxtaparanode (JXP) and internode are labeled. The node is contacted by processes from perinodal astrocytes in the CNS. The paranodal loops form a septate-like junction (SpJ) with the axon. The juxtaparanodal region resides beneath the compact myelin next to the paranode. The internode extends from the juxtaparanodes and lies under the compact myelin (adapted from Poliak and Peles, 2003).

These different regions are formed by specific interactions between myelinating glial cells and neuron. At the paranodal region, myelin is less compacted and forms loops containing small amount of cytoplasm. These loops are arranged in a regular and symmetric pattern at each side of the node of Ranvier. Cytoskeletal filaments tighten the axonal-paranodal apposition. Along myelinated axons, the internodes are separated by intervals where the axolemma is exposed, the node of Ranvier.

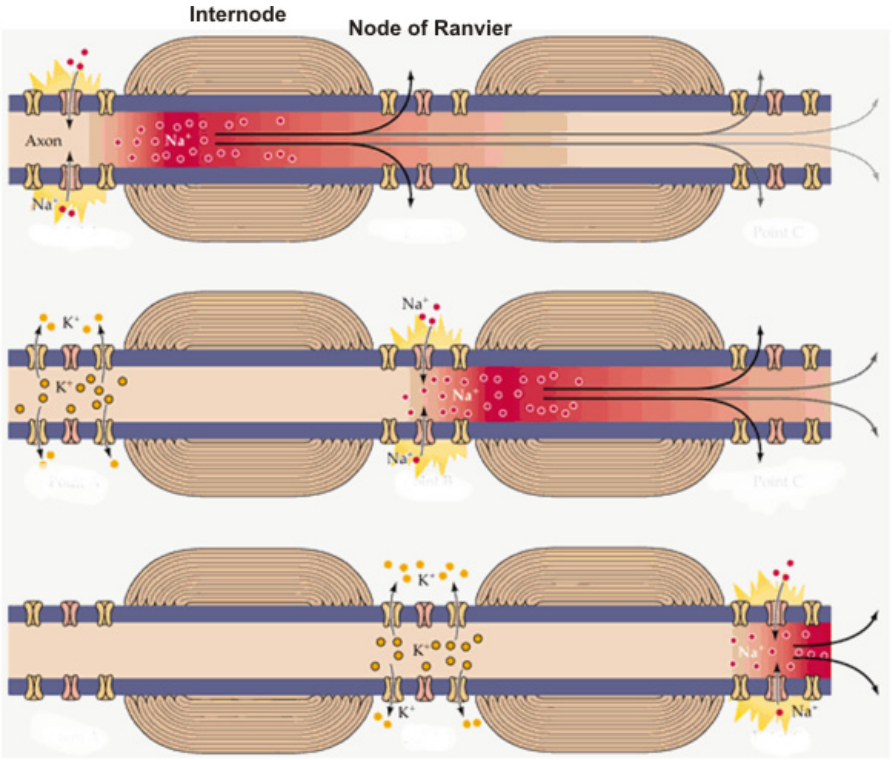

Figure 1.7: Diagram indicating saltatory action potential conduction along a myelinated axon. Inward Na^+ voltage-gated currents occur only at nodes of Ranvier (top), followed 1 ms later by outward K^+ current at the same node of Ranvier (adapted form Purves et al. 2001). The presence of myelin prevents the local current from leaking across the internodal membrane, flowing farther along the axon than in absence of myelin. The result is a greatly enhanced velocity of action potential conduction.

The nodes of Ranvier are essential for fast saltatory condunctance because they allow nerve impulses to jump from node to node rather than being slowly propagated along the axon, as in unmyelinated or demyelinates fibers (fig. 1.7, for review see Baumann and Pham-Dinh 2001; Hildebrand et al. 1993). Premyelinated axons exhibit a low density of sodium channels, uniformly distributed along the fiber whereas when myelination occurs sodium channels are clustered at the node of

Ranvier. This molecular organization enables the regeneration of action potentials at the node of Ranvier (for review see Waxman et al. 1994). Several studies demonstrated that oligodendrocytes are necessary to induce saltatory conductance by sodium channels clustering, by providing myelin insulation and furthermore by regulating axonal caliber (for review see Hildebrand et al. 1993; Waxman et al. 1994).

1.2.2 Physiological properties of oligodendrocytes

In the past, cells of the oligodendrocyte lineage have been extensively characterized in terms of electrophysiological properties providing a good tool for the study of glia cells during development, since defined stages could be identified with specific cell markers. These studies demonstrated a dramatic change in channel expression during development. The electrophysiological properties of glia precursor cells and oligodendrocytes were studied mainly in cell culture systems from rat optic nerve and mouse cortex and in situ (for review see Berger et al. 1995). The most prominent current expressed in precursor cells was a delayed rectifier potassium current. Other currents, such as Na^+, Ca^{2+}, A-Type K^+, inward rectifier and calcium-dependent K^+, were described (Blankenfeld Gv et al. 1992; Sontheimer et al. 1989). As precursor cells differentiate to oligodendrocytes these channels are lost and replaced by inwardly rectifying K^+ channels, the major channel type in promyelinating oligodendrocytes *in vitro* (Sontheimer et al. 1989) and *in situ* (Sontheimer and Waxman 1993). Mature oligodendrocytes show large passive currents during membrane de- and hyperpolarization. These outward and inward currents corresponding to de- and hyperpolarizing voltage steps show a strong decay with a voltage independent time constant. This current decay does not reflect the inactivation kinetics of the underlying channels but it is due to a shift of the K^+

gradient across the plasma membrane during the preceding depolarizing or hyperpolarizing voltage step. The ability of oligodendrocytes to move large amounts of K^+ across the membrane indicates that these cells can efficiently buffer $[K^+]_o$ by spatial buffer currents, thus rapidly removing the excess K^+ released from neurons following action potential (Berger et al. 1991; Chvatal et al. 1999; for potassium buffering see chapter 4.4).

1.3 Myelin related disorders

1.3.1 Hypomyelinating Leukodystrophies

Leukodystrophies are acquired or inborn diseases affecting the CNS myelin. Defects of leukodystrophies can be divided into hypo-, de- and dysmyelination. A well-characterized type of hypomyelinating disorders is the X-linked Pelizaeus-Merzbacher disease, which is caused by mutations in the proteolipid protein 1 (PLP1), one of the major components of myelin in CNS (Schiffmann and Boespflug-Tanguy 2001). Patients usually present with nystagmus, impaired motor development within the first months of life, ataxia and progressive spasticity. The phenotypical abnormalities clearly depend on whether there is duplicated, mutated or no PLP1 protein: mutated or duplicated Plp1 leads to marked death of murine oligodendrocytes, clearly due to an overload of Plp1 in the endoplasmic reticulum. In contrast, targeted null mutants are essentially healthy and fertile (Griffiths et al. 1998). Ultrastructural investigations of white matter from patients and mice lacking the PLP1/Plp1 gene revealed length-dependent axonal degeneration in the absence of demyelination (Garbern et al. 2002). These studies demonstrated that PLP1 is not fully necessary for proper myelination and assembly of myelin but rather for axonal integrity.

1.3.1.1 The Paelizeus-Merzbacher-like-disease

About 20 percent of patients with the clinical Pelizaeus-Merzbacher-disease (PMD) phenotype do not have *PLP1*-mutations and are therefore referred to as having Pelizaeus-Merzbacher-like-disease (PMLD; Garbern et al. 1999). Pelizaeus-Merzbacher-like-disease is a hypomyelinating leukodystrophy caused by mutations in the human Cx47 gene (Uhlenberg et al. 2004). Like the X-linked Pelizaeus-Merzbacher disease, which is caused by mutations in *PLP1*, PMLD is characterized by nystagmus, dysarthria, impaired motor development, progressive spasticity and ataxia. First symptoms, nystagmus and poor control of head and trunk movements, occur in early infancy. Ten different mutations including missense, nonsense and frameshift (fs) mutations of the *GJC2* gene encoding for Cx47 have been found in the genome of PMLD-affected patients to date: Cx47- P87S, R237stop, Y269D, M283T, P327fs (Uhlenberg et al. 2004), P128fs, G233S, L278fs (Bugiani et al. 2006), P304fs (Wolf et al. 2007), P305fs (Salviati et al. 2007).

PMLD patients carrying mutations in the *GJC2* gene show a mild peripheral phenotype in addition to hypomyelination in the CNS. All affected individuals harbored homozygous mutations or carried two different mutations of *GJC2* in their genome. People heterozygous for just one of the described mutations had no neurological symptoms and did not reveal hypomyelination in the CNS.

1.3.1.2 Hereditary Spastic Paraplegia

Recently Orthmann-Murphy et al. (2009), described a novel recessive inherited mutation in the *GJC2* gene encoding for connexin47 causing the hereditary spastic paraplegia, a hypomyelinating leukodystrophy characterized by a milder phenotype than the PMLD. Patients had a late-onset, slowly progressive, complicated spastic

paraplegia, with normal or near-normal psychomotor development and no nystagmus (Orthmann-Murphy et al. 2009).

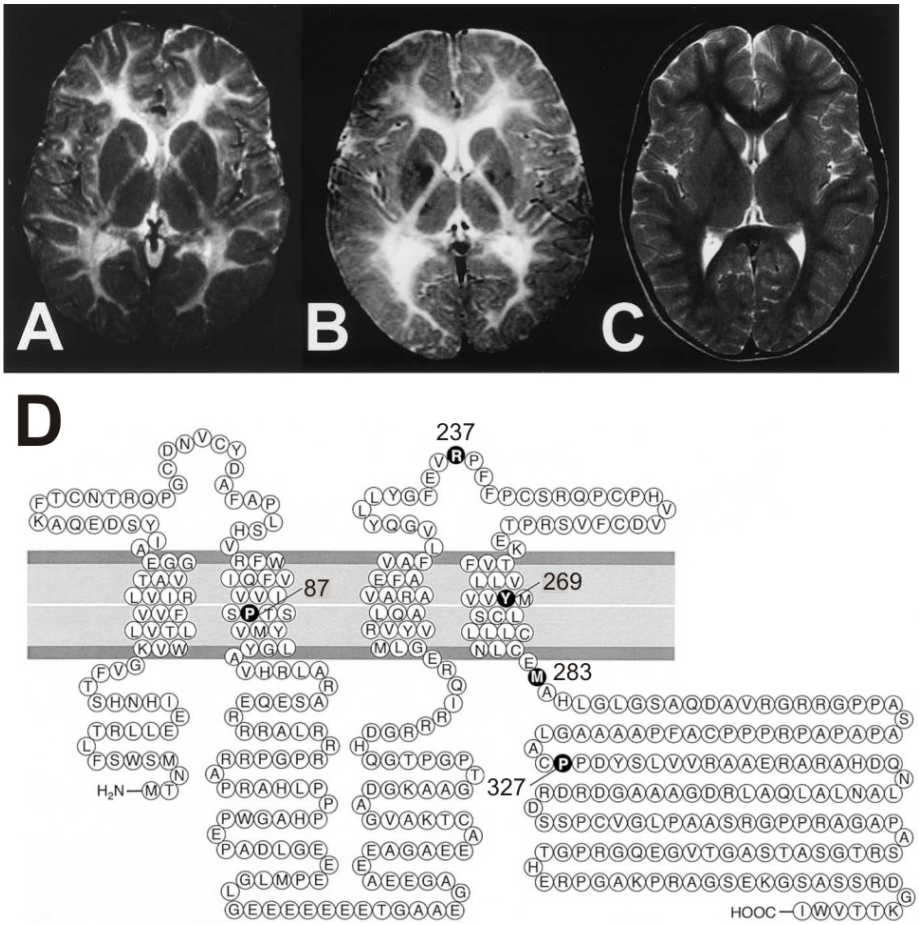

Figure 1.8: (A) Axial T2-weighted magnetic resonance images of the brain of PMLD and PMD patients. Diffuse enhanced signal intensity indicates that a 6 years old patient with PMLD shows nearly identical hypomyelination patterns of central white matter, compared to a 7 years old PMD patient (B). (C) Low signal intensity of normal myelination in an unaffected child. (D) Expression of *GJC2/Cx47* missense mutations associated with PMLD. This is a schematic drawing of human Cx47 illustrating position and nature of mutations associated with PMLD; note the three missense mutations P87S, Y269D and M283T, as well as R237stop and P327fs (black circle; adapted from Uhlenberg et al. 2004).

1.3.2 Inherited Demyelinating Neuropathies

Inherited demyelinating neuropathies are a genetically heterogeneous group of disorders including the demyelinating forms of Charcot-Marie-Tooth (CMT) disease (CMT1A, CMT1B and CMTX), the hereditary neuropathy with liability to pressure palsies (HNPP), as well as other more severe neuropathies such as the congenital hypomyelinating neuropathy and the Roussy-Lévy syndrome. These diseases affect

myelinated motor and sensory axons in a length dependent manner and they are caused by a variety of mutations in genes encoding myelin or Schwann cells specific proteins. Duplication of the *PMP22* gene, which encodes for the peripheral myelin protein 22, an intrinsic protein of the PNS compact myelin, causes the CMT1A and the corresponding deletion causes the HNPP. Mutations in the *P0* gene, which encodes for the major adhesive protein of compact myelin, are associated with several clinical phenotypes of CMT, as the CMT1B (for review see Scherer and Wrabetz 2008).

1.3.2.1. The X-linked Charcot-Marie-Tooth type 1

The X-linked Charcot-Marie-Tooth type 1 is a dominant inherited demyelinating neuropathy caused by mutations in the *GJB1* gene encoding for the gap junction protein connexin32 (Cx32; Bergoffen et al. 1993). More than 300 missense, nonsense and frameshift mutations in the *GJB1* gene have been found associated to the neuropathy. Several clinical studies on CMT1X patients with various mutations, including the loss of the *GJB1* gene, indicated that most of the Cx32 mutants cause neuropathy through loss of normal Cx32 function. Furthermore the clinical severity of the phenotype is not associated with particular Cx32 mutations. When expressed in heterologous cells most of the mutants do not form functional channels due to altered trafficking to the plasma membrane, hence they are degraded in proteasomes and lysosomes (for review see Scherer and Wrabetz 2008).

1.4 Gap Junction Proteins (Connexins) in the Central Nervous System

Gap junctions are formed by intercellular channels that span the plasma membrane of closely apposed cells and provide direct cytoplasmatic continuity. These intercellular channels allow diffusional exchange of ions, water and small metabolites up to a molecular weight of 1 kDa, thus enabling metabolic cooperation, spatial buffering and electrical coupling (for review see Bennett and Zukin 2004). Gap junction channels present a unique structure in comparison to other ion channels because each cell contributes one hemichannel, called the connexon. Two connexons interact in the extracellular space to form the complete gap junction channel, each of them formed by the hexamerization of the structural protein subunits termed connexins. Connexons can be composed of one or more type of connexins and are therefore defined as homomeric or heteromeric, respectively. Similarly gap junction channels can consist of apposing connexons that contain the same (homotypic) or different (heterotypic) connexins. In mammals there are at 20 different connexins, all encoded by a separated but related gene.

Connexin molecules consist of four relatively hydrophobic transmembrane regions connected by two extracellular loops, one central cytoplasmatic loop, with intracellular N- and C-terminal domains. The membrane spanning regions and the extracellular loops are highly conserved, while the cytoplasmatic loop and C-terminal domain are much more variable (for review see Bruzzone et al. 1996). Gap junctional hemichannels are assembled in post Golgi vesicles and transported to the plasma membrane where they are finally integrated. They diffuse laterally and appose to form the full channel or they dock to the plasma membrane as isolated hemichannel (Yeager et al. 1998). Degradation of gap junctions proceeds by

internalization of both junctional membranes in one of the adjoining cells. In many tissues the lifetime of connexins is relatively short, only few hours (Gaietta et al. 2002).

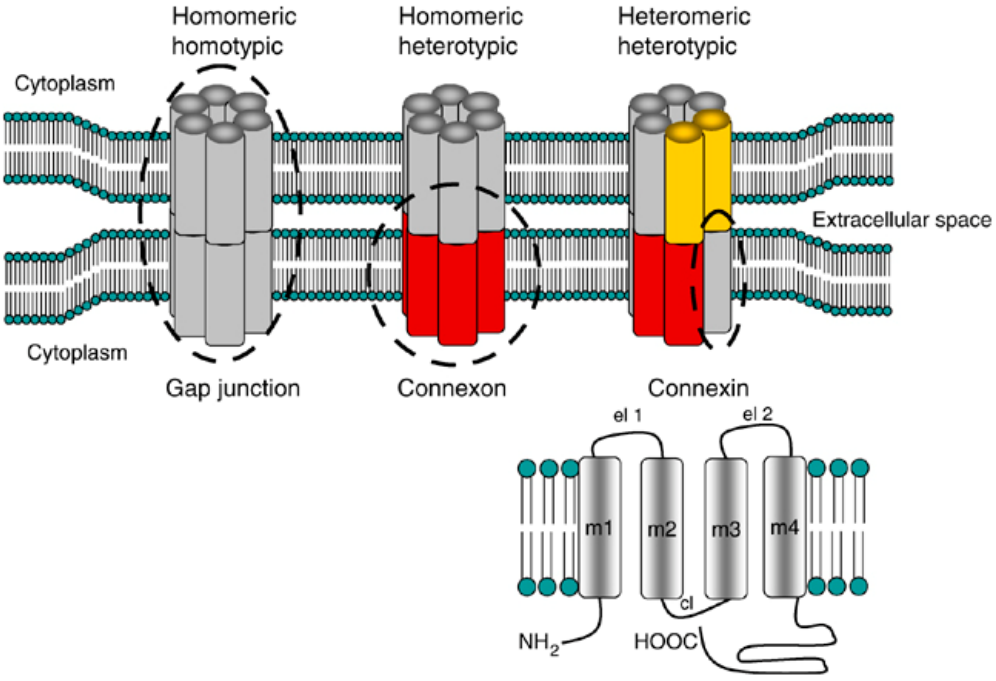

Figure 1.9: Diversity in gap junction channel formation between opposing membranes of neighboring cells. Connexins are protein subunits of hexameric hemichannels that dock to each other at apposed cell membranes to form a gap-junction intercellular channel. A homotypic channel consists of hemichannels composed of a single connexin type, a heterotypic channel consists of different hemichannels each composed of a single connexin type, and a heteromeric channel consists of mixed hemichannels. Lower panel shows a schematic representation relative to the plasma membrane of a generic connexin. Connexin molecules consist of four transmembrane domains (m1 - m4), two extracellular loops (el1 and el2) and three cytoplasmic portions: the amino-terminal and carboxy-terminal domains and the central cytoplasmic loop (cl). Adapted from Wagner 2008.

Numerous recent studies indicate that under physiological or pathological conditions gap junction proteins may form functional hemichannels, which could provide a pathway for release of intracellular components, such as ATP and glutamate, with the extracellular space (for reviews see Bennett et al. 2003; Spray et al. 2006). Under resting conditions connexin hemichannels have a low open probability, but they can be activated under certain stimuli such as low extracellular Ca^{2+} concentration, membrane depolarization, metabolic inhibition and mechanical membrane stress (for review see Evans et al. 2006).

At least 10 different connexins are expressed by the main three different cell types in the mammalian CNS: astrocytes (Cx43, Cx30, Cx26), oligodendrocytes (Cx47, CX32, Cx29) and neurons (Cx36, Cx45; for review see Bennett and Zukin 2004). In the adult brain, gap junctions couple mainly inhibitory interneurons and mediate electrical transmission that may provide for reduced latency of response or synchronization, including neuronal oscillatory activity. In terms of electrophysiological properties, electrical synapses are described as having low-pass filter characteristics (for review see Bennett and Zukin 2004; Sohl et al. 2005). The role of glial connexins will be described in details in paragraph *1.4.2* and *1.4.3*.

1.4.1 Physiological Properties of Gap Junctions

Electrophysiological analysis of single gap junction channels indicates rapid changes in junctional conductance similar to that exhibited by voltage-dependent or ligand-gated channels (for review see Harris 2001). Although gap junctions have commonly been regarded as the least selective channels, each different connexin can form channels with distinct unitary conductance, molecular permeability and gating sensitivities (Harris 2001). Voltage gating of gap junction channels can be mediated by either of its hemichannels, with greatest open probability at zero transjunctional voltage (V_j=0 mV) in homotypic channels. In most vertebrate connexins, junctional conductance is independent of the voltage between intracellular and extracellular space, however in heterotypic channels the two hemichannels can have different voltage-gate sensitivities that lead to asymmetry (rectification) in the current-voltage relationship (for review see Bennett and Zukin 2004). The gap junction permeability is also influenced by intracellular concentration of H^+ and Ca^{2+}, in fact junctional conductance rapidly decreases as the concentration of these two ions increases. Gating by pH depends on the C-terminus, since truncation of this region eliminates

pH sensitivity. An increase of intracellular Ca^{2+} in the range of 10 μM results in decreased junctional conductance, thus not likely affecting coupling under normal physiological conditions. A site sensitive to near-millimolar Ca^{2+} has been identified on the extracellular portion of the pore, explaining how hemichannels are held in the close position at high extracellular calcium (for review see Bennett and Zukin 2004; Spray et al. 2006). Gap junction channels are blocked by several chemical and pharmacological agents, such as the high-order alcohols heptanol and octanol, the anesthetic halothane, carbenoxolone, anandamide and the recently discovered endothelin 1 (Meme et al. 2009; for review see Harris 2001; Yeager and Harris 2007). Gap junctional conductance can also be modulated by phosphorylation at the consensus sites in the cytoplasmatic C-terminal domain of most connexins. Phosporylation may be considered a form of gating since the resulted increase or decrease in macroscopic conductance is associated to altered single channel conductance or open time.

1.4.2 Gap junctional coupling effects on cellular electrophysiological properties

It is a characteristic feature of cells displaying electrical or dye-coupling that the overall input conductance of the evoked current in response to voltage pulses is determined by both transmembrane and cell-to-cell conductances (Blomstrand et al. 2004; Harks et al. 2001; Postma et al. 1998). In coupled cells membrane capacitance and conductance of the adjacent cells contributes to the capacitative transient of the current response to a voltage clamp step. This capacitative transient is characterized by a slow and multiexponential initial decay, followed by a large prolonged steady state current. In uncoupled cells the capacitative transient can be monoexponential fitted and characterized by one decaying time constant. Therefore

whole cell current analysis of a coupled cell reveals an increased decaying multiexponential time constant of the capacitative transient with increasing number of adjacent coupled cells. In addition, electrical or dye-coupled cells display steady state currents characterized by lower input resistance (R_{in}) compared to uncoupled ones (Blomstrand et al. 2004; Meme et al. 2009; Postma et al. 1998). In hippocampus, electrically coupled astrocytes differ in their input resistance from uncoupled astrocytes (Meme et al. 2009). Dye-coupling experiments revealed that passive astrocytes coupled to neighboring astrocytes are characterized by lower input resistance compared to those with lower number of dye coupled cells (Blomstrand et al. 2004; Zhou et al. 2006). In line with these studies, hippocampal astrocytes from Cx30- and Cx43-double-deficient mice lack tracer coupling and display an increased membrane resistance (Wallraff et al. 2006).

1.4.3 The Panglia Syncytium

In the mouse brain oligodendrocytes and astrocytes express distinct sets of connexin proteins, which are capable of forming gap junction channels. Oligodendrocytes express the gap junctional proteins connexin47 (Cx47) (Menichella et al. 2003; Odermatt et al. 2003), Cx32 (Dermietzel et al. 1989; Scherer et al. 1995) and Cx29 (Altevogt et al. 2002; Altevogt and Paul 2004; Li et al. 1997; Nagy et al. 2003a; Nagy et al. 2003b). The postnatal expression profiles of Cx29, Cx32 and Cx47 mRNA in the brain are very similar to those of other genes during myelin development, suggesting that these connexins are associated with oligodendrocyte differentiation (reviewed by Sohl et al. 2004). The connexins expressed by astrocytes include Cx43 and Cx30 (Mercier and Hatton 2001; Nagy et al. 2001; Sohl et al. 2004). Expression of the Cx26 protein was also reported in astrocytes (Nagy et al. 2001), but could not

be confirmed by reporter gene analyses of mice expressing LacZ under control of the Cx26 promoter (Filippov et al. 2003; Nagy et al. 2001).

Immunocytochemical and ultrastructural studies suggest that oligodendrocytes share gap junctions exclusively with astrocytes, but not among each other (for review see Orthmann-Murphy et al. 2008). Freeze fracture analyses of mixed cultures of oligodendrocytes and astrocytes suggested inter-astrocytic gap junctions and heterologous astrocyte to oligodendrocyte gap junctions (Massa and Mugnaini 1985). Immunofluorescence analyses of spinal cord and brain tissue revealed co-localization of oligodendrocytic and astrocytic connexins on contact membranes between these two cell types (Kamasawa et al. 2005; Nagy et al. 2003b). Localizations of the different connexins within the oligodendrocyte plasma membrane are unique and diverse (Kleopa et al. 2004), suggesting distinct functions of the channels composed of different connexins. Cx47 is considered as the predominant oligodendrocytic connexin to form heterologous gap junctions with astrocytic Cx43, (Kamasawa et al. 2005), while Cx32 was colocalized with astrocytic Cx30 (Altevogt and Paul 2004). Furthermore, Cx32 was suggested to form autologous gap junctions at Schmidt-Lanterman incisures (Kamasawa et al. 2005). Based on its location on adaxonal oligodendrocytic membranes (Kamasawa et al. 2005), Cx29 has been suggested to form hemichannels but did not form functional homotypic gap junction channels in cell culture experiments (Ahn et al. 2008). Recently, by dual whole cell patch-clamp on cultured cells transfected with a distinct glia connexin, Cx32/Cx30 and Cx47/Cx43 were found to be the only functional heterotypic channels of all possible combinations (Orthmann-Murphy et al. 2007b).

Inter-astrocytic, inter-oligodendrocytic and astro-oligodendrocytic coupling was detected in cell culture experiments: cultured astrocytes are strongly coupled among each other via gap junctions (Kettenmann et al. 1983), while cultured

oligodendrocytes also form functional junctions, but to a smaller extent as revealed by electrophysiology and dye transfer (Kettenmann et al. 1983; Kettenmann et al. 1984). In addition, electrical coupling but no dye transfer of Lucifer Yellow (LY) between astrocytes and oligodendrocytes was reported (Ransom and Kettenmann 1990). In slices of early postnatal rat optic nerve, injected LY diffused only sparsely to nearby oligodendrocytes (Butt and Ransom 1989).

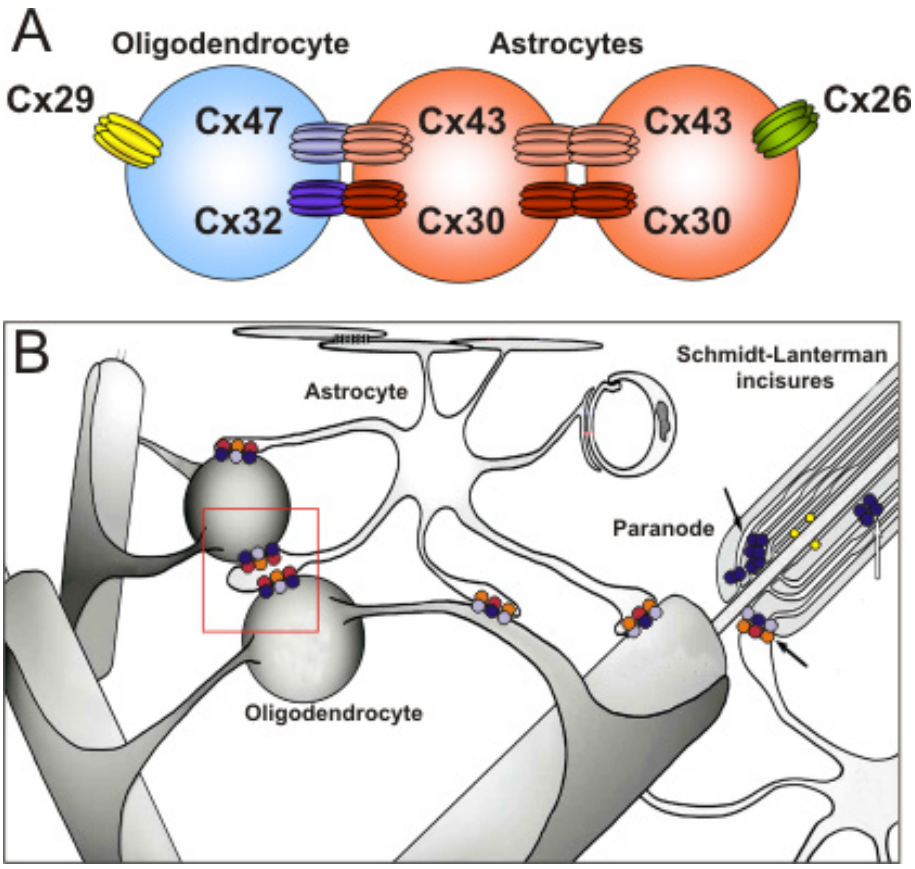

Figure 1.10: The gap junction network of astrocytes and oligodendrocytes. (A) Drawing depicts the gap junction proteins expressed by oligodendrocytes and astrocytes. Oligodendrocyte-to-astrocyte gap junctions contain Cx32/Cx30 and Cx47/Cx43 channels, while inter-astrocytic gap junctions are formed by homotypic Cx30/Cx30 and Cx43/Cx43 channels. (B) Diagram representing cells of the panglial syncytium linked by abundant gap junctions. Astrocytes act as “intermediaries” that couple oligodendrocyte somata, their “oligodendrite” processes, and their myelin segments to the astrocyte endfeet Homotypic Cx32/Cx32 channels connect layers of myelin sheath at the paranode and incisures (arrows). Cx29 hemichannels are localized to the adaxonal membrane of oligodendrocytes, apposing the axon. Blue connexons, Cx32; lilac connexons, Cx47; red connexons, Cx43; orange connexons Cx30; yellow connexons, Cx29 (adapted form Kamasawa et al.,2005).

In the gray matter of rat spinal cord, 18% of injected cells were strongly coupled, while in white matter no functional coupling was observed (Pastor et al. 1998). Also no LY spread was detected in acute slices of corpus callosum from juvenile mice

(Berger et al. 1991). In rabbit retina intercellular communication between oligodendrocytes and oligodendrocytes to astrocytes was detected by tracer transfer (Hampson and Robinson 1995; Robinson et al. 1993). Furthermore, functional gap junction dependent communication between astrocytes has been shown in the hippocampus (Wallraff et al. 2006), barrel cortex (Houades et al. 2008) and motor cortex (Haas et al. 2006) by biocytin tracer transfer experiments. Ablation of both connexins expressed in astrocytes, i.e. Cx30 and Cx43, did not result in gross behavioural abnormalities and the mice were fertile, even if inter-astrocytic coupling in the hippocampus was totally disrupted (Wallraff et al. 2006). However, recently Lutz et al. (2009) demonstrated that Cx43fl/fl Cx30-/- mice expressing Cre under the murine GFAP promoter (Cx43/Cx30-double knockout) display myelin vacuolization and glial edema in the hippocampal CA1 region. Functional inter-oligodendrocytic and astro-oligodendrocytic coupling remains yet to be identified in other parts of the brain.

1.4.4 Connexins and Myelination

Expression of connexins is crucial for oligodendrocytic function, since mutations in *CX32* (*GJB1*) or *CX47* (*GJC2*) genes result in severe myelin diseases in humans (Bergoffen et al. 1993; Bugiani et al. 2006; Kleopa and Scherer 2002; Uhlenberg et al. 2004). As already mentioned in paragraph *1.3.1.1*, missense mutations in *GJC2* cause the hypomyelinating leukodystrophy Pelizaeus-Merzbarcher-like disease 1 (Uhlenberg et al. 2004), while GJB1 mutations lead to the X-linked demyelinating peripheral neuropathy Charcot-Marie-Tooth type 1 (Bergoffen et al. 1993), which is associated with conduction slowing and in some cases with white matter lesions in the central nervous system (Hanemann et al. 2003). In contrast to the severe phenotype of PMLD patients, Cx47-deficient mice display only mild myelination

deficits in the CNS with no obvious behavioural abnormalities. Cx32-deficient mice develop a demyelinating peripheral neuropathy, indicating that loss of function in Schwann cells is sufficient to cause the disease, although neither Gjb1/Cx32-null mice nor GJB1/CX32-null humans exhibit a CNS phenotype, suggesting a different mechanism for the subclinical findings in CMTX1 patients (Hahn et al. 2000). However, Cx47- and Cx32-double-deficient mice have a similar phenotype to PMLD patients with missense or nonsense mutations in GJC2/CX47. These mice are severely impaired and develop tremor and ataxia as well as delayed myelination with abnormal vacuolation of the central white matter (Odermatt et al. 2003, Menichella et al. 2003). Interestingly, most of the patients with GJC2/CX47 mutations also revealed signs of peripheral neuropathy, in contrast to what has been found in mice, where Cx47 is not expressed in the peripheral nervous system. Altogether these findings suggest a functional redundancy of Cx47 and Cx32 within the glia syncytium and/or compensation for the loss of one connexin by the other. Recently Orthmann-Murphy et al. (2007a) showed that three of the missense mutations (P87S, Y269D, M283T) associated to PMLD result in a loss of function protein when expressed in communication-incompetent HeLa cells. These mutants were partially retained in the ER and failed to form functional homotypic channels suggesting that loss of function Cx47 mutants possibly result in PMLD phenotype by interfering with the normal function of Cx47/Cx43 gap junction channels. The possible role of the astro-oligodendrocytic coupling was recently reviewed by Orthmann-Murphy et al. (2008), but the situation is far from clear, since mice deficient for Cx32 and Cx47 in oligodendrocytes display a much more severe phenotype than mice deficient for the astrocytic Cx30 and Cx43 (Menichella et al. 2003; Lutz et al. 2009).

In addition interactions of Cx30 and Cx47 with the scaffolding protein zonula occludens-1 (ZO-1) and the transcription factor ZONAB were described (Li et al.

2004; Li et al. 2008; Penes et al. 2005). ZONAB was discussed to have a direct effect on the expression of the ErbB2 receptor for neuregulin (Balda and Matter 2000). The neuregulin-ErbB2 receptor signalling is involved in differentiation of oligodendrocytes and myelin development in the CNS (Kim et al. 2003).

1.4.5 The Potassium Siphoning Hypothesis

The possible biological function of oligodendrocytic coupling could be to provide pathways for controlling the homeostasis of K^+ during axonal activity, as originally proposed in the model of K^+ spatial buffering (Newman 1986; Orkand et al. 1966; for review see Orthmann-Murphy et al. 2008). Astrocytes are characterized by high permeability to K^+ and by extensive electrical coupling, which may be the prerequisites for redistributing K^+ from areas of high extracellular concentration to areas where the extracellular concentration is lower, without any net change in the glial intracellular [K^+], and thus maintaining proper axonal function (Newman 1986; Orkand et al. 1966).

However this model did not consider the role of oligodendrocytes in potassium homeostasis. A variety of inward rectifying and voltage-gated K^+ channels are localized at the juxtaparanodal membrane of CNS and PNS myelin (for review see Olsen and Sontheimer 2008). Influx of K^+ through these channels into internodal myelin would account for the depolarization of the peri-internodal compartment following axonal action potential. As suggested by Kamasawa et al. (2005), glial connexins could contribute to the redistribution of K^+ from the periaxonal cytoplasm by direct radial diffusion to the outer myelin layer by reflexive Cx32-contaning gap junctions in both paranodes and inscinsures.

At the outer myelin layer, gap junctions between oligodendrocytes and astrocytes could allow oligodendrocyte K^+ diffusion into the astrocyte syncytium, possibly

augmented by the high osmotic concentration and by the electrical potential difference between innermost myelin and astrocyte network. As originally proposed in the potassium buffer hypothesis the extensive gap junctional coupling of astrocytes provides a mechanism for K^+ dispersal at the capillaries and pia mater.

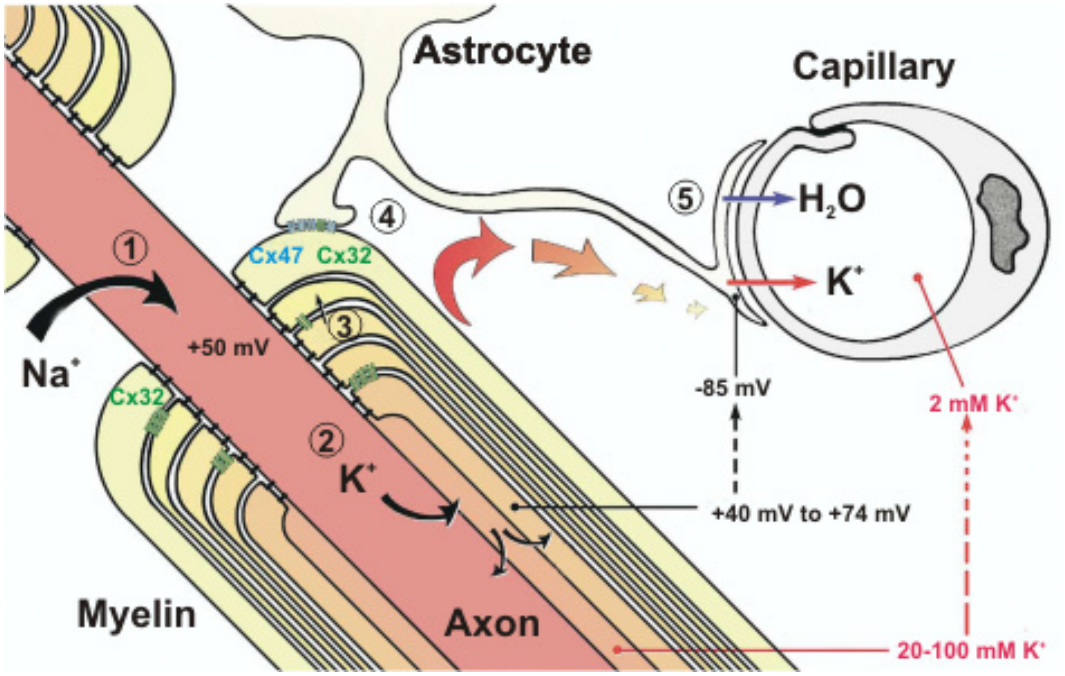

Figure 1.11: Diagram of pathways for "potassium siphoning" summarizing the movement of Na^+ at nodes of Ranvier (1), exit of K^+ at juxtaparanodal axonal plasma membrane (2), and intracellular and intercellular pathways for both K^+ and H_2O through Cx32-gap junctions linking successive layers of myelin (3) into the astrocyte syncytium via heterotypic (Cx47/Cx32: Cx43/Cx30) gap junctions (4), and ultimately to the astrocyte endfeet (5). Red-to-yellow gradient represents the charge gradient from areas of excess positive charge/positive membrane potential to lowest positive charge/highest negative membrane potential. Blue connexons, Cx47; green connexons, Cx32 (adapted from Kamasawaet al. 2005).

Recently Menichella et al. (2006) provided the first physiological evidence that neuronal activity correlates with the onset of myelin associated vacuolization in the CNS of Cx47/Cx32 double-deficient mice, thus consolidating the notion that oligodendrocytes play a critical role in buffering K+ ions released during neuronal activity.

2 Goals

Increased genetic evidence revealed the importance of oligodendrocytic connexins in proper myelin function, since CX32 (GJB1) or CX47 (GJC2) mutations cause severe human myelin related disorders (Bergoffen et al. 1993; Bugiani et al. 2006; Kleopa and Scherer 2002; Uhlenberg et al. 2004). According to ultrastructural and immunocytochemical studies oligodendrocytes share gap junctions exclusively with astrocytes, but not with each other (Kamasawa et al. 2005), while in cell culture experiments oligodendrocytes form functional gap junction channels (Kettenmann et al. 1983; Kettenmann et al. 1984). In order to understand the basis of the myelin related diseases caused by deletion or mutations of oligodendrocytic connexins, it is first of all necessary to determine which connexin forms functional gap junctions in the CNS white matter. Furthermore the impact of Cx47 mutants on Cx32 function has to be clarified, since mice lacking both Cx47 and Cx32 resemble the pathological phenotype of patients carrying GJC2 mutations, while Cx47-single-deficient animals show a relatively mild phenotype.

Therefore the specific aims of this study were to:

1. analyze functional inter-oligodendrocytic and oligodendrocyte-to-astrocyte coupling in the CNS white matter
2. investigate the role of Cx47 on oligodendrocytic coupling
3. characterize the effect of Cx47 mutants versus null Cx47 on inter-oligodendrocytic and oligodendrocyte-to-astrocyte coupling.

To address these questions functional coupling between oligodendrocytes was studied in acute slices of postnatal mouse corpus callosum from wildtype and different connexin-deficient mouse lines. As a model for PMLD mice carrying the Cx47M282T point mutation were used. The ortholog human mutation Cx47M283T

was the only missense mutation found homozygously in PMLD patients described by Uhlenberg et al. (2004). Using the whole cell patch-clamp technique single oligodendrocytes were dialysed with the gap junction permeable tracer biocytin and the labeled cells were identified via cell-type specific markers.

3 Material and Methods

3.1 Chemicals

Table 3.1 List of chemicals

Name	Company
Alexa Fluor 594	Invitrogen, Karlsruhe, Germany
Aqua Poly/Mount	Polysciences Inc., Eppelheim, Germany
Biocytin	Sigma-Aldrich, Munich, Germany
Bovine Serum Albumin (BSA)	Fluka Chemie, Buchs, Switzerland
$CaCl_2 \cdot 2H_2O$	Carl Roth GmbH, Karlsruhe, Germany
$C_6H_{12}O_6$	Carl Roth GmbH, Karlsruhe, Germany
Diaminobenzidine (DAB)	Sigma-Aldrich, Munich, Germany
Dimethylsulfoxide (DMSO)	Sigma-Aldrich, Munich, Germany
Ethylene glycol tetraacetic acid	Sigma-Aldrich, Munich, Germany
HEPES	Carl Roth GmbH, Karlsruhe, Germany
Invisorb® Spin Tissue Mini Kit	Invitek, Berlin, Germany
KCl	Carl Roth GmbH, Karlsruhe, Germany
$K_2HPO_4 \cdot 3H_2O$	Merck, Damstadt, Germany
$MgCl_2 \cdot 6H_2O$	Carl Roth GmbH, Karlsruhe, Germany
NaCl	Carl Roth GmbH, Karlsruhe, Germany
$NaHCO_3$	Carl Roth GmbH, Karlsruhe, Germany
$NaH_2PO_4\ H_2O$	Carl Roth GmbH, Karlsruhe, Germany
$Na_2HPO_4\ 2H_2O$	Carl Roth GmbH, Karlsruhe, Germany
Normal Goat Serum (NGS)	Gibco, Eggenstein, Germany
β-Gal Staining Set solution	Roche Diagnostics GmbH, Mannheim, Germany
Glycerol	Sigma-Aldrich, Munich, Germany
Paraformaldehyde	Merck, Damstadt, Germany
Streptavidin-Cy3 Conjugate	Jackson ImmunoResearch/Dianova, Hamburg, Germany
Tris-HCl	Carl Roth GmbH, Karlsruhe, Germany
Triton X-100 (TX-100)	Carl Roth GmbH, Karlsruhe, Germany
Vectastain Elite ABC kit Standard	Axxora, Grünberg, Germany

3.1.1 Intra and extracellular solutions

Table 3.2 Solutions for acute brain slices

	Artificial Cerebral Spinal Fluid (aCSF)	Standard Intracellular Solution
NaCl	134 mM	4 mM
KCl	2.5 mM	120 mM
$C_6H_{12}O_6$	10 mM	5 mM
$MgCl_2 \cdot 6H_2O$	1.3 mM	4 mM
$CaCl_2 \cdot 2H_2O$	2 mM	0.5 mM
$K_2HPO_4 \cdot 3H_2O$	1.25 mM	-
$NaHCO_3$	26 mM	-
HEPES	-	10 mM
EGTA	-	5 mM
Biocytin	-	0.5 - 0.6%
pH	7.4	7.4
Osmolarity (mmol/kg)	340	285

3.1.2 Antibodies and solutions for Immunohistochemistry

Table 3.3 List of primary antibodies

Name	Company
Chicken polyclonal anti-eGFP	Chemicon, Millipore GmbH, Schwalbach/Ts., Germany
Mouse polyclonal anti-CNPase	Covance/HISS Diagnostic GmbH, Freiburg, Germany
Rabbit monoclonal anti-Olig2	a kind gift from David Rowitch, Boston, USA
Rabbit polyclonal anti-eGFP	Invitrogen, Karlsruhe, Germany
Rabbit polyclonal anti-GFAP	DAKO, Hamburg, Germany
Rabbit polyclonal anti-NG2	Chemicon, Millipore GmbH, Schwalbach/Ts., Germany

Table 3.4 List of secondary antibodies

Name	Company
Cy5-conjugated donkey anti-mouse IgG	Jackson ImmunoResearch/Dianova, Hamburg, Germany
Cy5-conjugated donkey anti-rabbit IgG	Jackson ImmunoResearch/Dianova, Hamburg, Germany
DyeLight 488-conjugated donkey anti-rabbit IgG	Jackson ImmunoResearch/Dianova, Hamburg, Germany
FITC-conjugated donkey anti-chicken IgG	Jackson ImmunoResearch/Dianova, Hamburg, Germany
FITC-conjugated donkey anti-mouse IgG	Jackson ImmunoResearch/Dianova, Hamburg, Germany

Table 3.5 Solutions for Immunohistochemistry

Solution	Assay	Content	pH
ABC-Kit dilution buffer	DAB	0.5% BSA, 0.25% DMSO, 0.05M TBS	7.4
DAB incubation buffer	DAB	0.025% DAB, 0.03% NiCl, 0.1M TB	7.6
DAB pre-incubation buffer	DAB	0.025% DAB, 0.03% NiCl, 0.002% H_2O_2, 0.1M TB	7.6
Phosphate buffer (PB) 0.1M	other	0.2M Na_2HPO_4 $2H_2O$, 0.2M NaH_2PO_4 H_2O	7.4
Blocking/permealizing buffer	other	2% TX-100, 2% BSA and 10% NGS, 0.1M PB	7.4
Dilution buffer	other	2% TX-100, 2% BSA and 5% NGS, 0.1M PB	7.4
Blocking/permealizing buffer	DAB	2% BSA, 0.25% DMSO, 0.05M TBS	7.4
Peroxidases blocking buffer	DAB	1% H_2O_2, 0.1M TB	7.4
Tris-HCl buffer (TB) 0.1M	DAB	100 mM Tris-HCl	7.4
Tris-HCl buffer (TB) 0.1M	DAB	100 mM Tris-HCl	7.6
Tris buffered saline (TBS) 0.1M	DAB	100 mM Tris-HCl, 100mM NaCl	7.4
Tris buffered saline (TBS) 0.05M	DAB	100 mM Tris-HCl, 50mM NaCl	7.4

3.1.3 Primers, solutions and reagents for genotyping PCR

Table 3.6 List of oligonucleotides

PCR reaction	Primer	Sequence (5'-3')
Cx29	Cx29 forward (1)	ATA GGC CCA GAG AAG CTT GAG
	LacZ reverse (2)	CCT CTT CGC TAT TAC GCC AG
	Cx29 reverse (3)	TGG TGT TTG ATC AAC TTT GGA G
Cx43 fl/fl	Cx43 fl/fl UMP (forward) (1)	TCA TGC CCG GCA CAA GTG AGA C
	Cx43 fl/fl UMPR (reverse) (2)	TCA CCC CAA GCT GAC TCA ACC G
hGFAP-Cre	GFAP LZ1 (forward) (1)	ACT CCT TCA TAA AGC CCT CG
	Cre LZ4 (reverse) (2)	ATC ACT CGT TGC ATC GAC CG
Cx47	Cx47 forward (1)	CAG GAT CAA TGG AAG ATT CTC GGT CCC
	Cx47 reverse (2)	GCC AAG CGG TGG ACT GCA TAG CCC AGG
	eGFP reverse (3)	GAC ACG CTG AAC TTG TGG CCG TTT ACG
Cx47 M282T	Cx47 (M282T) forward (1)	CAG AGA GAG GAG CTG TTC TTG GTC C
	LacZ reverse (2)	CCG GTC GCT ACC ATT ACC AGT TGG

	Cx47 (M282T) reverse (3)	GCA GCA GAG ACG GCA AGG CCA CC
Cx30	Cx30 forward (1)	GGT ACC TTC TAC TAA TTA GCT TGG
	LacZ reverse (2)	AGC GAG TAA CAA CCC GTC GGA TTC
	Cx30 reverse (3)	AGG TGG ACC CAT TGT AGA GGA AG
Cx32	Cx32 forward (1)	AGA TAA GCT GCA GGG ACC ATA GG
	Cx32 reverse (2)	CCA TAA GTC AGG TGT AAA GGA GC
	Neo reverse (3)	ATC ATG CGA AAC GAT CCT CAT CC
NG2	NG2 forward (1)	TGA CCT TGG ATT CTG AGC
	eYFP reverse (2)	ACA GCT TTC CTT CCA GAC
	NG2 reverse (3)	TGA CCT TGG ATT CTG AGC

Table 3.7 Solutions for genotyping PCR reactions

Reagents	**Cx29**	**Cx30**	**Cx32**	**Cx43 fl/fl**	**hGFAP-Cre**	**Cx47**	**Cx47 M282T**	**NG2**
10 X PCR Buffer	2.50 µl	2.50 µl	2.50 µl	2.50 µl	2.50 µl	2.50 µl	2.50 µl	2.50 µl
DMSO	-	1.00 µl	-	1.00 µl	-	-	-	-
dNTPs	1 mM	1 mM	1 mM	1 mM	1 mM	1 mM	1 mM	1 mM
$MgCl_2$	1.50 µl	-	1.50 µl	-	1.50 µl	1.50 µl	1.50 µl	1.50 µl
(1) Primer	0.2 pM	0.2 pM	0.2 pM	0.2 pM	0.2 pM	2 pM	0.2 pM	0.2 pM
(2) Primer	0.2 pM	0.2 pM	0.2 pM	0.2 pM	0.2 pM	2 pM	0.2 pM	0.2 pM
(3) Primer	0.2 pM	0.2 pM	0.4 pM	-	-	0.2 pM	0.2 pM	0.2 pM
TAQ polimerase	0.25 µl	0.25 µl	0.25 µl	0.25 µl	0.25 µl	0.25 µl	0.25 µl	0.25 µl
Genomic DNA	1.5 µl	0.5 µl	1.5 µl	1.0 µl	1.5 µl	1.5 µl	1.5 µl	1.5 µl
Final Volume	25 µl	25 µl	25 µl	25 µl	25 µl	25 µl	25 µl	25 µl

Table 3.8 List of PCR reagents

Name	Company
dNTPs	Invitek, Berlin-Buch, Germany
$MgCl_2$	Invitrogen, Karlsruhe, Germany
Primers	Metabion international AG, Martinsried, Germany
TAQ polimerase	Invitrogen, Karlsruhe, Germany
TAQ polimerase*	Roche Diagnostics GmbH, Mannheim, Germany

** for Cx30 and Cx43 fl/fl PCR reactions*

3.1.4 Equipments, apparatus, and computer software

Table 3.9 List of equipments and apparatus

Name	Company
Amplifier (EPC-9.2)	HEKA Elektronik, Lambrecht, Germany
Amplifier (EPC-10)	HEKA Elektronik, Lambrecht, Germany
Capillaries (borosilicate) Inner diameter 0.87 mm/outer diameter 1.5 mm	Hilgenberg, Malsfeld, Germany
Digital camera (Sensi Cam)	PCO Computer Optics GmbH, Kelheim, Germany
Digital camera (Spot PURSIUT)	Olympus Life Science Europa GmbH, Hamburg, Germany
Digital camera (AxioCam)	Zeiss, Oberkochen, Germany
DIC optics	Zeiss, Oberkochen, Germany
Filter set ALPHA Vivid XF100-2 for EGFP	Omega Optical, Austin, TX, USA
Filter set Leica set 15 for Cy3 [1]	Leica, Solms, Germany
Filter set Leica set GFP for EGFP and FITC [1]	Leica, Solms, Germany
Filter set Leica set I3 for EGFP and FITC [2]	Leica, Solms, Germany
Filter set Leica set N2.1 for Cy3 [2]	Leica, Solms, Germany
Filter set Multi band XF53 for EGFP and Alexa Fluor 594	Omega Optical, Austin, TX, USA
Filter set U-MSP101v1 MFISH for FITC	Olympus Life Science Europa GmbH, Hamburg, Germany
Filter set U-MSP102v1 MFISH for Cy3	Olympus Life Science Europa GmbH, Hamburg, Germany
Filter set U-MSP104v1 MFISH for Cy5	Olympus Life Science Europa GmbH, Hamburg, Germany
Filter tips for internal solution (0.22 µm)	Millipore, Carrigtwohill, Ireland

Glass cover slips 13mm	Glaswarenfabrik Karl Hecht KG, Sandheim, Germany
Lamp HBO 50W mercury [2]	Leica, Solms, Germany
Lamp HBO 100W mercury [1]	Leica, Solms, Germany
Lamp X-Cite-120W metal halide	Olympus Life Science Europa GmbH, Hamburg, Germany
Micromanipulator (Patchman)	Eppendorf, Hamburg, Germany
Microscope (Axioskop 2FS plus)	Zeiss, Oberkochen, Germany
Microscope (DM TCS SP2, confocal)	Leica, Solms, Germany
Microscope (System mikroskop BX 51)	Olympus, Hamburg, Germany
Microscope (TCS SP5, confocal)	Leica, Solms, Germany
Monochromator (Polychrom IV)	Till Photonics, Graefelfing, Germany
Objective 4X U Plan Semi Apo – na 0.3	Olympus, Hamburg, Germany
Objective 10X UM Plan FL – na 0.3w	Olympus, Hamburg, Germany
Objective 20X HCX PL Apo – na 0.7oil/glyc/w [1]	Leica, Solms, Germany
Objective 20X HCX PL Apo – na 0.7 [2]	Leica, Solms, Germany
Objective 20X U Plan Semi Apo – na 0.5	Olympus, Hamburg, Germany
Objective 40X U Plan Semi Apo – na 0.75	Olympus, Hamburg, Germany
Objective 40X Achroplan– na 0,8w	Zeiss, Oberkochen, Germany
Objective 40X HCX PL Apo – na 1.25-0.75oil [1]	Leica, Solms, Germany
Objective 40X HCX PL Apo – na 1,25oil [2]	Leica, Solms, Germany
Pipette Puller (P-2000 Laser Based)	Sutter Instrument, Novato, CA, USA
Superfrost Plus slides	Menzel GmbH & Co KG, Braunschweig, Germany
T3000 Thermocycler	Whatman, Biometra
Vibratome (HM 650V)	Microm, Walldorf, Germany
Vibratome (VT 1000 S)	Leica, Solms, Germany

[1] *TCS SP5 confocal setup*
[2] *DM TCS SP2 confocal setup*

Table 3.10 List of computer software

Name	Company
Adobe Photoshop CS 8.0	Adobe Systems Inc., San Jose, CA, USA
Axiovision 4.7.2	Zeiss, Göttingen, Germany
CorelDRAW Graphic Suite X3	Corel Corporation, Fremont, USA
Image Pro 5.0	Media Cybernetics, Bethesda, MD, USA
Image Pro Plus	Media Cybernetics, Bethesda, MD, USA
Imaging Cells Easily (ICE) 3.6.1	Max-Delbrück-Center for molecular medicine, Berlin, Germany
LAS AF Lite	Leica, Solms, Germany
LCS Lite	Leica, Solms, Germany
Metamorph	Visitron Systems GmbH, Puchheim, Germany
Microsoft Office 2003	Microsoft, Redmond, WA, USA
SPSS 11.5.1	SPSS Inc, Chicago, IL, USA
TIDA Version 5.20	HEKA Elektronik, Lambrecht, Germany
Origin 7	OriginLabCorporation, Northampton, USA

3.2 Animals

All mice used for this study were kept under standard housing conditions with a 12-hour/12-hour dark-light cycle and with food and water ad libitum. All experiments were performed according to the guidelines of the German law for animal protection. Mice used for experiments had a genetic background of 93% C57BL/6N. In the Cx47-deficient (Cx47 eGFP(-/-)) mouse line, the Cx47 coding region had been replaced by cDNA encoding the enhanced variant of the green fluorescent protein (eGFP; Odermatt et al. 2003). Cx32-deficient mice were generated by inserting the neomycin resistance gene cassette into exon 2 of the Cx32 gene, 30 codons after the translational start site (Nelles et al. 1996). To obtain Cx47- and Cx32-double-deficient mice, Cx47 eGFP(-/-) male mice were crossbred with Cx32(-/-) female mice. Female Cx47- and Cx32-double-heterozygous were crossed with male Cx32 –

deficent and Cx47-heterozygous. Because Cx32 gene is X-linked, one of eight males was deficient for both connexins. In the Cx29-deficient mice the Cx29 coding region was replaced by a lacZ reporter gene that was driven by the endogenous Cx29 promoter (Eiberger et al. 2006). Conditional Cx43-deficient mice were obtained by interbreeding of Cx43 (fl/fl) mice with mice carrying the hGFAP-Cre transgene (Theis et al. 2003). In Cx43fl/fl:hGFAP-Cre mice the astrocyte specific deletion of Cx43 resulted in expression of the reporter gene LacZ. Since the widely used hGFAP-Cre transgene exhibits variable recombination activity (Requardt et al. 2009) all mice used in experiments were tested for LacZ expression by β-galactosidase staining (see paragraph *3.4.3*). Cx43- and Cx30-double-deficient mice were obtained by interbreeding of the Cx43fl/fl:hGFAP-Cre mice with mice lacking the astrocytic Cx30. In the Cx30-deficient mouse line the Cx30 coding region was replaced by the reporter gene lacZ and a Neo resistance cassette (Teubner et al. 2003). Heterozygous NG2-EYFP knockin mice were used to examine coupling with oligodendrocyte precursor cells. These heterozygous mutants were generated inserting cDNA encoding the enhanced variant of the Yellow Fluorescent Protein (EYFP) into exon 1 of the NG2 gene (Karram et al. 2008). Mice carrying the point mutation Cx47M282T, i.e. the ortholog of the human mutation Cx47M286T were generated in Prof. Willecke's laboratory (Tress et al., unpublished). Expression of the mutant *GJC2* gene in transgenic animals resulted in a bicistronic mRNA coding for Cx47M282T and the reporter gene LacZ, which could be detected by X-Gal staining. Translation of the LacZ gene was mediated by the IRES cassette. For experiments, 10 to 15 day old mice were used, unless otherwise specified.

3.2.1 Genotyping PCR protocols

For all genotyping PCR reactions, genomic DNA was isolated using the Invisorb® Spin Tissue Mini Kit, according to manufacturer instructions.

Diagnostic PCR of tail-tip DNA was performed to genotype mice for occurrence of wildtype and knock out Cx47 eGFP alleles using a Cx47 intron-specific sense primer (for sequences and solutions see paragraph *3.1.4*, table *6*), which was combined with Cx47 exon-specific and EGFP-specific antisense primers under the following conditions: 5 min of DNA denaturation at 95°C, followed by 40 cycles of 94°C for 45 sec, 64°C for 45 sec, and 72°C for 1 min, and final elongation at 72°C for 10 min. The PCR yielded a 530 bp amplicon specific for wildtype and a 340 bp fragment for the mutated Cx47 allele (Odermatt et al. 2003).The Cx32 genotype (the Cx32 gene is located on the X chromosome) was tested by tail-tip PCR with some modifications of the original protocol described (Anzini et al. 1997). In details: The PCR reaction product was denatured at 95°C for 5 min, followed by 40 cycles (95°C, 30 sec; 62°C, 30 sec; 72°C, 35 sec) and a final extension at 72°C for 10 min. The wildtype Cx32 and the mutated allele were represented as a 550 bp and a 414 bp fragment, applying two primers complementary to Cx32 gene sequences and an additional oligonucleotide primer binding to the neo resistance cassette sequences. Cx29-deficient mice were genotyped by PCR of tail-tip DNA, according to the protocol described by Eiberger et al. (2006), with some modifications. Cx29 intron-specific sense primer was combined with Cx29 exon-specific and lacZ-specific antisense primers under the following conditions: 5 min of DNA denaturation at 94°C, followed by 35 cycles of 94°C for 30 s, 58°C for 30 s, and 72°C for 30 s and a final elongation at 72°C for 10 min. The PCR yielded a 555 bp wildtype specific amplicon and a 394 bp fragment for the mutated Cx29 allele. Genotyping of mice lacking Cx43 in astrocytes was performed according to Theis et al. (2001), with some modifications.

For simultaneous detection of the Cx43 floxed allele and the Cx43 wildtype allele, primers UMP and UMPR were applied. PCR conditions were 2 min at 94° C for denaturation, 34 cycles of 92° C for 60 sec, 65° C for 60 sec, 72°C for 90 sec and a final elongation of 72° C for 10 min. A 1 kb floxed amplicon and a 900 bp wildtype amplicon were generated. Cre transgene was detected adapting the protocol described in Theis et al. (2003). GFAP LZ1 and Cre LZ4 primers were combined under the following PCR conditions: 60 sec denaturation at 94° C, 29 cycles of 94° C for 60 sec, 60° C for 60 sec, 72° C for 60 sec and final elongation at 72° C for 10 min, generating a 200 bp fragment. Mice deficient for the astrocytic Cx30 were genotyped for occurrence of wildtype and mutated alleles using Cx30 intron-specific sense primer combined with Cx30 exon-specific and lacZ exon-specific primers (Teubner et al. 2003). A 544 bp wildtype amplicon and a 460 bp transgene amplicon were generated using the following conditions: denaturation at 94° C for 5 min, 34 cycles of 94° C for 45 sec, 60°C for 45 sec, 72° C for 45 sec and 72°C for 10 min for final elongation. The genetic identity of Cx47 M282T heterozygous and homozygous animals was verified by three primer PCR analysis which yield a 575 bp product for the wildtype allele and a 730 bp product for the transgenic Cx47M282T allele. PCR conditions were: denaturation at 95°C for 5min, 29 cycles of 95° C for 30 sec, 61° C for 30 sec, 72° C for 45 sec and a final elongation at 72° C for 10 min. The DNA was subjected to PCR amplification to distinguish between the normal and mutant gene, where a normal band of 900 bp and a mutant band of 750 bp were observed. PCR analysis was performed at the following conditions: 95° C denaturation for 3 min, 34 cycles of 95°C for 60 sec, 56°C for 30 sec, 72°C for 60 sec and 72° C for 10 min for final elongation (Karram et al. 2008).

3.3 Acute brain slice preparation

Acute brain slices were prepared from postnatal days (p) 10–15 old mice; adult slices from p20-25 old mice, as previously described (Haas et al. 1996). In brief, mice were decapitated, brains were carefully removed and mounted in a chamber with ice-cold bicarbonate-buffered artificial cerebrospinal fluid (aCSF), composed as already described in the material and methods chapter, paragraph *3.1.2*. The buffer solution was saturated with carbogen (95%O_2, 5%CO_2). Coronal slices of 110 µm were prepared at 4°C using a vibratome HM 650 V. They were then gently transferred and stored in aCSF at room temperature (21–25°C) for at least 30 min before the experiments were conducted.

3.4 Dye-coupling experiments

3.4.1 Visualization of oligodendrocytes

Acute brain slices were placed in a holding chamber mounted on the stage of an upright light microscope Axioskop 2 FS plus. To secure the acute brain slices without damaging the area of interest, they were positioned on a glass coverslip and a U-shaped platinum grid lined with thin nylon threads. To maintain constant condition during experiments, the chamber was continuously perfused with standard aCSF. Specimens were viewed at different magnification using 10X or 40X water immersion objectives. In some experiments, the cells of interest were visualized by DIC using a 40X DIC water immersion objective. For fluorescence detection, excitation beams of specific wavelengths were generated by a monochromator Polychrome IV, controlled by TIDA software via EPC 9.2 or EPC 10 amplifiers. The emitted light was detected by an appropriate set of filters specific for the fluophore used (see paragraph *3.1.5*, table *9*). In the mouse corpus callosum oligodendrocytes were recognized in the

bright phase by their somata often located in a row parallel to the fibers. In Cx47-deficient and Cx47/32-double-deficient mice, the Cx47 coding region was replaced by cDNA encoding eGFP (Odermatt et al. 2003), therefore oligodendrocytes were identified by their eGFP fluorescence at an excitation and emission wavelength of 488 and 530 ± 10 nm, respectively. Images were captured with a SensiCam CCD camera, using the software Imaging Cell Easily 3.6.1.

3.4.2 Setup and equipments

Dye coupling experiments and electrophysiological recordings were carried out using setup described in paragraph *3.1.5.* Patch pipettes were pulled from borosilicate capillaries (inner diameter 0.87 mm; outer diameter 1.5 mm) using a P-2000 laser-based pipette puller and filled with standard intracellular (pipette) solution described in paragraph *3.1.2*. To assess gap junctional coupling biocytin (0.5-0.6%) was included to the pipette solution and Alexa Fluor 594 (10 µg/ml) was added to confirm intracellular access. Prior to use, this solution was passed through a filter tip (0.22 µm) to avoid blockage of pipette tips. During each patch-clamp experiment, the filled pipette was secured on a Cl^--coated silver electrode and then guided towards the chosen cell using a micromanipulator. Mild positive pressure was always applied to the pipette in order to avoid tip contamination and to help navigation through the cell layers. Electrical potential and current between the patch electrode and the ground electrode inserted in the perfusion were recorded with EPC 9.2 or EPC 10 amplifiers and monitored using TIDA software. Pipette resistance (R_p) ranged from 3 to 7 MΩ. All experiments were performed at room temperature.

3.4.3 Electrophysiological recordings and biocytin injection

Membrane current recordings and biocytin injection were performed in the conventional whole cell voltage-clamp configuration (Hamill et al. 1981). Briefly, the patch pipette was placed close to the cell membrane and a slight suction was applied, leading to the formation of a seal between membrane and pipette. The seal was accompanied by an increase in the resistance to >1GΩ. At this stage, to reach the whole cell mode, the membrane patch was ruptured by suction and applying a large hyperpolarizing voltage step (1 V) for 0.1-10 ms (also called “zap”). Electrode capacitance was compensated by TIDA software.

During recordings, the membrane was continuously de- and hyperpolarized between - 170 and + 50 mV in 10 mV steps for 50 ms (fig. 3.1). Current signals were amplified (EPC 9/2 or EPC10 amplifiers), filtered (3 kHz), sampled (5 kHz), and monitored with TIDA software.

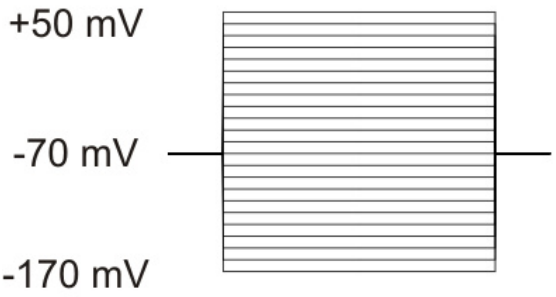

Figure 3.1: Stimulation protocol for recording membrane currents. Cells were clamped to a holding potential of -70 mV. A series of de- and hyperpolarizing voltage jumps ranging from -170 mV to +50 mV at 10 mV increments were applied for 50 ms.

Resting membrane potentials of the recorded cells were identified with a TIDA routine. Membrane capacitance (C_m) values were calculated based on the equation $C_m = \int I*dt / \Delta U$, measuring with TIDA software the transient currents evoked in response to a depolarizing +10mV step from a holding potential of -70 mV (50 ms). Membrane capacitance values depending on the transient current kinetics were determined applying the equation $C_m = \tau / R_s$, where τ indicates the decay time constant of the transient current elicited at +30 mV from a holding potential of -70

mV. Decay time constants and amplitudes of slow and fast components were determined by biexponential fit of the evoked capacitative transient current between 2 ms and 49 ms after the voltage step. The series resistance (R_s) was calculated by the Ohmic law ($R_s = \Delta U / I_{max}$). Input resistance (R_{in}) values were determined from the steady state current response to a depolarizing voltage step of 10 mV from a holding potential of - 70 mV (50 ms), applying the equation: $R_{in} = \Delta U / I_{off}$. In each individual slice only a single cell was filled via the patch pipette during whole cell recordings (20 min) (Kressin et al. 1995). Only cells with stable membrane potential V_m (ranging from -42 mV to -68 mV) and R_s over the 20 min period were considered for data analysis.

Cells filled with Alexa Fluor 594 were detected by fluorescence microscopy with excitation at 589 nm generated by a monochromator Polychrome IV. The emitted light at 616 ± 4 nm was visualized with standard fluorescence optics and captured with a CCD camera SensiCam, using the software Imaging Cell Easily 3.6.1 (ICE, Max-Delbrück-Center for molecular medicine, Berlin, Germany). The volume of the patched cells was quantified on images acquired as described above. The perimeter of each cell filled with Alexa Fluor 594 was tracked manually and measured with the *Measurement* tool of AxioVision 4.7.2 software. From the obtained value the cell volume (V) was then calculated applying the formula $V = 4/3\ \pi\ r^3$.

3.5 Immunohistochemistry

After recording and dialysis the slices were fixed for 1 hour in a solution of 4% paraformaldehyde in 0.1 M phosphate buffer (pH 7.4) at 4°C and processed for biocytin visualization with diaminobenzidine (DAB) or fluorochrome conjugated streptavidin combined with immunostaining. To detect spontaneous loss of hGFAP-cre activity (Requardt et al. 2009), slices obtained from all the Cx43- deficient and

Cx43/Cx30-double-deficient mice used in experiments were tested for LacZ expression.

3.5.1 Biocytin labeling with DAB reaction

Hundred-ten µm thick slices were processed for DAB-biocytin detection according to the free floating method described in D'Ambrosio et al. (1998) with the modifications applied by Haas et al. (2006). Briefly, after fixation the tissue was first rinsed in 0.1M phosphate buffer (PB) and then 0.1M Tris-HCl buffer (TB), pH 7.4. Endogenous peroxidases were suppressed with 1% H_2O_2 for 2 hours. To reduce nonspecific background and to permealize membranes, sections were incubated with 2% bovine serum albumin (BSA) and 0.25% dimethylsulfoxide (DMSO) in 0.05M Tris buffered saline (TBS), pH 7.4 for 1 hour. Then samples were incubated with Vectastain Elite ABC kit Standard for 48 hr at 4°C, according to manufacturer's instructions. After preincubation with 0.025% DAB and 0.03% NiCl in 0.1M TB, pH 7.6 for 15 minutes to increase stainining density, fresh DAB and NiCl solution containing 0.002% H_2O_2 was added. After 60 minutes, the DAB reaction was stopped adding 0.1M TB pH 7.4 and slices were mounted, dried and embedded in Aqua Poly/Mount mounting medium on gelatin coated slides. Images were taken with an AxioCam digital camera and appropriate software AxioVision 4.7.2.

3.5.2 Biocytin labeling with Cy3 conjugated streptavidin combined with immunostaining

In order to identify the population of coupled cells within the network, biocytin labeling with Cy3 conjugated streptavidin was combined with the oligodendrocyte marker CNPase immunostaining, the astrocytic marker GFAP or the oligodendrocyte precursor markers NG2 and Olig2, respectively. To identify oligodendrocyte

precursors I also used heterozygous NG2-EYFP knock in mice, in which the NG2 coding region was replaced by the gene encoding the EYFP protein. In Cx47-deficient and in Cx47/32-double-deficient mice oligodendrocytes were identified by immunostaining against eGFP, specifically expressed under the Cx47 promoter. After fixation slices were incubated in a solution containing 2% Triton X-100 (TX-100), 2% BSA and 10% normal goat serum (NGS) in phosphate buffer at pH 7.4 for 4 hours to permeabilize and to block nonspecific binding of the primary antibodies. Cy3 conjugated streptavidin (1:200), mouse anti-CNPase oligodendrocyte cell marker (1:200), rabbit polyclonal anti-GFAP (1:1,000), rabbit polyclonal anti-NG2 (1:100), rabbit anti-Olig2 (1:10,000) and chicken polyclonal anti-eGFP antibodies (1:500) were diluted in 0.1 M phosphate buffer containing 2% TX-100; 2% BSA; 5% NGS. A rabbit polyclonal anti-EGFP antibody recognizing EYFP (1:200) was used to amplify staining of NG2-EYFP cells. The floating slices were incubated with the primary antibodies for 48 h at 4°C. Primary antibodies were visualized by application of FITC-conjugated donkey anti-mouse IgG (1:200), Cy5-conjugated donkey anti-mouse IgG (1.200), Cy5-conjugated donkey anti-rabbit IgG (1:200), DyeLight 488-conjugated donkey anti-rabbit IgG (1:200) or by FITC-conjugated donkey anti-chicken IgG (1:200) for 2 hours at 4°C. Specificity of secondary antibody was tested applying all secondary antibodies to control slices labeled with each single primary antibody alone. No unspecific cross reaction between secondary antibodies was observed. Slices were rinsed and mounted with Aqua Poly/Mount mounting medium. Images were acquired by confocal microscopy (Leica DM TCS SP2 or Leica TCS SP5) with Leica software (LCS Lite or LAS AF Lite, respectively). All scannings were performed sequentially with an Argon laser (488nm) and two Helium-Neon lasers (543 and 633nm), with appropriate excitation beam splitter.

3.5.3 Detection of hGFAP-cre activity by β-galactosidase staining

All Cx43-deficient and Cx43/Cx30-double-deficient mice used for experiments were monitored for loss of Cre activity by β-galactosidase staining with the β-Gal Staining Set solution. According to the manufacturer instruction, fixed slices were incubated overnight in the X-Gal solution diluted in iron buffer (1:19 dilution) at 37°C. The reaction was stopped by rinsing the sections with PB 0.1 M, pH 7.4 at RT. Slices were mounted and embedded in Aqua Poly/Mount mounting medium on gelatin coated slides. Images were acquired with Spot PURSIUT digital camera and MetaMorph software. Only slices obtained from animals expressing the LacZ gene were further analyzed by biocytin injection. In Cx43/Cx30-double-deficient mice both Cx43fl/fl and Cx30 coding regions were replaced by the reporter gene LacZ. Therefore LacZ expression driven under the Cx43 promoter was distinguished by comparison with the specific expression pattern observed in Cx43fl/fl:hGFAP-Cre mice (fig. 3.2).

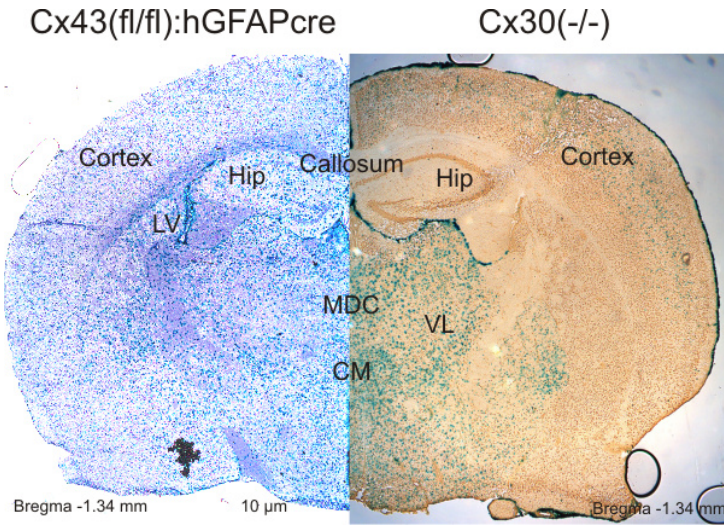

Figure 3.2: Histochemical staining for lacZ-encoded β-galactosidase reporter expression in forebrain of Cx43fl/fl:hGFAPcre and Cx30-deficent mice (the reporter indicates where the ablated connexin would have been expressed). LacZ expression (blue) is strong in cortex and hippocampus of Cx43fl/fl:hGFAP-cre mice. Cx30-deficient mice show high levels of lacZ reporter expression in thalamus, but weak in cortex. Note the typical expression pattern of Cx30 in cells of the leptomeninges. (Abbreviations: CM, central medial thalamic nucleus; Hip, hippocampus; LV, lateral ventricle; MDC, mediodorsal thalamic nucleus, central; VL, ventrolateral thalamic nucleus). Adapted from Söhl, unpublished.

3.6 Oligodendrocyte morphology: measurement of the processes orientation

To quantify the processes orientation of the injected oligodendrocytes, images were acquired as described in paragraph *3.3*. In order to correct for the angular displacement of the fibers, the angle between each single process and an arbitrary axis (x) normal to the fibers direction was tracked manually and measured using the *Measurement* function of the AxioVision 4.7.2 software.

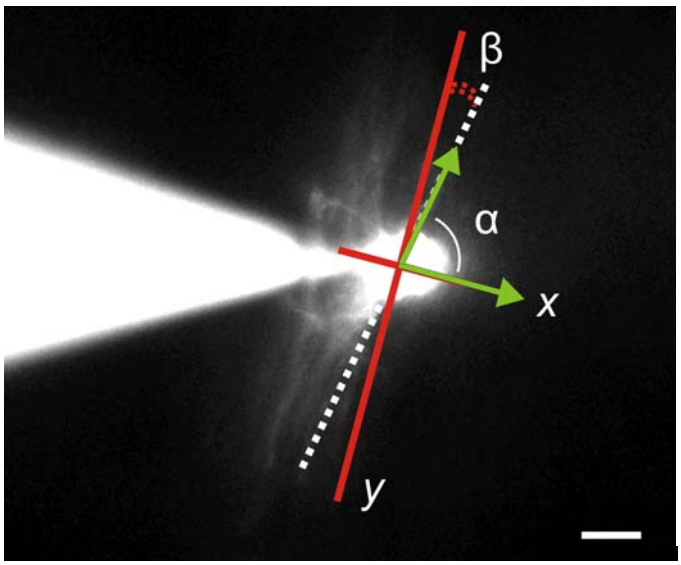

Figure 3.3: Measurement of the orientation of oligodendrocytic processes. Sample image of oligodendrocytic processes visualized by intracellular injection of the dye Alexa 594. The angle (α) between a single process (dotted line) and an arbitrary axis normal to the fibers (x) was tracked manually (green arrows). The absolute value of the angle (β) between the process (dotted line) and the axis parallel to the fibers (y) was calculated as $\beta = |\alpha - 90°|$.

All the measured angles (α) had a value α between 0° and 180°. I then calculated the absolute value of the angles (β) between the process and the axis (y) normal to the arbitrary x axis, thus parallel to the fibers, by subtracting 90° from the measured angle α ($\beta = |\alpha - 90°|$). Figure 3.3 represents an example of measurement.

3.7 Dye coupling quantification

To evaluate dye coupling biocytin filled cells were counted on sequential confocal stacks (0.2-0.8 µm steps) of the 110 µm thick slices with the Image Pro plus and Image Pro 5.1 software. The maximum network diameter, which represents the detectable extent of tracer spread, was measured as distance between the two more

distal somata within the network with the same software used for image acquisition. For CNPase and eGFP colocalization experiments on Cx47-deficient mice cells were counted with the Image Pro 5.0 software on 30 confocal stacks (686 µm x 686 µm x 10 µm), pooling data of 5 slices obtained from 3 animals. Densitometric mean of streptavidin-Cy3 intensity in the coupled cells was assessed and corrected for a reference blank area on single optical slices of sequential confocal stacks with AxioVision 4.7.2 software.

3.8 Statistical analysis

Electrophysiological data were analyzed and plotted using TIDA and Origin software. The frequency distribution of the number of oligodendrocytic processes oriented with an angle β was derived by pooling data from 20 coupled and 5 uncoupled oligodendrocytes of wildtype animals, and plotted by binning angle values into 13 groups ranging from 0 to 48 degrees. For angle measurements data analysis was performed applying the non-parametric Mann-Whitney test with SPSS software. Frequency distribution of the β angle values per oligodendrocytic process was plotted by binning β angle values in 14 groups ranging from 0° to > 48°. For dye coupling experiments differences between groups were evaluated by Student's two-tailed t-Test or one-way ANOVA, as stated in the results chapter (chapter *4*). *Post-hoc* analysis for comparing means was performed using the Bonferroni test. Data regarding the number of oligodendrocytes forming networks (networks %) were analyzed with the Chi-Square Test (SPSS software). Each single group was tested versus the control (wildtype mice). All values are expressed as mean ± standard error of the mean (SEM). P-values of <0.05 were considered statistically significant.

4 Results

4.1 Oligodendrocytic coupling in the young postnatal corpus callosum

In order to determine whether white matter oligodendrocytes are coupled, cells in the corpus callosum of acute coronal slices obtained from brains of wildtype C57BL/6N mice (postnatal day 10-15) were dialysed with the gap junction permeable tracer biocytin (Fig. 4.1A-F). Only one cell per slice was dialysed with biocytin. Oligodendrocytes were recognized in the light microscope by their slightly oval shaped somata often located in a row parallel to the fibers and were approached with glass pipettes with R_p ranging between 3-7 MΩ. This identification was confirmed by recording membrane currents with the patch-clamp technique. Applying a standardized pulse protocol, the membrane was clamped at a holding potential of -70 mV and jumped stepwise to increasingly de- and hyperpolarizing potentials ranging from + 50 mV to - 170 mV (10 mV increment) for 50 ms. These cells were characterized by the presence of voltage independent membrane currents which typically showed some decay during the voltage step and large symmetrical tail currents, i.e. a characteristic feature of mature oligodendrocytes (Fig. 4.1C; Berger et al. 1991). Their identity was further confirmed after dialysis of the cells with the fluorescent dye Alexa Fluor 594 (10 µg/ml) which revealed that these cells characteristically expressed sparsely branched, long processes which were oriented in parallel to the fibers (Fig. 4.1D).

After recording and biocytin dialysis, the slices were fixed. The extent of cell coupling was revealed by either localizing biocytin with the DAB reaction or by fluorochrome-conjugated streptavidin.

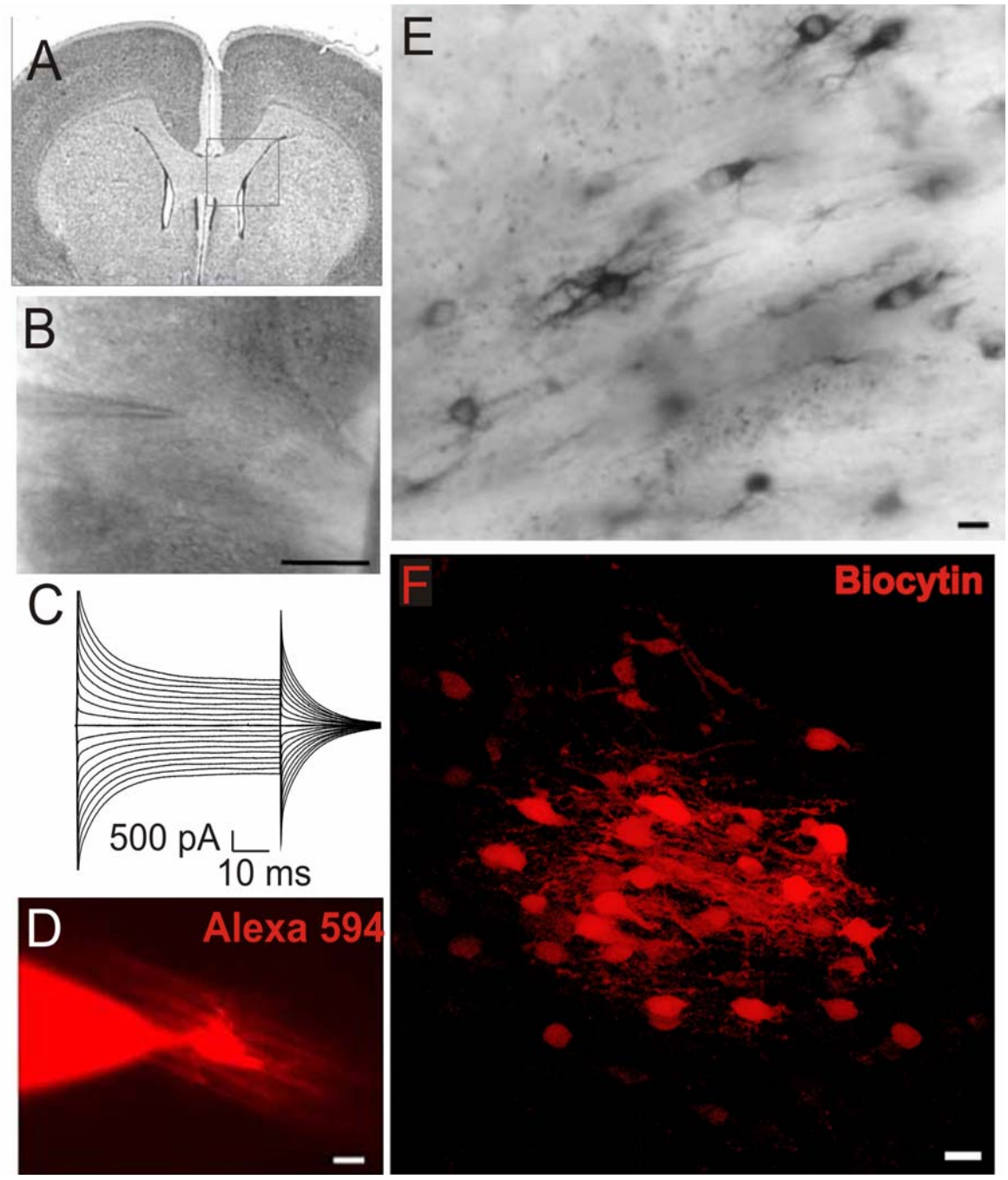

Figure 4.1: Oligodendrocytic coupling in the corpus callosum of postnatal day (p) 10-15 wildtype (WT) mice: (A) Image of a coronal slice from mouse brain with marked corpus callosum and (B) bright field of the area of interest. Bar denotes 100 µm. (C) Membrane currents of an oligodendrocyte were recorded in response to a series of voltage steps ranging from - 170 and + 50 mV (50 ms, 10 mV increments) from a holding potential of - 70 mV (p13 mouse). (D) Typical oligodendrocyte morphology revealed by injection of the fluorescent dye Alexa 594. (E-F) After injection into a single oligodendrocyte, biocytin spread to a network of neighbouring cells as revealed by DAB (E) or streptavidin-Cy3 labeling (F). Bars denote 10 µm.

The latter procedure could be combined with analyses of markers for the identification of oligodendrocytes and astrocytes using immunolabeling with antibodies to CNPase and GFAP, respectively. DAB labeling indicated a network of

coupled cells in 16 out of 17 slices (94% form networks, n=16, 4 mice). In these 16 networks, the tracer could be clearly recognized in 24 ± 4 cells (Fig. 4.1E).

I also measured the distance between somata of the coupled cells in the network that were most distant from each other which represents the detectable spatial extent of the tracer. I shall refer to this value as extent of tracer spread and found an average value of 213 ± 22 µm for the 16 experiments. Similar results were obtained by localizing biocytin with fluorochrome-conjugated streptavidin. The streptavidin/biocytin labeled cells were analyzed with a confocal microscope, which allowed me to recognize more cells as compared to the DAB approach. In 20 out of 24 slices (83% form networks, 16 mice) biocytin spread from the injected cell into 61 ± 10 neighbouring cells (n=20), within an average tracer spread of 203 ± 15 µm (n=20; Fig. 4.1F).

4.1.1 Morphological characterization of coupled and uncoupled oligodendrocytes

Myelinating oligodendrocytes can be distinguished from radial oligodendrocyte precursors by their parallel longitudinal processes, oriented along the fibers (Butt and Ransom 1993). To analyze the morphology of coupled and uncoupled oligodendrocytes, I measured the processes orientation for each injected cell by quantification of the angle β between the processes and an arbitrary axis parallel to the fibers (see paragraph *3.5*). The frequency distribution of the oligodendrocytic processes oriented with a certain angle β was derived to compare the orientation of the processes belonging to coupled and uncoupled cells. Oligodendrocytes were dialyzed with the fluorescent dye Alexa Fluor 594 (10 µg/ml) which clearly revealed from 5 up to 16 processes per cell. In coupled oligodendrocytes, the angle β ranged from 0.01° to 39.59° (average 10.4° ± 0.8°, n=166 processes, 20 cells), indicating a

population of oligodendrocytes extending mainly parallel processes (Fig. 4.2A-C). In uncoupled oligodendrocytes, the angle varied from 0.21° to 71.34° (average 18.5° ± 2.9°, n=44 processes, 5 cells), therefore uncoupled cells more frequently exhibited radial processes (Mann-Whitney U Test, p=0.0153, Fig. 4.2D-H). Figure 4.2 shows an example of the processes orientation in coupled and uncoupled oligodendrocytes in the young postnatal corpus callosum.

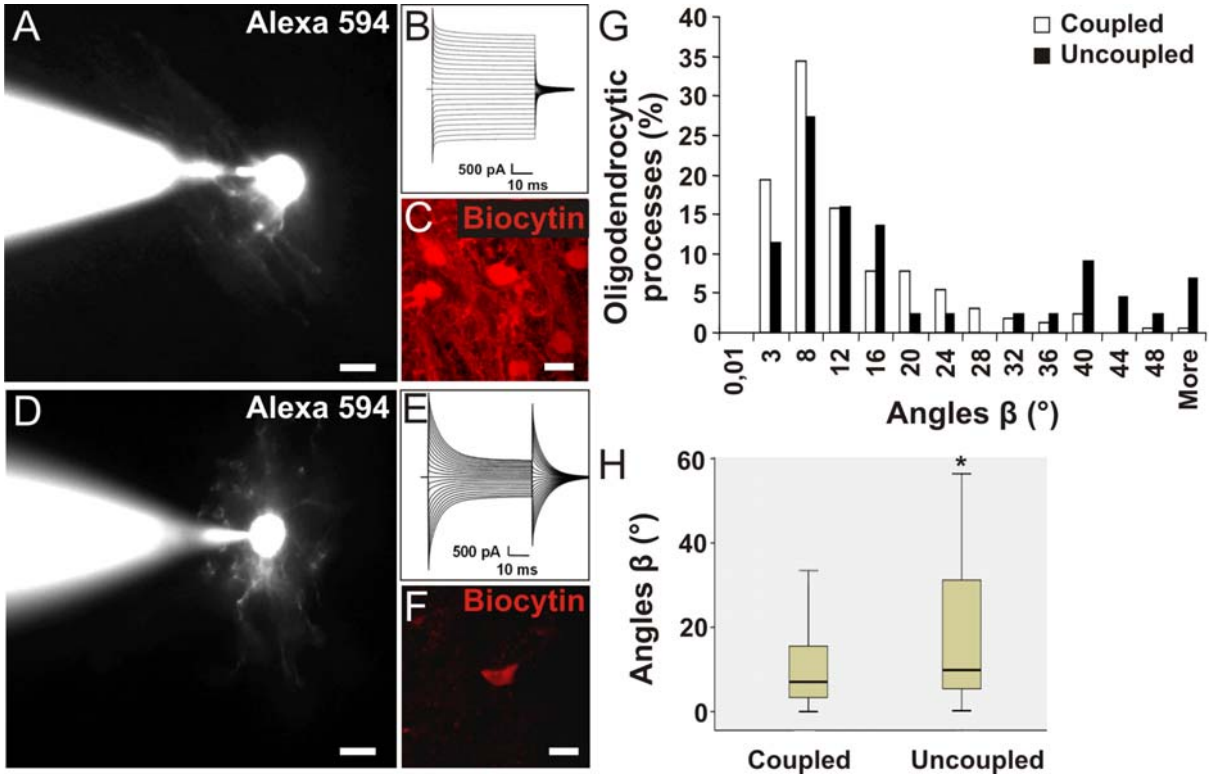

Figure 4.2: Morphological characterization of coupled and uncoupled oligodendrocytes in p10-15 old wildtype mice. (A-C) Images show an example of coupled oligodendrocyte, characterized by parallel processes as revealed by dialysis with the fluophore Alexa Fluor 594 (Alexa 594, A). (B) Morphological identification of the injected cell was confirmed by the current profile recorded from a holding potential of - 70 mV (+ 50 mV to – 170, 50 ms, 10 mV increments). (C) Confocal image of the cells coupled to the injected one, as revealed by biocytin/streptavidin-Cy3 labeling. Bars denote 10µm. (D-F) Images illustrating the typical radial morphology of an uncoupled oligodendrocyte and recorded current profile. (D) Injection of the dye Alexa Fluor 598 revealed an oligodendrocyte characterized by radial processes. (E) Membrane currents of the injected cell, typical of oligodendrocytes. (F) Confocal image show the uncoupled biocytin-positive oligodendrocyte, as visualized by streptavidin-Cy3 reaction. Bars denote 10 µm. (G) Frequency distribution of the percentage of oligodendrocytic processes oriented with a certain β angle in coupled and uncoupled oligodendrocytes. Note that in coupled cells almost 35% of the oligodendrocytic processes were oriented with a β angle of a value within 3° and 8° compared to the fibers direction, while uncoupled oligodendrocytes displayed more often angles between 28° and 44°, or more. (H) Boxplot indicates the median (50%, dark line) of the β angles in coupled (n=166 processes) and uncoupled (n=44 processes) oligodendrocytes (Mann-Whitney U Test, *p=0.0153). Lower and upper hinges represent the 25% and 75% of the angles distribution in each group, while whiskers are the lowest and the highest observed values, not statistically outliers.

4.1.2 Oligodendrocytes are more extensively coupled to each other than to astrocytes

To identify the type of coupled cells within the network, I colocalized biocytin with the oligodendrocyte marker CNPase and the astrocyte marker GFAP by confocal microscopy in coronal sections of the corpus callosum (110 µm thick). When easily recognizable in the network, all the injected cells were identified as CNPase-positive (not shown). 77 ± 2% biocytin-positive coupled cells were CNPase-positive, indicating that the network mainly consisted of oligodendrocytes (20 slices; Fig. 4.3A,B,C,F). Only 9 ± 2% of biocytin-positive cells were GFAP-positive, and thus were concluded to be astrocytes (18 slices; Fig. 4.3A,D,E,F). A considerable population of coupled cells (14 ± 3% of cells in 20 networks) was negative for both CNPase and GFAP (Fig. 4.3A-F).

To compare the level of biocytin in oligodendrocytes versus astrocytes the densitometric mean intensity of the streptavidin-Cy3 fluorescence was determined in the biocytin-positive cells. Streptavidin-Cy3 intensity was measured in single images from confocal stacks of ten networks with a mean astrocyte to oligodendrocyte ratio of 0.3 ± 0.02 (89 cells). The average densitometric mean intensity of the dye in 64 CNPase-positive cells was 84.5 ± 8 and 60 ± 8 in 25 GFAP-positive cells (Student's two-tailed t-Test, $p<0.05$; Fig. 4.3G-L). Moreover the biocytin/streptavidin-Cy3 positive astrocytes were often observed at the periphery of the network rather than between the coupled oligodendrocytes. Taken together, these experiments demonstrate that oligodendrocytes couple more frequently to each other (and to oligodendrocyte precursors, see below) and less efficiently to astrocytes.

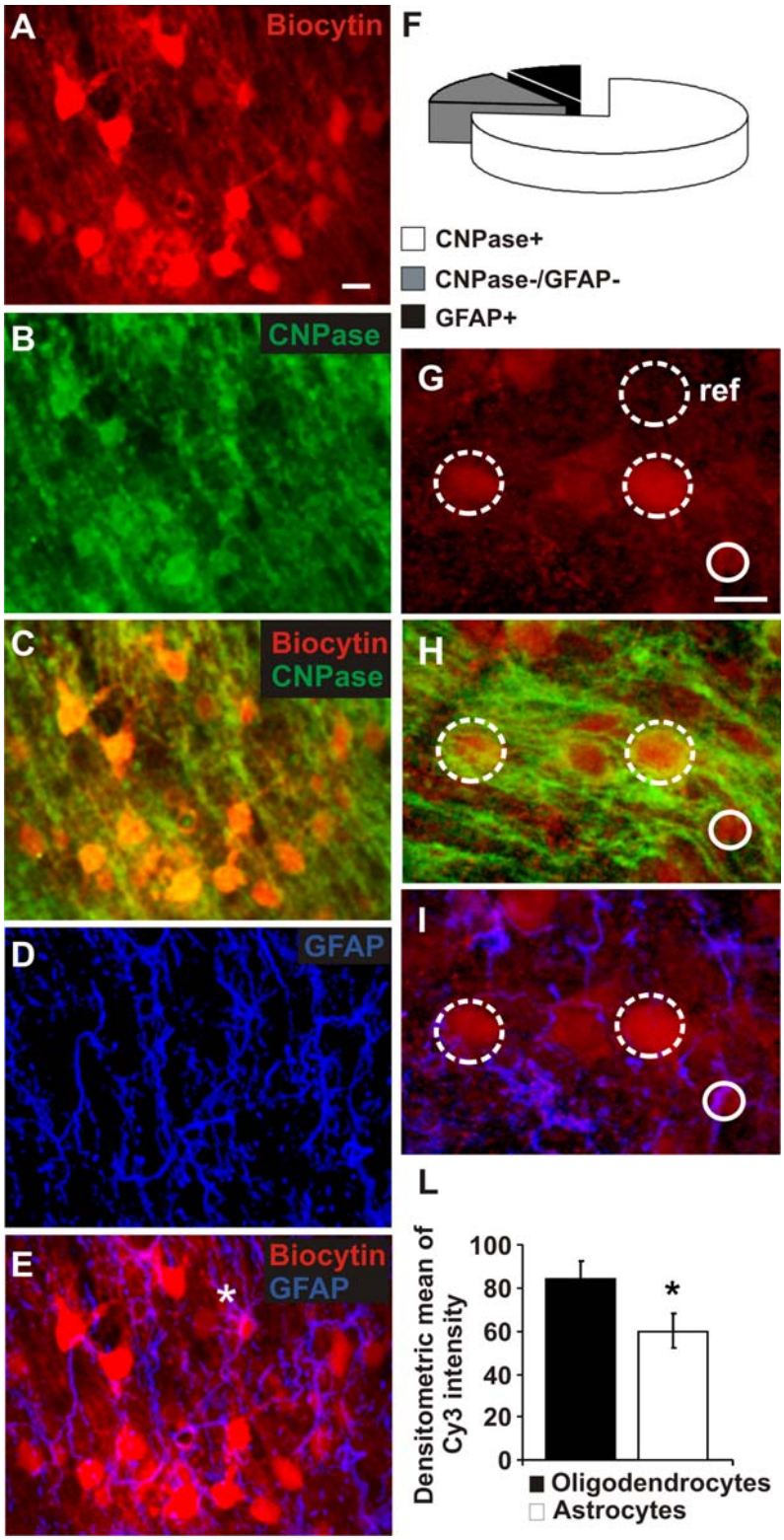

Figure 4.3: Cell type identification of coupled cells in wildtype mice. (A-E) Biocytin injection into an oligodendrocyte of a p13 wildtype mouse. Biocytin was labeled with streptavidin-Cy3 (A) and oligodendrocytes were identified by CNPase immunostaining (B). (C) Overlay of A and B. (D) Immunolabeling of the same section for the astrocytic marker GFAP. (E) Overlay of A and D Note a coupled cell expressing GFAP (white asterisk). (F) Streptavidin-Cy3 intensity measurement in oligodendrocytes and astrocytes. (G-I) Single confocal stack of biocytin-positive cells (G, red) stained for the astrocytic marker GFAP (H, blue) and for the oligodendrocytic marker CNPase (I, green). The circles represent an example of quantification of the streptavidin-Cy3 intensity in astrocytes (full-line) or in oligodendrocytes (dotted-line), with reference background. Note the brighter Cy3-streptavidin labeled oligodendrocytes. (C) Biocytin uptake in oligodendrocytes versus astrocytes was determined by measuring the densitometric mean intensity of the streptavidin-Cy3 fluorescence in CNPase-positive oligodendrocytes and in GFAP-positive astrocytes. Streptavidin-Cy3 intensity was measured in single images from confocal stacks of ten networks with a mean astrocyte to oligodendrocyte ratio of 0.3 ± 0.02 (n=89). The average densitometric mean intensity of the dye in oligodendrocytes was 84.5 ± 8 (n=64) and 60 ± 8 in astrocytes (n=25, Student's two-tailed t-Test, $p<0.05$), indicating that oligodendrocytes contain significantly more biocytin than astrocytes. Bars, 10 µm.

4.1.3 A heterogeneous population of oligodendrocyte precursors is coupled to the oligodendrocyte network

To address the identity of the CNPase- and GFAP-negative cells in the network, I studied the expression of the markers for immature oligodendrocytes NG2 (Karram et al. 2005; Nishiyama et al. 2009), and the bHLH transcription factor Olig2, which is expressed by both precursors and mature oligodendrocytes (Lu et al. 2002). Biocytin was injected into oligodendrocytes of NG2-EYFP heterozygous animals. These heterozygous mutants express the enhanced yellow fluorescent protein (EYFP) under the control of the endogenous NG2 promoter and the NG2 protein, allowing an easy identification of NG2 cells (Karram et al. 2008). Experiments were carried out in the corpus callosum as described above and biocytin/streptavidin-Cy3 labeling was combined with immunostaining for EYFP (to enhance the signal of the NG2-EYFP cells) and CNPase. In these mice the number of oligodendrocytes forming network (12 networks out of 14 injected cells, 86% formed network) and the number of coupled cells within a given network (average 34 ± 6 coupled cells, n=12, 7 mice) did not differ from wildtype. In all the networks 4 ± 2% of biocytin-positive cells were EYFP-positive (Fig. 4.4A,B,D,F) and 81 ± 4% of coupled cells were CNPase-positive (Fig. 4.4.A,C,E,F), while 15 ± 4% cells within the network were negative for both CNPase and EYFP (Fig. 4.4A-F). Similar results were obtained performing the same experiments on wildtype mice and using an NG2 antibody to identify cells. Biocytin/streptavidin-Cy3 was colocalized with CNPase and NG2, markers for mature and immature oligodendrocytes respectively. In 10 networks out of 12 slices (average 53 ± 10 coupled cells; n=10, 5 mice) 6 ± 2% biocytin-positive cells expressed only NG2 (Fig. 4.4G,H,J,L) and 78 ± 5% were CNPase-positive (Fig. 4.4G,I,K,L), while 15 ± 5% coupled cells were negative for both markers (Fig. 4.4G-

L). Further characterization of the CNPase- and GFAP-negative subpopulation of coupled cells was performed combining biocytin/streptavidin-Cy3 labeling with immunostaining for CNPase and Olig2.

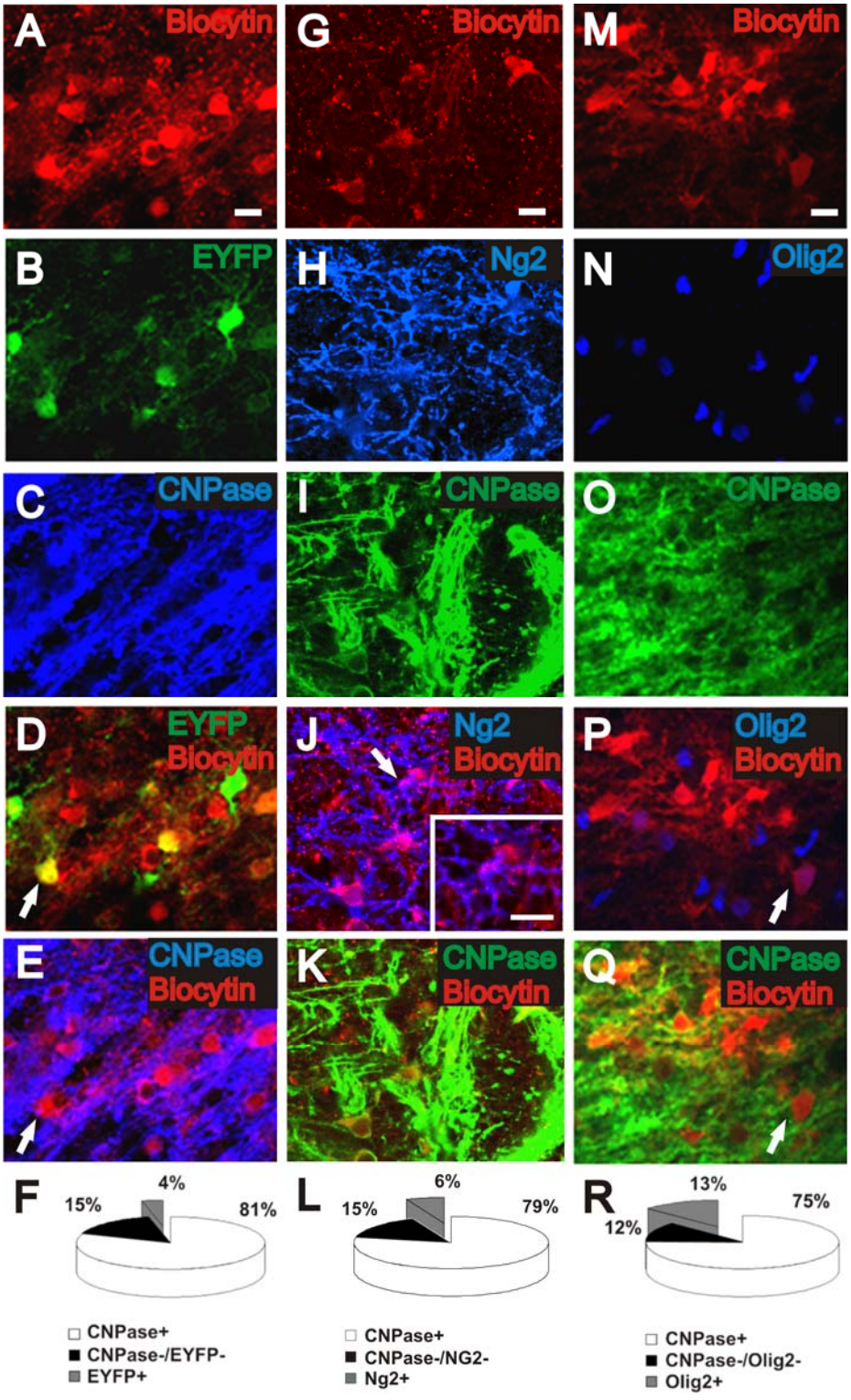

Figure 4.4: Characterization of CNPase- and GFAP-negative coupled cells in heterozygous NG2-EYFP and wildtype mice. For quantification all values are expressed as percentage of the mean of

coupled cells in the network. (A-E) In a p13 NG2-EYFP heterozygous mouse, in which the enhanced yellow fluorescent protein (EYFP) is expressed under the NG2 promoter, biocytin/streptavidin-Cy3 labeling was performed with EYFP and CNPase immunostaining. (A) shows biocytin labeling, (B) the EYFP fluorescence, (C) CNPase staining. (D) is an overlay of A and B. Note a coupled cell in which the NG2 promoter activity is indicated by EYFP expression (white arrow). (E) Overlay of A and C. The same cell as in D was CNPase-negative (white arrow) and is an oligodendrocyte precursor cell.
(F) Quantification of the population of coupled cells positive for CNPase (CNPase+), positive for EYFP (EYFP+), and for none (CNPase-/EYFP-). A subpopulation of CNPase-negative cells coupled within the oligodendrocytic network expressed EYFP under the NG2 promoter (4 ± 2%), thus identified as oligodendrocyte precursors.
(G-M) In a p14 wildtype mouse biocytin/streptavidin-Cy3 labeling was combined with CNPase and NG2 immunostaining. (G) shows the biocytin labeling. (H) is the CNPase and (I) the NG2 staining. (J) is an overlay of biocytin and CNPase, (M) biocytin and NG2 staining. The white arrows in (J) and (M) indicate a NG2-positive, CNPase-negative oligodendrocyte precursor cell coupled to the oligodendrocytic network, displayed at higher magnification in the insert (M).
(N) Quantification of the population of coupled cells positive for CNPase (CNPase+), positive for EYFP (EYFP+), and for none (CNPase-/EYFP-). A subpopulation of CNPase-negative cells coupled within the oligodendrocytic network expressed NG2 (6 ± 2%), marker for oligodendrocyte precursors.
(O-S) In a p15 wildtype mouse biocytin/streptavidin-Cy3 labeling (O) was performed with immunostaining for CNPase (P) and for Olig2 (Q), marker for cells belonging to the oligodendrocytic lineage. (R) Overlay of biocytin and CNPase, (S) biocytin and Olig2 staining. Note a CNPase-negative coupled cell in which the transcription factor Olig2 is expressed (white arrow).
(T) Quantification of the population of coupled cells positive for CNPase (CNPase+), positive for Olig2 only (Olig2+), and for none (CNPase-/Olig2-). A subset of CNPase-negative cells coupled to the oligodendrocytic network expressed Olig2 (13 ± 4%), thus identified as oligodendrocyte precursors. All together these data indicate that a subpopulation of CNPase-negative, coupled cells expressed NG2 (4 ± 2% and 6 ± 2%) or Olig2 (13 ± 4%), thus belonging to the oligodendrocytic lineage.

In 10 networks out of 13 slices (average 44 ± 9 coupled cells; n=10, 5 mice) 13 ± 4% of the coupled cells expressed only Olig2 and not CNPase (Fig. 4.4M,N,P,R), 75 ± 5% of biocytin-positive cells were CNPase-positive (Fig 4.4M,O,Q,R), while a population of coupled cells was negative for both markers (12 ± 3%; Fig. 4.4M-R). These findings indicate that the majority (around 88%) of the coupled cells belong to the oligodendrocytic lineage, being CNPase-positive oligodendrocytes, NG2- or Olig2-positive precursor cells.

4.1.4 Oligodendrocytic coupling during development from p10 to p25 tends to decrease

Coupling in p20-25 old wildtype mice was also studied with the same approach described above (Fig. 4.5A-K). In 4 out of 6 experiments, biocytin spread to a mean of 32 ± 2 coupled cells (67% form networks, n=4, 3 mice) with a tracer extent up to

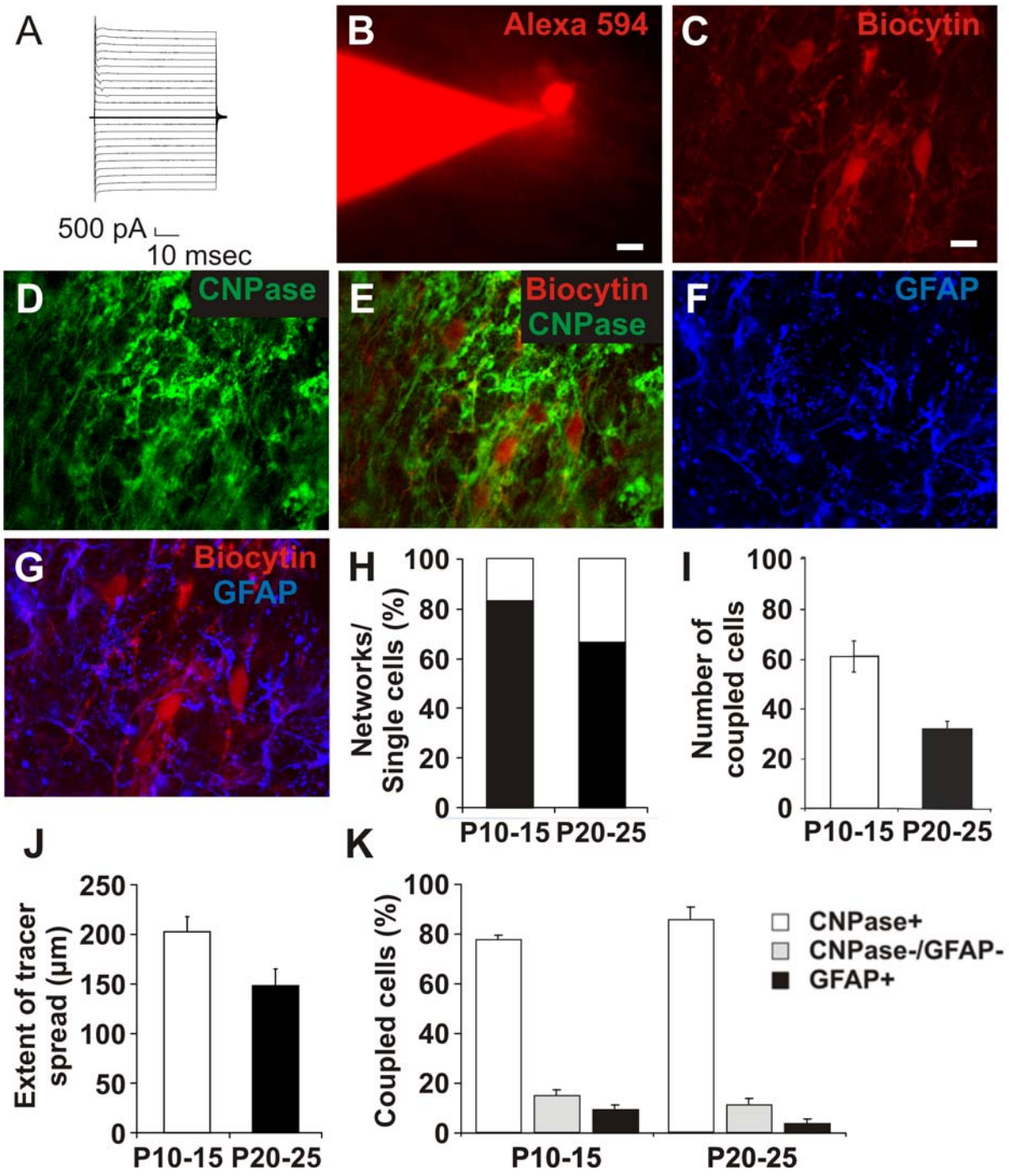

Figure 4.5: Oligodendrocytic coupling in the corpus callosum of wildtype mice at postnatal day 20-25. (A) Membrane currents of a single oligodendrocyte injected with the gap junction permeable tracer biocytin in response to depolarizing and hyperpolarizing voltage steps from a holding potential of -70 mV (50 ms, 10 mV increment). (B) Oligodendrocyte morphology revealed by dialysis with the fluophore Alexa 594. (C) In a p25 old mouse biocytin, as revealed by strepdavidin-Cy3 reaction, spread to an average of 32 ± 2 neighboring cells. (D-G) Characterization of the population of biocytin-positive cells (C) by immunostaining for the oligodendrocytic marker CNPase (D) and for the astrocytic marker GFAP (F). (E) indicates the merge of biocytin and CNPase while (G) depicts the merge of biocytin and GFAP. (H-J) Quantification of networks of p20-25 old wildtype mice. (H) Percentage of injected cells which were coupled to at least one other cell and thereby formed a network. (I) Average number of coupled cells in a network. (J) Extent of tracer spread as defined by the largest distance between two somata of within the network. (K) Quantification of the identified cells coupled within the network. As observed in p10-15 old wildtype mice, the majority of coupled

cells expressed the oligodendrocyte marker CNPase and only 3% percent were GFAP-positive astrocytes. However the remaining 11% of the biocytin labeled cells did not express CNPase or GFAP, most likely being oligodendrocyte precursors. Although the population of coupled cells expressing CNPase increased while the CNPase- and GFAP-negative coupled cells decreased, in line with a more advanced developmental stage of white matter oligodendrocytes, no significant difference was observed compared to p10-15 old wildtype mice

184 µm (average 148 ± 17 µm). Althought the number of coupled cells and the extent of biocytin spread were decreased compared to p10-15 old wildtype mice, this reduction was not significant. Immunohistochemical analysis of CNPase and GFAP expression revealed an increase in the biocytin labeled cells expressing CNPase (average 86 ± 6%, n=4 networks, 3 mice; Fig 4.5C,D,E,K), while the GFAP-positive coupled cells were diminished (average 3 ± 2% n=4; Fig.4.5C,F,G,K). The minor increase in CNPase-positive cells within the network together with the decreased number of coupled cells expressing GFAP did not significantly differ form p10-15 old wildtype mice. The remaining 11 ± 3% was negative for both CNPase and GFAP (Fig. 4.5C-E,K), most likely belonging to the oligodendrocytic lineage (see paragraph *4.1.4*).

Despite the decreased number of coupled cells and extent of tracer spread in the network of p20-25 old mice compared to p10-15 old animals (Fig. 4.5I,J), oligodendrocytic coupling does not significantly change during development from p10 to p25. Additionally, at p20-25 the population of coupled oligodendrocytes slightly increases along with the reduction in the number of coupled oligodendrocyte precursors and astrocytes. Although not significant, the observed changes are consistent with an advanced developmental stage.

4.2 In Cx47-deficient mice oligodendrocytic coupling is reduced

Cx47 is the major connexin expressed by oligodendrocytes (Menichella et al. 2003; Odermatt et al. 2003). To determine the importance of Cx47 for oligodendrocytic coupling I used a Cx47-deficient mouse line, in which the Cx47 coding region was

replaced by the cDNA encoding for the reporter protein eGFP (Odermatt et al. 2003). Oligodendrocytes could easily be identified by eGFP fluorescence. Similar to wildtype slices, oligodendrocytes were further characterized by processes parallel to the fiber orientation which were well visible after dialysis with Alexa Fluor 594 and by passive, often decaying membrane currents (Fig. 4.6A,B).

In Cx47-deficient mice, I found coupling of oligodendrocytes identified with the DAB reaction in 11 out of 15 slices (78% form networks, 7 mice; Fig. 4.6C,D).

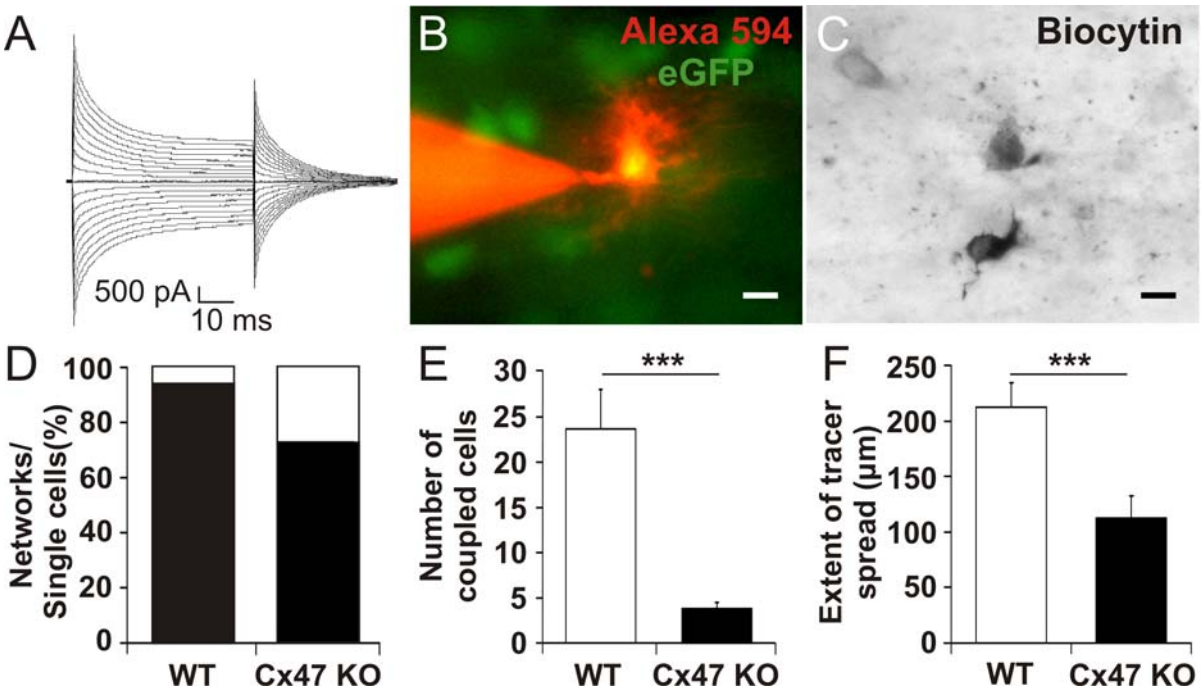

Figure 4.6: Oligodendrocytic coupling in p10-15 old Cx47-deficient mice revealed by DAB labeling. (A) Oligodendrocytes were identified by their typical membrane currents, often decaying, during depolarizing and hyperpolarizing voltage steps, from a holding potential of -70 mV (50 ms, 10 mV increment) and by their eGFP fluorescence (B). In this mouse strain the reporter gene eGFP replaced the Cx47 coding region and was thus expressed under control of the Cx47 promoter. (C) Biocytin injected into a single oligodendrocyte of a p 13 mouse spread to 3 neighboring cells, as revealed by DAB reaction. (D-F) Quantification of networks revealed by DAB reaction in p10-15 old wildtype and Cx47-deficient mice. (D) Percentage of injected cells which were coupled to at least one other cell and thereby formed a network. (E) Average number of coupled cells in a network. (J) Extent of tracer spread as defined by the largest distance between two somata within the network. Note the significant reduction in the number of coupled and extent of tracer spread in Cx47-deficient mice (Student's two-tailed t-Test, *** $p<0.001$, n=11).

However, relative to wildtype slices, these networks consisted of significantly fewer cells (4 ± 1, n= 11; Student's two-tailed t-Test, $p<0.001$; Fig. 4.6E) and,

consequently, the spatial extent of biocytin diffusion was significantly reduced, on average 112 ± 20 µm (Student's two-tailed t-Test, $p<0.001$, n=11; Fig. 4.6F).

Similar results were obtained by biocytin labeling with streptavidin conjugated to the fluorochrome Cy3 (Fig 4.7A-E). In 13 out of 20 slices (65% form networks; 9 mice), the networks consisted of 13 ± 3 cells (one-way ANOVA, $p<0.001$; Bonferroni *post-hoc* analysis for comparison of means, $p<0.001$, n=13), with an extent of tracer spread of 132 µm (± 11 µm; one-way ANOVA, Tukey *post-hoc* analysis for comparison of means, $p<0.05$, n=13), which is significantly smaller as compared to wildtype (Fig. 4.8F-H).

As in wildtype mice the population of coupled cells was identified by combining biocytin-streptavidin/Cy3 labeling with immunostaining for eGFP, expressed under the Cx47 promoter, and for the astrocytic marker GFAP. All biocytin-positive cells were eGFP-positive (average 13 ± 3, n= 13, Fig. 4.7C). No cells colabeled with GFAP antibodies (Fig 4.7C). The pronounced reduction in the number of coupled cells in Cx47 KO mice indicates that oligodendrocytic coupling among each other and to other cell types is mainly due to expression of Cx47. To further characterize the population of eGFP-positive cells, slices obtained from the same animals used for dye coupling experiments were stained with antibodies to eGFP and the oligodendrocytic marker CNPase. 77 ± 2.6% of the eGFP-positive cells were identified as CNPase-positive, while 23 ± 2% were CNPase-negative and therefore immature oligodendrocytes (Fig. 4.7D-E).

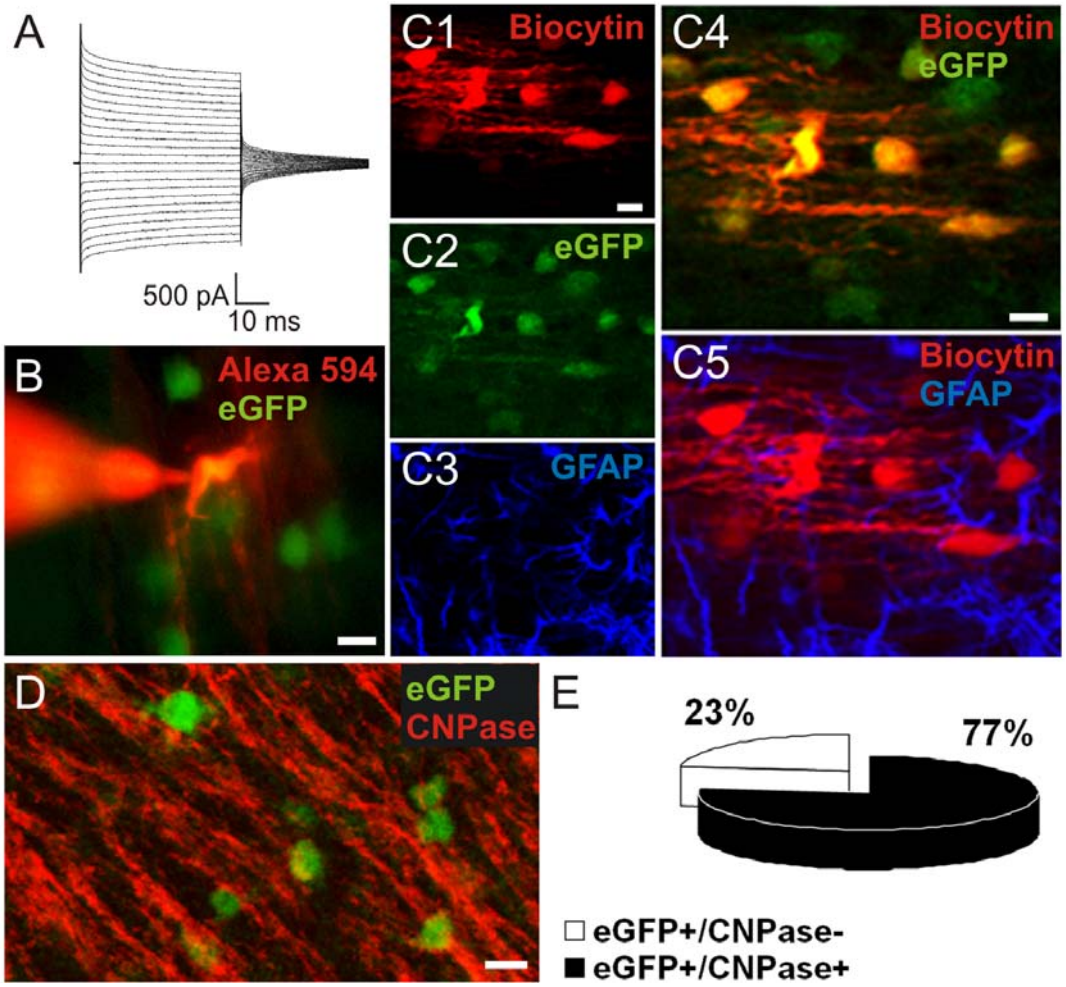

Figure 4.7: Glial cell-type identification of coupled cells in the corpus callosum of p10-p15 Cx47-deficient mice. In this mouse line, the Cx47 coding region was replaced by cDNA encoding for the reporter protein eGFP. (A) Membrane currents of an oligodendrocyte were recorded in response to a series of voltage steps ranging from - 170 and + 50 mV (50 ms, 10 mV increments) from a holding potential of - 70 mV (p15 mouse). (B) Oligodendrocytes were identified by their eGFP fluorescence and by their typical morphology as revealed by dialysis with the fluorescent dye Alexa 594. (C) Identification of the biocytin-positive cells by immunostaining for the reporter protein eGFP, expressed by oligodendrocytes under control of the Cx47 promoter, and for the astrocytic marker GFAP. Biocytin injection into a single eGFP-positive oligodendrocyte of a p15 Cx47-deficient mouse revealed 11 coupled cells. All the coupled cells were eGFP-positive, therefore oligodendrocytes. No GFAP-positive astrocyte was ever observed within the network of biocytin labeled cells. (D-E) Quantification of Cx47-eGFP and CNPase expression in Cx47-deficient mice in which the Cx47 coding region was replaced by eGFP. (D) Confocal image of eGFP positive cells stained for the oligodendrocytic marker CNPase. Thirty confocal stacks (686 µm x 686 µm x 10 µm) of slices with eGFP/CNPase labeling were analyzed. CNPase immunostaining revealed that 77 ± 3% of the cells were positive for eGFP, the reporter for Cx47 expression (E). Bar denotes 10 µm.

4.3 Cx32- and Cx29- deficiency does not affect oligodendrocytic coupling

To determine the role of Cx32 and Cx29 for oligodendrocytic coupling, I injected biocytin into oligodendrocytes of Cx32- (Nelles et al. 1996) and Cx29-deficient

(Eiberger et al.. 2006) animals. Experiments were performed in the corpus callosum as described in paragraph *4.1*. In Cx32-deficient mice, biocytin as revealed by streptavidin conjugated to Cy3 spread up to a mean of 72 ± 12 cells in 14 out of 20 slices (70% form networks, n=14, 13 mice, Fig. 4.8A, F-H). The number of coupled cells was not significantly different as compared to the wildtype. In 6 slices, only the injected, uncoupled cell was found. The extent of the tracer spread was on average 240 ± 25 µm. Immunofluorescence analysis showed that 83 ± 5% of the coupled cells in 14 networks were CNPase-positive and only 9 ± 3% were GFAP-positive. Eight ± 3% of the biocytin-positive cells lacked CNPase or GFAP expression (n=14, Fig. 4.10C).

In Cx29-deficient mice, I found oligodendrocyte networks consisting on average of 37 ± 8 coupled cells in 9 out of 13 slices (69% form networks, n=9, 3 mice, Fig. 4.8B, F-H). The observed reduced number in comparison to wildtype was not significantly different. Biocytin intercellularly spread up to a diameter of 316 µm (average 218 ± 17 µm, n=9). Similar to the observations in wildtype mice, 85 ± 4% of the coupled cells were CNPase-positive and 5 ± 2% GFAP-positive. 10 ± 4% of cells in the network did not express CNPase or GFAP (n=9, Fig. 4.10C). These findings indicate that loss of Cx32 or Cx29 does not significantly affect the inter-oligodendrocytic coupling or the heterotypic oligodendrocyte-to-astrocyte coupling.

4.4 Oligodendrocytes are not coupled in mice deficient for both Cx47 and Cx32

As previously described (Menichella et al. 2003; Odermatt et al. 2003), Cx47/Cx32-double-deficient mice display strong vacuolization in nerve fibers in all regions of the central nervous system, develop an action tremor and die on average after postnatal day 51. As in Cx47-deficient mice, the Cx47 coding region was replaced by the

cDNA encoding for the reporter protein eGFP. Oligodendrocytes were identified by eGFP fluorescence and further characterized by morphology and by passive, decaying membrane currents. In the corpus callosum, when biocytin was injected into a single oligodendrocyte, it failed to spread to any neighboring cell (Chi-Square Test, Chi Square= 29.601, $p<0.001$, n=19, 5 mice; Fig. 4.8C, F-H). This result indicates that the lack of both Cx47 and Cx32 totally abolishes oligodendrocytic coupling to other oligodendrocytes as well as to astrocytes.

4.4.1 Increased oligodendrocytic coupling correlates with low input resistance

According to several *in vitro* and *in situ* studies, cells displaying electrical or dye-coupling are characterized by lower input resistance (R_{in}) compared to uncoupled ones (Blomstrand et al. 2004; Meme et al. 2009; Postma et al. 1998). An increased input resistance would therefore be expected when oligodendrocytic coupling is completely abolished by lack of Cx47 and Cx32.

Therefore I analysed the input resistance for coupled and uncoupled oligodendrocytes of acutely isolated corpus callosum slices from wildtype and Cx47- and Cx32-double-deficient mice, respectively. The input resistance was determined from the steady state current response to a depolarizing voltage step of 10 mV from a holding potential of - 70 mV (50 ms; Fig. 4.9A,B). Coupled oligodendrocytes from wildtype mice showed an input resistance ranging from 13 MΩ to 56 MΩ (average 33 ± 4 MΩ, n=16), linearly decreasing with the increased number of coupled cells (Fig. 4.9C). Accordingly, in uncoupled oligodendrocytes from Cx47- and Cx32-double-deficient mice an approximately 10 fold increase in input resistance was observed (average 369 ± 83 MΩ; Student's two-tailed t-Test, $p<0.001$, n=19; Fig. 4.9D).

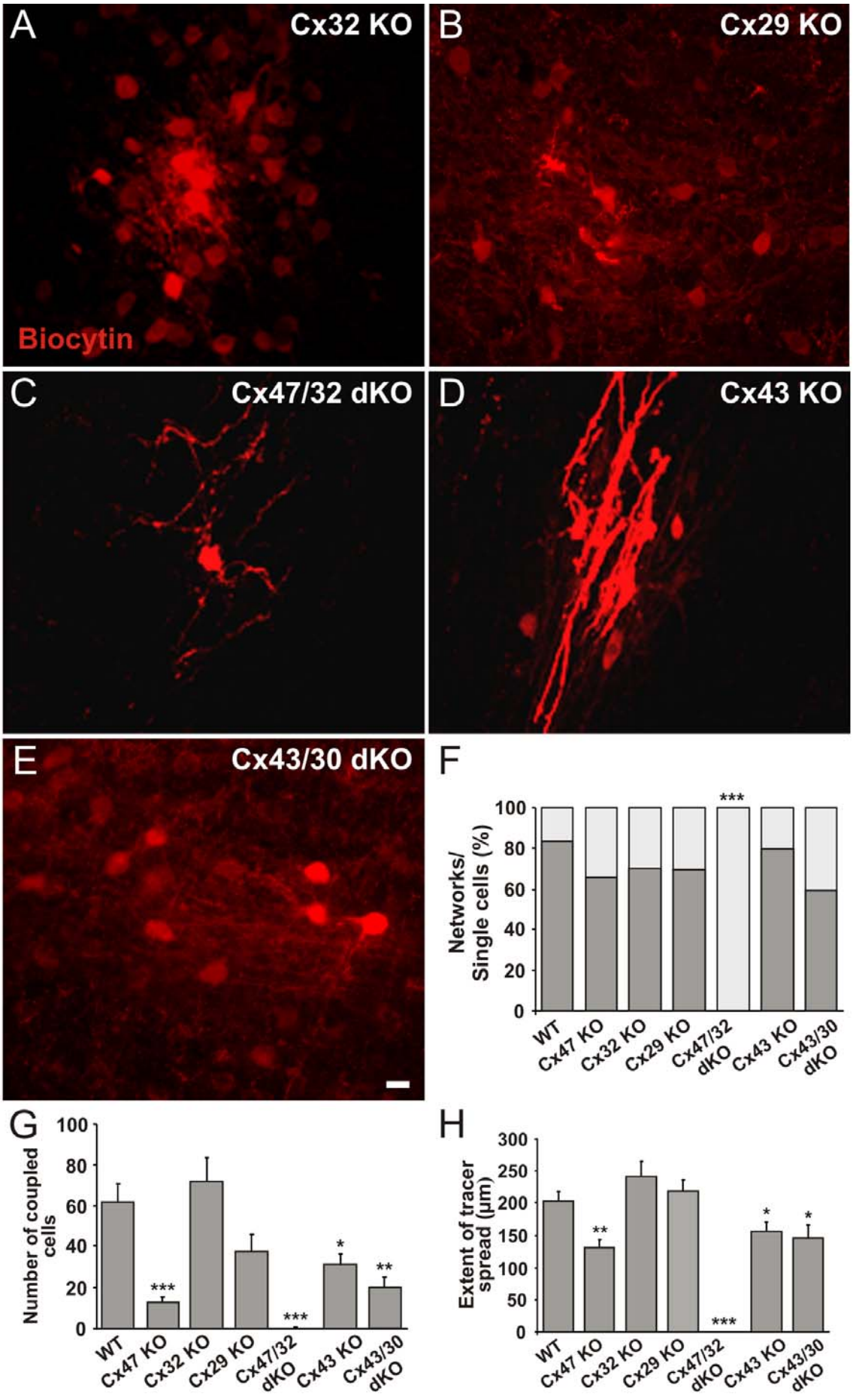
A
Cx32 KO
Biocytin
B
Cx29 KO
C
Cx47/32 dKO
D
Cx43 KO
E
Cx43/30 dKO
F
Networks/ Single cells (%)
100
80
60
40
20
0
***
WT
Cx47 KO
Cx32 KO
Cx29 KO
Cx47/32 dKO
Cx43 KO
Cx43/30 dKO
G
Number of coupled cells
100
80
60
40
20
0
***
***
*
**
WT
Cx47 KO
Cx32 KO
Cx29 KO
Cx47/32 dKO
Cx43 KO
Cx43/30 dKO
H
Extent of tracer spread (µm)
300
250
200
150
100
50
0
**
***
*
*
WT
Cx47 KO
Cx32 KO
Cx29 KO
Cx47/32 dKO
Cx43 KO
Cx43/30 dKO

Figure 4.8: Networks of coupled cells in mice single- and double-deficient for specific oligodendrocytic or astrocytic connexins. (A-E) Confocal images showing biocytin/streptavidin-Cy3 labeling of coupled cells in slices from a p13 Cx32 KO (A), p15 Cx29 KO (B), p15 Cx47/32 double (d) KO (C), p15 Cx43 KO (D) and p15 Cx43/30 dKO (E) mouse. While in Cx32- and Cx29-deficient mice the networks are in size and number of cells similar to wildtype mice, in Cx43-deficient and in Cx43/30-double-deficient mice the networks are generally smaller. Note that in Cx47/Cx32-double-deficient animals biocytin labeling is restricted to a single cell (C). Bars denote 10 µm. (F-H) Quantification of networks in connexin-deficient and wildtype mice. (F) Percentage of injected cells which were coupled to at least one other cell and thereby formed a network (gray) versus injected uncoupled cells (light gray). Note that in Cx47/Cx30 dKO only the single injected cells were detected (Chi-Square Test, Chi Square= 29.601, ***p<0.001). (G) Average number of coupled cells in a network. Asterisks indicate statistical significance (one-way ANOVA, p<0.001; Bonferroni *post-hoc* analysis for comparison of means, *p<0.05, **p<0.01, ***p<0.001). (H) Extent of tracer spread as defined by the largest distance between two somata of the network. Asterisks indicate statistical significance (Student's two-tailed t-Test, *p<0.05, **p<0.01, ***p<0.001).

Electrical coupling between cells can be detected measuring membrane capacitance (C_m) by single whole-cell configuration recordings (de Roos et al. 1996). Therefore the total C_m of coupled and uncoupled oligodendrocytes was calculated integrating the capacitative current and applying the formula $C_m = \int I*dt / \Delta U$ (see paragraph *3.4.3*). Uncoupled cells displayed a C_m consisting in average of 150 ± 15 pF (n=19), significantly higher than in the coupled ones, in which the average C_m was 32 ± 4 pF (Student's two-tailed t-Test, p<0.001, n=16; Fig. 4.9E). This result is in contrast to what reported in *in vitro* experiments, where C_m linearly increased with coupled cell number (de Roos et al. 1996, Postma et al. 1998).

To determine a possible morphological difference that could affect the membrane capacitance of uncoupled oligodendrocytes in the Cx47- and Cx32-double-deficient mice, I calculated the volume of the recorded cells from the measured perimeter (see paragraph *3.4.3*). Although uncoupled cells from Cx47- and Cx32-double-deficient mice showed an increased volume (average 812 ± 101 µm^3, n=19 cells) compared to wildtype coupled cells (average 685 ± 77 µm^3, n=16 cells), this difference was not significant. However, C_m significantly correlated with the calculated volume in both coupled (R=0.57, n=16, p<0.05) and uncoupled oligodendrocytes (R=0.58, n=17, p<0.05). Figure 4.9E shows a diagram in which membrane capacitance of coupled and uncoupled cells was plotted versus the calculated cell volume.

I also determined the slow and fast capacitative transients of the evoked current to compare decay time constants (τ) and capacitance between coupled and uncoupled cells. In electrically coupled cells the slow capacitative transients (C_s) represent the capacitative current response of the neighboring cells, while the fast capacitative transients (C_f) represent the response of the recorded cell. In coupled oligodendrocytes the evoked current could be fit by a biexponential. These cells exhibited a C_s of 26.9 ± 5.6 pF average (n= 16 cells), while C_f was 9.9 ± 2.1 pF (n=16 cells). Uncoupled cells showed a significantly higher C_s in comparison to coupled oligodendrocytes (average 124.6 ± 17.5 pF, Student's two-tailed t-Test, $p<0.001$, n=19 cells), while no difference was observed in C_f (average 22.9 ± 6.7 pF, n=19 cells). The observed significant increase in C_s of uncoupled cells is in contrast with several *in vitro* studies demonstrating that C_s increases linearly with increased gap junctional coupling (de Roos et al. 1996; Harks et al. 2001; Postma et al. 1998). However, no significant difference between the decaying time constants of coupled and uncoupled cells was found. Coupled oligodendrocytes showed a fast time constant (τ_{fast}) ranging from 1.4 to 12.8 ms (average 3.9 ± 0.8, n= 16 cells), while the slow time constant (τ_{slow}) varied from 6.5 to 47.9 ms (average 18.4 ± 2.5 ms, n= 16 cells; Fig. 4.9F). In uncoupled oligodendrocytes the evoked currents could also be fit by a biexponential and were characterized by a τ_{fast} of 2.9 ± 0.3 ms average (n=19 cells), while τ_{slow} ranged from 5.3 to 21.0 ms (average 12.8 ± 0.9 ms, n= 19 cells; Fig. 4.9F).

In addition I quantify the contribution of C_s and C_f to the total capacitative current amplitude that was 448 ± 79 pA average (n= 16 cells) in coupled oligodendrocytes and 1696 ± 238 pA average (n=19 cells) in uncoupled oligodendrocytes. The amplitude of slow and fast current transients accounted for 45 ± 5 % (197 ± 51 pA

average, n=16) and 55 ± 5 % (average 251 ± 50 pA, n=16 cells) of the total current in coupled and for 66 ± 5% (average 1028 ± 141 pA, n=19 cells) and 34 ± 5% (668 ± 170 pA, n=19 cells) in uncoupled cells. Therefore uncoupled cells showed a significant increase in the slow component over the fast component of the transient currents (Student's two-tailed t-Test, p<0.01, n=19 cells). This is in contrast to the

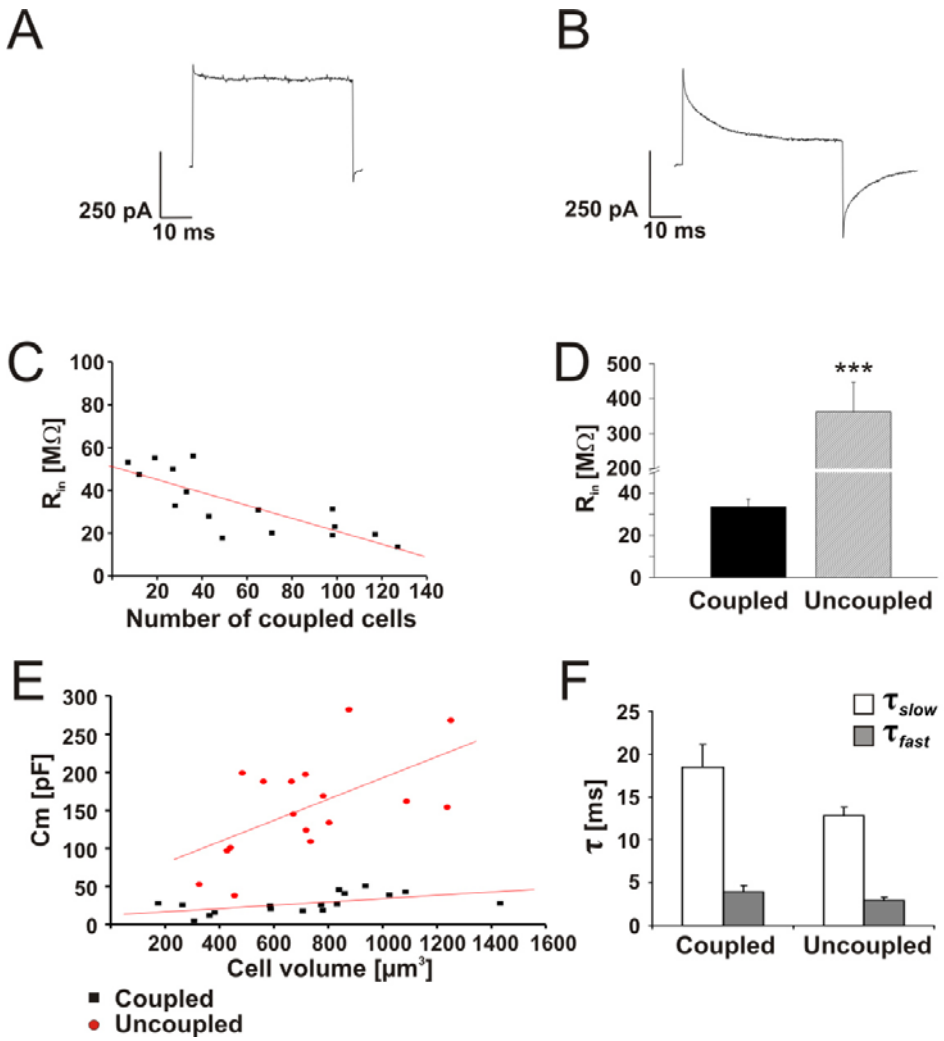

Figure 4.9: Currents, membrane capacitance and input resistance in coupled versus uncoupled oligodendrocytes. (A, B) Membrane currents in response to a 10 mV voltage step from the holding membrane potential of -70 mV from a coupled oligodendrocyte of a wildtype mouse (A; p13 mouse) and in an uncoupled cell of a Cx47/Cx32 double deficient mouse (B; p15 mouse). (C) Plot of the input resistance (R_{in}) versus the number of cells coupled to the injected oligodendrocytes, in wildtype mice. Note the decrease in input resistance correlated with increased number of coupled cells (interpolating line: y=a+b*x, a=51.09 ± 4.21, b= -0.30 ± 0.06; R= -0.79, n=16, p<0.001). (D) Plot of the input resistance in coupled (wildtype) and uncoupled oligodendrocytes obtained from Cx47/32 double deficient mice. Note the approximately 10 fold higher R_{in} value in uncoupled oligodendrocytes. (E) Diagram correlating membrane capacitance (Cm) to cell volume of coupled (wildtype; interpolating line: y=a+b*x, a=12.51 ± 6.18, b=0.02 ± 0.01, R=0.57, n=16, p<0.05) and uncoupled oligodendrocytes of p10-15 old mice (interpolating line: y=a+b*x, a=53.12 ± 38.73, b= 0.1 ± 0.05, R=0.58, n=17, p<0.05). Asterisks indicate statistical significance (Student's two-tailed t-Test, ***p<0.001).
(F) Graph indicates the decay time constants of slow (τ_{slow}) and fast (τ_{fast}) current transient in coupled and uncoupled oligodendrocytes. No significant difference was observed in τ_{slow} or τ_{fast} between the two groups.

reduced C_s contribution described in uncoupled cells *in vitro* (de Roos et al. 1996; Harks et al. 2001; Postma et al. 1998).

All together these data indicate that low input resistance correlates with increased gap junctional coupling. However, uncoupled cells displayed decaying time constants, capacitance and current amplitude of the slow current transients in compared to what reported by others a significant discrepancy. One can assume that uncoupled oligodendrocytes obtained from Cx47- and Cx32-double-deficient mice display physiological and morphological differences compared to wildtype oligodendrocytes, yet to be investigated.

4.5 Cx43-deficiency restricts the network to oligodendrocytes and astrocytes

Cx43 is the major astrocytic connexin colocalized with Cx47 at oligodendrocyte-to-astrocyte heterologous gap junctions (Kamasawa et al. 2005) and forming functional heterotypic channels with Cx47 in transfected mammalian cells (Orthmann-Murphy et al. 2007b). To test the possible contribution of the astrocytic Cx43 to oligodendrocytic coupling biocytin was injected in slices obtained from mice lacking Cx43. Since Cx43-deficient mice were described to be embryonically lethal, I used Cx43fl/fl:hGFAP-Cre mice, which allowed us to selectively ablate Cx43 in GFAP expressing astrocytes (Theis et al. 2003; Wallraff et al. 2006). To detect spontaneous loss of hGFAP-Cre activity (Requardt et al. 2009), all mice used in experiments were tested for expression of the LacZ reporter gene by X-Gal staining. Only slices of brains positively tested for β-galactosidase expression were analyzed. Oligodendrocytes were identified by their typical morphology in bright phase microscopy as described above. In 23 out of 29 (79% form networks, 12 mice) biocytin injected slices we detected networks consisting on average of 31 ± 5 cells

(one-way ANOVA, $p<0.001$; Bonferroni *post-hoc* analysis for comparison of means, $p<0.05$, n=23) with a mean extent of tracer spread of 156 ± 15 µm (n=23; Fig. 4.8D, F-H). The number of coupled cells was lower as compared to wildtype yet with a low significance, while the extent of tracer spread was not significantly different. Immunofluorescence analysis showed a significant increase in the number of CNPase-positive cells coupled within the network (92 ± 2%, one-way ANOVA, $p<0.001$; Bonferroni *post-hoc* analysis for comparison of means, $p<0.001$, n=23; Fig. 4.10A1,A2,A4,C). The remaining 8 ± 2% of coupled cells were GFAP-positive (Fig. 4.10A1,A3,A5,C). In contrast to wildtype, all biocytin-positive cells expressed either CNPase or GFAP (one-way ANOVA, $p<0.001$; Bonferroni *post-hoc* analysis for comparison of means, $p<0.001$, n=23; Fig. 4.10A1-A5, C). These findings indicate that deletion of the Cx43 gene impairs the coupling of oligodendrocytes to the subpopulation of immature oligodendrocytes and also to the still unidentified population negative for all markers. However, Cx43-deficiency did not compromise the spread of biocytin from oligodendrocytes to astrocytes.

4.6 Cx43- and Cx30-double-ablation reduces the number of cells coupled within the oligodendrocyte syncytium

To assess whether oligodendrocytic coupling was mediated by heterotypic gap junctions to astrocytes, biocytin was injected into oligodendrocytes of mice lacking the astrocytic connexins Cx43 and Cx30 (Wallraff et al. 2006). Cx43- and Cx30-double-deficient mice were obtained by interbreeding Cx43fl/fl:hGFAP-Cre mice and Cx30-deficient mice. I monitored hGFAP-Cre activity in all mice used for experiments by X-Gal staining for expression of the LacZ reporter gene.

In double-deficient mouse line both Cx43fl/fl and Cx30 coding regions were replaced by the reporter gene LacZ; efficient Cre-mediated deletion of Cx43 was therefore

confirmed by the specific LacZ expression pattern in cortex and hippocampus where Cx30 expression is weak (Requardt et al. 2009). Only slices with appropriate localization of the LacZ signals were considered for statistics. Experiments were performed as previously described. In 10 out of 17 slices (i. e. 64 % form network, 3 mice) biocytin injected into a single oligodendrocyte spread up to 44 neighboring cells (average 20 ± 5, n=10) with a mean extent of 145 ± 21 µm (Fig. 4.8E, F-H). Both number of coupled cells and extent of tracer spread were significantly reduced in comparison to wildtype mice (one-way ANOVA, p<0.001, Bonferroni post-hoc

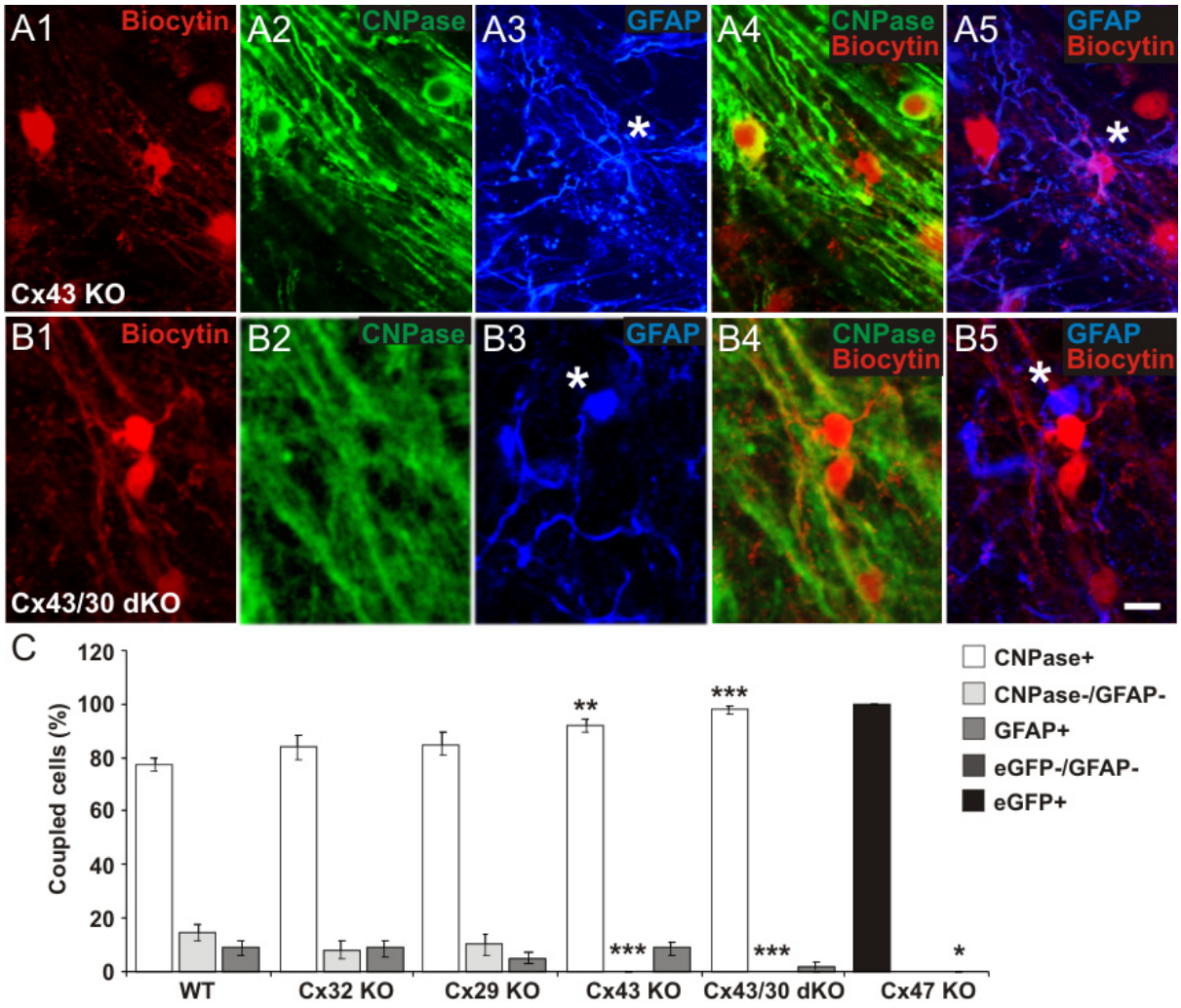

Figure 4.10: Identification of glial cell-types within the networks in mice single- and double-deficient for specific oligodendrocytic or astrocytic connexins. (A1-A5) Example of cell-type identification in biocytin labeled networks of Cx43- deficient mice (p10-15). Biocytin was detected with streptavidin-Cy3 (A1) and oligodendrocytes were identified by CNPase immunostaining (A2). (A3) Immunolabeling of the same section for the astrocytic marker GFAP. (A4) Overlay of A1 and A2. (A5) Overlay of A1

and A3. Note a coupled cell expressing GFAP (asterisk). (B1-B5) Biocytin labeling with streptavidin-Cy3 (B1) combined with immunostaining for CNPase (B2) and GFAP (B3). (B4) Overlay of B1 and B2. (B5) overlay of B1 and B3. Note the GFAP-positive astrocyte (asterisk) not labeled with biocytin adjacent to two biocytin-positive cells expressing CNPase. (C) Quantification of cell types within the network in wildtype, Cx32 KO, Cx29 KO, Cx43 KO, Cx43/Cx30 dKO and Cx47 KO mice. Values are expressed as percentage of the mean of coupled cells per network. In wildtype mice the majority of coupled cells were CNPase-positive (77 ± 2%, n=20), a small population lacked immunopositive signals for both CNPase and GFAP (14 ± 3%, n=20), while only few GFAP-positive cells were found (9 ± 2%, n=18). Cx32- and Cx29-ablation in comparison to wildtype tissue did not result in significant differences regarding the population of coupled cells. In Cx43 KO mice, immunostaining revealed that the large majority of coupled cells were CNPase-positive (92 ± 2%, one-way ANOVA, $p<0.001$; Bonferroni *post-hoc* analysis for comparison of means, $p<0.01$; n=23). No cells negative for both CNPase and GFAP were detected in these networks (one-way ANOVA, $p<0.001$; Bonferroni *post-hoc* analysis for comparison of means, $p<0.001$; n=23). In Cx43/Cx30 dKO mice CNPase-positive cells coupled within the network significantly increased as compared to wiltype animals (98 ± 1%, one-way ANOVA, $p<0.001$; Bonferroni *post-hoc* analysis for comparison of means, $p<0.001$; n=10). Deletion of the astrocytic Cx43 and Cx30 resulted in an almost complete loss of GFAP-positive cells coupled to the oligodendrocytic network. As observed in Cx43 KO mice, no coupled cells negative for both CNPase and GFAP were ever observed (one-way ANOVA, $p<0.001$; Bonferroni *post-hoc* analysis for comparison of means, $p<0.001$; n=10). In Cx47 KO mice, all coupled cells were identified as eGFP-positive, i.e. oligodendrocytes. No coupled cell negative for GFAP or for both eGFP and GFAP was observed.

analysis for comparison of means, $p<0.01$; Student's two-tailed t-Test, $p<0.05$, respectively; n=10). In Cx43- and Cx30-double-deficient mice the population of biocytin-positive cells consisted almost exclusively of CNPase-positive oligodendrocytes (98 ± 1%, one-way ANOVA, $p<0.001$, Bonferroni post-hoc analysis for comparison of means, $p<0.001$, n=10; Fig. 4.10B1,B2,B4,C). Only in two larger networks (44 coupled cells each, 2 mice) biocytin injection into a single oligodendrocyte spread to 3 and 6 GFAP-positive astrocytes, respectively (average 2 ± 1%, n=10; Fig. 4.10B1,B3,B5,C). As in Cx43-single-deficient mice the population of cells both negative for CNPase and GFAP was never observed (one-way ANOVA, $p<0.001$, Bonferroni post-hoc analysis for comparison of means, $p<0.001$, n=9; Fig. 4.10B1-B5,C). According to these data, deficiency of both astrocytic Cx43 and Cx30 results in a significant reduction of the number of coupled cells belonging to the oligodendrocytic network. In addition oligodendrocyte-to-astrocyte coupling is almost completely abolished. The residual astrocytic coupling is most likely due to the already described heterogeneity of hGFAP-Cre mediated ablation of Cx43 within the

astrocytic population of a given brain region (Requardt et al. 2009; Wallraff et al. 2006).

4.7 The Cx47M282T mutant causes a loss of function

Mutations in the *GJC2* gene encoding for the human Cx47 cause the hypomyelinating leukodistrophy PMLD. To determine a possible dominant negative effect of Cx47 mutants on oligodendrocytic coupling *in vivo,* mice carrying the Cx47M282T point mutation were used. The Cx47M282T knock in ($Cx47^{M282T/M282T}$) mice were generated as mouse model for the PMLD (Tress et al., unpublished), since the ortholog human mutation Cx47M286T was the only missense mutation found homozygously in PMLD patients (Uhlenberg et al. 2004).

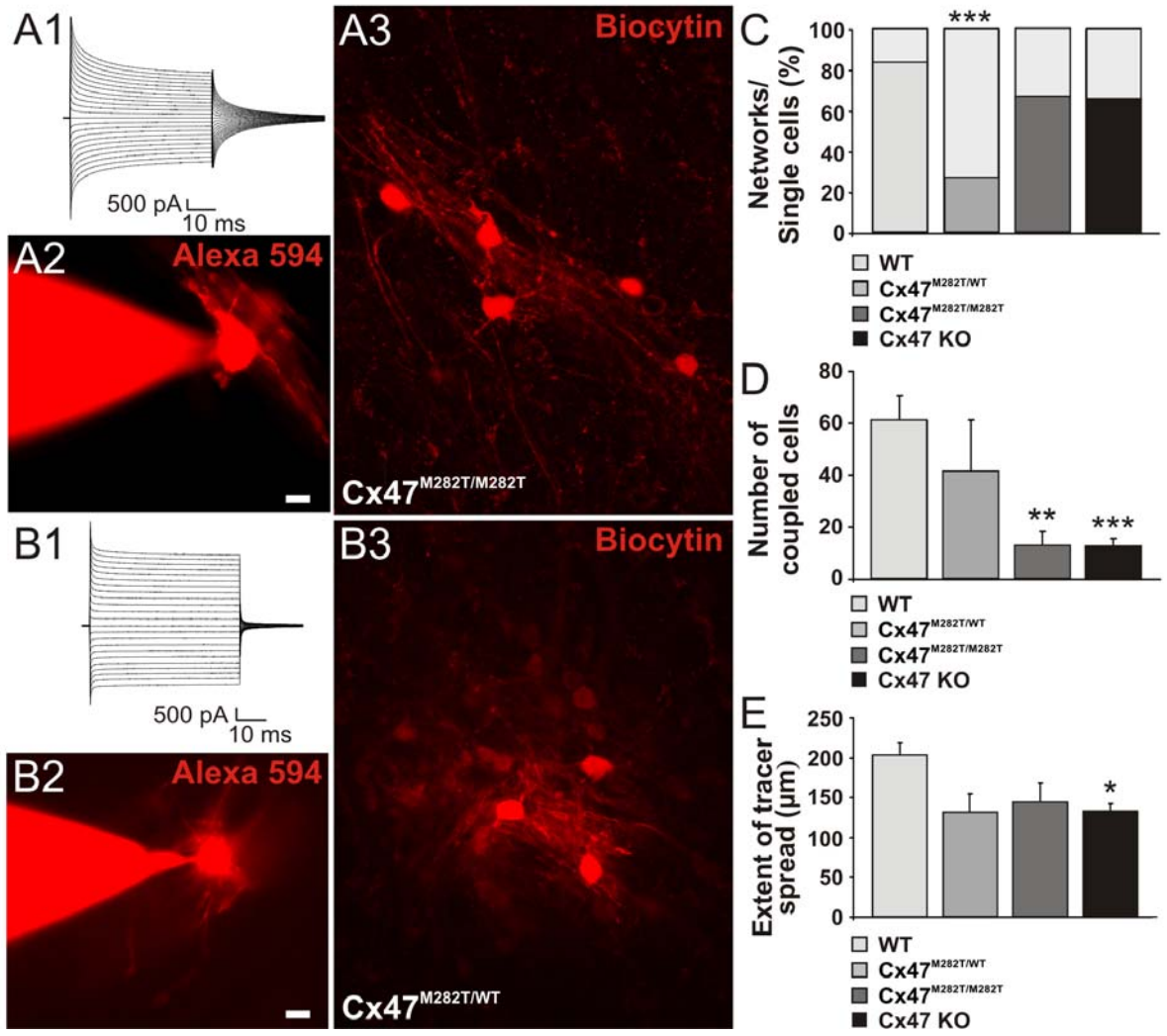

Figure 4.11: Oligodendrocytic coupling in the corpus callosum of p10-15 old homozygous ($Cx47^{M282T/M282T}$) and heterozygous ($Cx47^{M282T/WT}$) Cx47M282T mutant mice. (A1-A3) Biocytin injection and coupling in a p14 old $Cx47^{M282T/M282T}$ mouse. (A1) Membrane currents of the recorded oligodendrocyte injected with the gap junction permeable tracer biocytin in response to depolarizing and hyperpolarizing voltage steps from a holding potential (V_h) of -70 mV (50 ms, 10 mV increment). (A2) Oligodendrocyte morphology revealed by dialysis with the fluophore Alexa 594. (A3) Confocal image of the oligodendrocytic network. Biocytin, as revealed by strepdavidin-Cy3 reaction, spread to 16 neighboring cells. Bars denote 10 µm. (B1-B3) Biocytin injection and coupling in a p15 old $Cx47^{M282T/WT}$ mouse. (B1) Current profile of the recorded oligodendrocyte injected with biocytin (+50 to -170 mV, V_h= -70 mV). (B2) Oligodendrocyte morphology revealed by dialysis with the dye Alexa 594. (B3) Confocal image of the oligodendrocytic network. Biocyitin, as revealed by streptavidin-Cy3 labeling, spread to 53 adjacent cells. (C-E) Quantification of networks in Cx47M282T mutants, Cx47-deficient and wildtype mice (p10-15). (C) Percentage of injected cells which were coupled to at least one other cell and thereby formed a network versus injected uncoupled cells (light gray). Note that in $Cx47^{M282T/WT}$ only 27% of injected oligodendrocytes were found coupled. Asterisks indicate statistical significance (Chi Square Test, ***p<0.001). (D) Average number of coupled cells in a network. Asterisks indicate statistical significance (one-way ANOVA, p<0.001; Bonferroni *post-hoc* analysis for comparison of means, **p<0.01, ***p<0.001). (I) Extent of tracer spread as defined by the largest distance between two somata of the network. Asterisks indicate statistical significance (one-way ANOVA, p<0.05; Bonferroni *post-hoc* analysis for comparison of means, *p<0.05).

Experiments were performed in the corpus callosum and oligodendrocytes were identified by their typical morphology in bright phase microscopy, as described in paragraph *4.1* (Fig 4.11A1-A3). In Cx47M282T knock in mice, biocytin as revealed by streptavidin-Cy3 labeling spread to 13 ± 5 neighboring cells average, in 10 out of 15 slices (67% form networks; n=10, 3 mice), with a mean tracer extent of 143 ± 27 µm. The number of coupled cells in these networks was reduced by 79% in comparison to wildtype (one way ANOVA, p<0,001, Bonferroni *post-hoc* analysis for comparison of means, p<0.001; n=10), although the tracer spread to an extent not significantly different as was observed in wildtype (Fig. 4.11C-E). Immunostaining for the oligodendrocytic marker CNPase and the astrocytic marker GFAP indicated a reduction by 66% in the number of GFAP-positive cells labeled with biocytin/streptavidin-Cy3 as compared to wildtype (Fig. 4.12A1,A3,A5,C). However this reduction was not significant (3 ± 2%, n=10). The majority of coupled cells were CNPase-positive (93 ± 3%, one way ANOVA, p<0.001, Bonferroni *post-hoc* analysis for comparison of means, p<0.001; n=10; Fig. 4.12A1,A2,A4,C) while the population CNPase- and GFAP-negative was significantly reduced to 4 ± 2% (one way ANOVA

p<0.01, Bonferroni *post-hoc* analysis for comparison of means, p<0.01; n=10; Fig.4.12A1-A5,C).

The same experiments were performed also in heterozygous Cx47M282T ($Cx47^{M282T/WT}$) mice (Fig. 4.11B1-B3). In this mouse line only 4 out of 15 biocytin injections into single oligodendrocytes revealed intercellular coupling (27% form networks, 4 mice; Fig. 4.11C), with networks consisting of 41 ± 20 cells average (n=4; Fig. 4.11D) and tracer extent up to 193 μm (average 131 ±24 μm, n=4; Fig. 4.11E). The observed reduction in the number of oligodendrocytes forming networks was significantly different in comparison to wildtype mice (Chi-Square Test, Chi Square= 12.523, p<0.001). However, the number of coupled cells and extent of biocytin spread were not significantly different from wildtype animals. Similarly to wildtype networks the majority of biocytin-positive cells were CNPase-positive (87 ± 6%, n=4; Fig. 4.12B1,B2,B4,C), 3 ± 2% coupled cells were CNPase- and GFAP-negative (Fig. 4.12B1-B5,C), while the remaining 10 ± 4% were GFAP-positive astrocytes (Fig. 4.12B1,B3,B5,C).

Altogether these results indicate that homozygous Cx47M282T mutants cause a reduction in the number of cells coupled within the network. Moreover coupling of oligodendrocytes to GFAP-positive astrocytes is impaired, although not significantly, similarly to Cx47-deficient mice in which oligodendrocyte-to-astrocyte coupling was completely abolished.

In addition, heterozygous Cx47M282T mutants cause a reduction by 68% in the number of oligodendrocytes forming networks in comparison to wildtype animals. However, in $Cx47^{M282T/WT}$ mice neither the number of coupled cells within the oligodendrocyte syncytium nor coupling of oligodendrocytes to astrocytes is significantly affected.

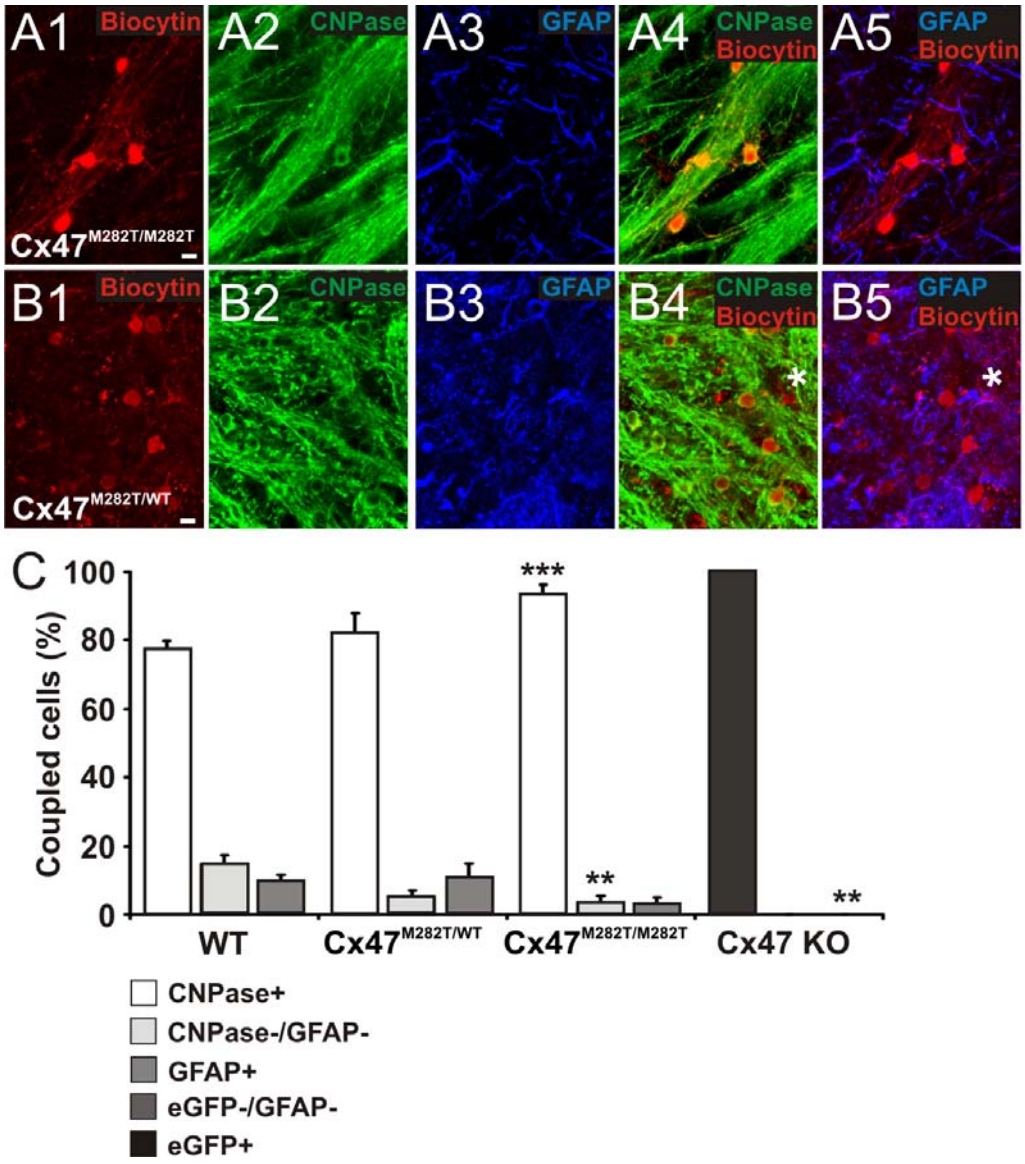

Figure 4.12: Identification of glial cell-types within the networks in p10-15 old homozygous ($Cx47^{M282T/M282T}$) and heterozygous ($Cx47^{M282T/WT}$) Cx47M282T mutant mice. (A1-A5) Confocal images showing an example of cell-type identification in biocytin labeled networks of a p14 old $Cx47^{M282T/M282T}$ mouse. Biocytin was detected with streptavidin-Cy3 (A1) and oligodendrocytes were identified by CNPase immunostaining (A2). (A3) Immunolabeling of the same section for the astrocytic marker GFAP. (A4) Overlay of A1 and A2. (A5) Overlay of A1 and A3. In this network no coupled cell expressed GFAP. (B1-B5) Biocytin labeling with streptavidin-Cy3 (B1) combined with immunostaining for CNPase (B2) and GFAP (B3). (B4) Overlay of B1 and B2. (B5) overlay of B1 and B3. Note the GFAP-positive astrocyte (asterisk) labeled with biocytin. The same cell was CNPase-negative (B4, asterisk). (C) Quantification of cell types within the network in wildtype, $Cx47^{M282T/WT}$, $Cx47^{M282T/M282T}$ and Cx47 KO mice. Values are expressed as percentage of the mean of coupled cells per network. In $Cx47^{M282T/M282T}$ mice the majority of coupled cells was CNPase-positive (93 ± 3%, one-way ANOVA, $p<0.001$; Bonferroni *post-hoc* analysis for comparison of means, $p<0.001$; n=10), while the population of CNPase- and GFAP-negative cells was significantly reduced in comparison to wildtype mice (3 ± 2%, one way ANOVA $p<0.01$, Bonferroni post-hoc analysis for comparison of means, $p<0.01$; n=10). Only few GFAP-positive cells were found, although the observed reduction was not significant as compared to wildtype animals (3 ± 2%, n=10). The heterozygous Cx47M282T mutation compared to wildtype did not result in significant differences regarding the population of coupled cells. As already described in paragraph *4.2*, in Cx47 KO mice immunostaining for the reporter protein eGFP, which replaced the Cx47 coding region, revealed that all coupled cells were identified as eGFP-positive and therefore oligodendrocytes. No GFAP-positive cells were found (one-way ANOVA, $p<0.01$; Bonferroni *post-hoc* analysis for comparison of means, $p<0.01$; n=13).

4.8 Summary of results

Functional coupling among oligodendrocytes and astrocytes in the corpus callosum from wildtype and different connexin-deficient mouse lines has been investigated. In addition dye transfer experiments were performed in mice carrying the Cx47M282T mutation ($Cx47^{M282T/M282T}$) associated to the human leukodistrophy Paelizeus-Merzbacher-like-disease (PMLD). Using the patch-clamp technique the gap-junction-permeable tracer biocytin was injected into single oligodendrocytes in acute slices of corpus callosum (p10-15) and visualized with streptavidin-Cy3 labeling.

In wildype mice oligodendrocytic coupling was investigated also at a later developmental time point (p20-25).

Oligodendrocytes and astrocytes were identified by expression of the oligodendrocytic marker CNPase and the astrocytic marker GFAP, respectively. In wildtype, CNPase- and GFAP-negative coupled cells were identified as oligodendrocyte precursors expressing NG2 and Olig2, markers for immature oligodendrocytes. Therefore the population of CNPase- and GFAP-negative coupled cells was considered as oligodendrocyte precursors in all the other mouse lines except for Cx47-deficient mice. In these animals oligodendrocytes were identified by expression of eGFP, which replaced the Cx47 coding region and was thus expressed under control of the Cx47 promoter. Immunostaining for CNPase identified 77 ± 2% eGFP-positive cells as CNPase-positive in the corpus callosum of the same mice used for experiments. The remaining 23 ± 2% did not expressed CNPase, thus being immature oligodendrocytes. However a direct comparison between oligodendrocyte precursors coupling in Cx47-deficient mice wildtype and the other mouse lines, was not possible (see † in table 4.1).

	Formed Networks (%)	***Number of coupled cells***	***Extent of tracer spread (µm)***	***O coupled***	***OPC coupled***	***A coupled***
WT (p10-15)	83%	61 ± 10	203 ± 15.64	77 ± 2%	14 ± 3%	9 ± 2%
WT (p20-25)	67%	32 ± 2	148 ± 17	86 ± 6%	11 ± 3%	3 ± 2%
Cx47 KO	65%	13 ± 3***	132 ± 11*	100 ± 0%†	-†	-*
Cx32 KO	70%	72 ± 12	240 ± 25	83 ± 5%	8 ± 3%	9 ± 3%
Cx29 KO	69%	37 ± 8	218 ± 17	85 ± 4%	10 ± 4%	5 ± 2%
Cx47/Cx32 dKO	-***	-***	-***	-	-	-
Cx43 KO	79%	31 ± 5*	156 ± 15	92 ± 2%**	-***	8 ± 2%
Cx43/Cx30 dKO	64%	20 ± 5**	145 ± 21*	98 ± 1%***	-***	2 ± 1%§
Cx47$^{M282T/WT}$	27%***	41 ± 20	121 ± 34	87 ± 6%	3 ± 2	10 ± 4%
Cx47$^{M282T/M282T}$	67%	13 ± 5***	143 ± 27	93 ± 3%***	4 ± 2%**	3 ± 2%

Table 4.1: Summary of gap junctional coupling in mice single- and double-deficient for specific glial connexins and in mice carrying the Cx47M282T mutation compared to wildtype. O, oligodendrocytes; OPC, oligodendrocyte precursor cells; A, astrocytes.
Note the complete lack of oligodendrocytic coupling in Cx47/Cx32-double-deficient mice. The number of coupled cells is significantly reduced by deletion of Cx47, Cx43 or double deletion of both Cx43 and Cx30. The extent of biocytin spread was significantly impaired only in Cx47-deficient and Cx43/Cx30-double-deficient mice. Lack of Cx47 completely disrupted oligodendrocyte-to-astrocyte coupling.
(†) In Cx47-deficient oligodendrocytes were identified by expression of eGFP under control of the Cx47 promoter. Immunostaining for CNPase in the corpus callosum identified 77 ± 2% eGFP-positive cells as CNPase-positive. The remaining 23 ± 2% did not expressed CNPase, thus being immature oligodendrocytes.
(§) The residual oligodendrocyte-to-astrocyte coupling detected in Cx43/Cx30-double-deficient mice is probably due to the heterogeneity of hGFAP-Cre mediated ablation of Cx43. Asterisks indicate significance (*p<0.05; **p<0.01; ***p<0.001, see chapter *4* for performed statistic).

In wildtype mice between p10-15 and p20-25 no significant difference was observed, althought at the later time point number of coupled cells and extent of biocytin spread tended to decrease. Consistent with a more advanced developmental stage, the number of oligodendrocytes found coupled increased, though not significantly.

Lack of both Cx47 and Cx32 completely abolished oligodendrocytic coupling.

In Cx47-deficient, Cx43-deficient and Cx43/Cx30-double-deficient mice the number of coupled cells was significantly reduced compared to wildtype. The extent of biocytin spread was significantly impaired only in Cx47-deficient and Cx43/Cx30-double-deficient mice in comparison to wildtype.

Lack of Cx47 completely abolished oligodendrocyte-to-astrocyte coupling. Ablation of Cx43 resulted in an increased number of oligodendrocytes within the syncytium and in the loss of coupling to oligodendrocyte precursors, in both Cx43-deficient and Cx43/Cx30-double-deficient mice. The residual oligodendrocyte-to-astrocyte coupling detected in Cx43/Cx30-double-deficient mice was probably due to the heterogeneity of hGFAP-Cre mediated ablation of Cx43 (see [§] in table 4.1). Homozygous expression of Cx47M282T mutants caused a significant reduction in coupled cells, similarly to Cx47 deletion. In Cx47M282T/M282T the population of coupled cells consisted almost exclusively of oligodendrocytes and coupling to astrocytes was reduced by 66% compared to wildtype, although not significant. All data are summarized in table 4.1.

5 Discussion

5.1 Oligodendrocytes form a network in the corpus callosum

In contrast to the notion that oligodendrocytes couple to astrocytes and not among each other (for review see Orthmann-Murphy et al. 2008), my present work provides the first functional demonstration of direct oligodendrocyte-to-oligodendrocyte coupling in white matter of juvenile mouse brain. I was able to identify coupling by injection of the gap junction permeable tracer biocytin, although the fluorescent dye Alexa Fluor 594 rarely revealed coupling. However, not all the injected oligodendrocytes formed functional gap junctions. Morphological analysis revealed that these uncoupled cells were characterized by more radial processes as compared to coupled cells, thus most likely being immature oligodendrocytes (see paragraph *1.2.1.1*).

Oligodendrocytic coupling had been documented for cultured cells (Kettenmann et al. 1983; Kettenmann et al. 1984) and for oligodendrocytes in slices of gray matter spinal cord and retina (Pastor et al. 1998; Robinson et al. 1993). In white matter, no evidence was found for inter-oligodendrocytic gap junction formation *in situ* based on immunocytochemical and freeze fracture studies (Kamasawa et al. 2005; Massa and Mugnaini 1982; Nagy and Rash 2000).

In accordance with previous observations that injection of the fluorescent dye Lucifer Yellow did not spread to neighboring oligodendrocytes in the gray matter, I conclude that the increased sensitivity of the biocytin approach reveales oligodendrocytic coupling. I then assume that the strength of coupling between oligodendrocytes is lower than between astrocytes in which the spread of fluorescent dyes has frequently been reported. This is supported by previous studies in cell culture where

70% of the injected oligodendrocytes were found to form Lucifer Yellow permeable gap junction channels to at least one and up to five neighboring cells, whereas astrocytes were always found extensively coupled (Kettenmann et al. 1983). A difference in sensitivity was observed also in slices were oligodendrocytes were injected with either Lucifer Yellow or biocytin (Pastor et al. 1998). The latter labeled a much larger network. Accordingly, in gray matter astrocytes the amount of intercellular coupling detected by biocytin injection was increased when compared to the dye sulforhodamine B, as shown by Houades et al. (2008).

This frequently observed discrepancy is likely due to the different permeability of gap junctions to the tracers described above. Although gap junctions are considered as non-selective channels allowing the passage of molecules up to 1 kD (Neijssen et al. 2005), several studies have reported a variable size and charge selectivity among them (Bedner et al. 2006; Bruzzone et al. 1996; Elfgang et al. 1995; Harris 2007). The remarkable sensitivity of biocytin could be explained by its better permeability due to lower molecular weight, ionic charge and method of detection (Gu et al. 2003).

5.2 During development from p10 to p25 oligodendrocytic coupling tends to be impaired

Here, for the first time, I demonstrate functional oligodendrocytic coupling in the mouse CNS white matter around the third postnatal week, when myelination is the most active (for review see Baumann and Pham Dinh 2001). In p20-25 old mice the number of coupled cells and the extent of biocytin spread showed a tendency to decrease in comparison to p10-15 old animals, but the observed reduction was not significant. Immunohistochemical identification of the coupled cells revealed a 10% increase in the number of CNPase-positive oligodendrocytes, while the population of

oligodendrocyte precursors was reduced by 25%. These findings, even if not significantly different from p10-15 old mice, are consistent with oligodendrocyte development (see paragraph *1.2.1.1*). The number of GFAP-positive coupled cells decreased by 61%, indicating a possible reduction in oligodendrocyte-to-astrocyte coupling along development. The observed impairment of inter-oligodendrocytic and oligodendrocyte-to-astrocyte coupling could be possibly due to a down-regulation of Cx47 expression at this time point. Cx47 transcription was first detected 1 week after birth and reached a maximum at approximately p14, while in the adult mouse Cx47 mRNA levels decreased again to approximately one-third of the level seen around the second postnatal week (Teubner et al. 2001). Several studies reported a maximum expression of Cx32 around p20 (Dermietzel et al. 1989; Nadarajah et al. 1997; Prime et al. 2000), which matched the time point in which I performed the dye transfer experiments. The expression peak reached by Cx32 at p20, when Cx47 mRNA levels start to decrease, could account for the oligodendrocytic coupling detected, despite the tendency to diminish.

The extent of gap junctional coupling in glial cells of the adult mouse brain has not yet been extensively characterized. Studies performed by biocytin injection into single astrocytes revealed extensive networks in hippocampal acute slices of p14-p28 and p30-p90 old mice (Rouach et al. 2008; Wallraff et al. 2006) and in the mouse striatum between the 8th and 12th postnatal week (Wang et al. 2008).

These findings are consistent with the expression levels of the astrocytic Cx30 and Cx43 in the adult rodent brain. Significant amounts of the Cx30 mRNA were detected in 2 weeks old mice, becoming more abundant in adult animals (Dahl et al. 1996). Protein expression of Cx43 starts at embryonic day 18 and increases during the second postnatal week, being stable during rodent adulthood (Dermietzel et al. 1989). However, astrocytic networks in the adult cortex could be rarely found, as

detected by biocytin injection (Peters et al. 2009). In accordance, discrepancies between time course of connexins mRNA expression and extent of dye coupling were already described in rat neocortical neurons (Rorig et al. 1996). The variability in astrocytic coupling observed in these studies, in which the same functional assay was applied, could also be due to different expression levels of connexin proteins in specific brain regions at a certain age.

Altogether my findings indicate that development from p10 to p25 does not significantly affect oligodendrocytic coupling. However further experiments at later time points would be required to determine whether oligodendrocytic coupling diminishes with the full establishement of myelination.

5.3 Connexin47 and -32 are necessary for oligodendrocytic coupling

My results indicate that for inter-oligodendrocytic gap junctional coupling Cx47 plays a dominant role as indicated by the significant reduction in number of coupled cells and in extent of biocytin spread in Cx47-deficient mice. The remaining oligodendrocytic coupling observed in Cx47-deficient mice is most likely mediated by the oligodendrocytic Cx32. In Cx47-deficient mice a dramatic increase in Cx32 expression along myelinated fibers, which could then compensate for the loss of Cx47, was already reported by Li et al. (2008).

For intercellular coupling Cx32 seems to be less important, since the oligodendrocytic network was not significantly reduced after deletion of Cx32, thus supporting the paramount role of Cx47 for oligodendrocytic coupling. Cx32, however, still contributes to oligodendrocytic coupling, since the residual network in Cx47-deficient mice was completely absent in mice lacking both Cx47 and Cx32. The partial redundancy observed here could explain why Cx32-deficient mice (Nelles et

al. 1996), as well as mice lacking Cx47, display no severe pathological phenotypic abnormalities in the CNS, while animals deficient for both Cx47 and Cx32 develop a dramatic CNS demyelination (Menichella et al. 2003; Odermatt et al. 2003).

Furthermore, my results indicate that Cx29, which is also expressed in oligodendrocytes, does not contribute to the establishment of the network, since in Cx29-deficient mice the number of coupled cells, although decreased, was not significantly different from wildtype mice. In addition, biocytin injected into single oligodendrocytes spread to an extent comparable to what observed in wildtype animals. According to immunohistochemical studies, Cx29 is mainly localized at the adaxonal membrane of small myelin sheaths and therefore it has been speculated that Cx29 forms only hemichannels (Kamasawa et al. 2005). Scrape-loading assays and fluorescence recovery after photobleaching (FRAP) analysis on stable transfected cells expressing Cx29 showed no dye transfer into neighbouring cells (Ahn et al. 2008). In addition, recordings by dual whole cell patch-clamp of Neuro2A cells transiently expressing Cx29 revealed lack of junctional conductance (Altevogt et al. 2002). The present findings support the notion that Cx29 does not form functional gap junctions, in accordance with the studies described above.

5.4 Increased oligodendrocytic coupling correlates with low input resistance

In hippocampus, electrically coupled astrocytes differ in their input resistance from uncoupled astrocytes (Meme et al. 2009). Dye-coupling experiments revealed that passive astrocytes coupled to neighboring astrocytes are characterized by lower input resistance compared to those with lower number of dye coupled cells (Blomstrand et al. 2004; Zhou et al. 2006). In line with these studies, hippocampal astrocytes from Cx30- and Cx43-double-deficient mice lack tracer coupling and

display an increased membrane resistance (Wallraff et al. 2006). Accordingly, my studies demonstrate that the degree of tracer coupling contribute to some extent to the passive electrophysiological properties of oligodendrocytes. Therefore, loss of oligodendrocytic gap junctional communication by Cx47- and Cx32-deficiency results in an increase of the oligodendrocytic input resistance.

Despite several electrophysiologycal studies reported that decay time constant of the slow current transients as well as membrane capacitance increase linearly with the number of coupled cells (de Roos et al. 1996; Harks et al. 2001; Postma et al. 1998), here uncoupled oligodendrocytes showed evoked currents which could be fit by a biexponential and display decay time constants comparable to coupled cells. Furthermore, uncoupled oligodendrocytes were characterized by a significantly higher membrane capacitance evoked by slow transient currents in comparison to coupled cells. This discrepancy could be due to morphological differences or altered physiological properties, yet to be defined, in oligodendrocytes of mice deficient for both Cx47 and Cx32.

5.5 Oligodendrocyte-to-astrocyte coupling is relatively weak but promotes oligodendrocytic coupling

Although astrocytes in gray matter are highly coupled among each other (Houades et al. 2008; Wallraff et al. 2006), biocytin injection into single astrocytes of the corpus callosum did not reveal networks of coupled astrocytes in brain slices obtained from juvenile mice (Haas et al. 2006). Here I found that some astrocytes are part of the oligodendrocytic network, but the majority of cells within a given network belong to the oligodendrocytic lineage.

In the retina, coupling between astrocytes and oligodendrocytes has been described (Robinson et al. 1993). In accordance to this study, injected Lucifer Yellow did reveal

heterotypic coupling among glial cells but spread from astrocytes into oligodendrocytes instead of spreading from oligodendrocytes into astrocytes. The unidirectional coupling model proposed by these authors has been deeply criticized, since asymmetrical dye transfer between coupled cells violates the second law of thermodynamics (Finkelstein 1994). Furthermore the electrical rectification displayed by oligodendrocyte-to-astrocyte heterotypic Cx32/Cx30 channels (Dahl et al. 1996), while heterotypic Cx47/Cx43 channels exhibit more symmetric voltage dependent properties, can not account for unidirectional coupling since pore size and single-channel conductance are not simply related (for review see Orthmann-Murphy et al. 2007b). Despite most of the electrophysiological studies on mammalian cells transfected with different combination of glial connexins focused on the physiological properties of heterotypic Cx47/Cx43 and Cx32/Cx30 channels, there is evidence that Cx47 and Cx32 can mediate electrical coupling and thus form functional homotypic channels (Elfgang et al. 1995; Teubner et al. 2001). In the present work I clearly demonstrate that oligodendrocytes in corpus callosum directly couple to other oligodendrocytes by homotypic gap junctions formed by the oligodendrocytic Cx47 and Cx32, rather than to astrocytes.

However, oligodendrocyte-to-astrocyte coupling is a prerequisite for extending the oligodendrocytic syncytium, since ablation of the oligodendrocytic Cx47 or both astrocytic Cx43 and Cx30 results in a reduction of the oligodendrocytic network size. Oligodendrocytes can therefore exchange metabolites, ions and other gap-junction permeable molecules much easier among each other than with astrocytes.

On the other hand, astrocyte connexins influence the oligodendrocytic network size. I can, therefore, not exclude the option that oligodendrocytes couple not only directly, but also through very small astrocytic compartments. If true, I have to postulate that these compartments are only poorly connected to the soma and other processes of

the astrocyte from which they arise. Then one could assume that biocytin travels through that astrocytic compartment to other oligodendrocytes without spreading into the astrocyte. Indeed, such structures have been found in Bergmann glial cells termed microdomains. These structures form compartments which are connected to the rest of the cell by a very thin stalk (Grosche et al. 1999). Computational modelling of the microdomains indicated that each is electrotonically independent of the stem process from which it arises, as well as of neighbouring domains (Grosche et al. 2002). Even if this is true however, the fact remains that oligodendrocytes can exchange metabolites, ions and other gap-junction permeable molecules much easier among each other than with astrocytes.

Recently, Orthmann-Murphy et al. (2007b) proposed a model of glial connexin channels based on electrophysiological studies on pairs of cultured mammalian cells, each transfected with a distinct connexin. By dual whole cell patch-clamp, Cx32/Cx30 and Cx47/Cx43 were found to be the only functional heterotypic channels of all possible combinations. Here I demonstrate that in the postnatal corpus callosum Cx47-containing gap junctions are required for heterologous coupling between oligodendrocytes and astrocytes. I also observed that oligodendrocyte-to-astrocyte coupling was almost completely abolished in Cx43- and Cx30-double-deficient mice but still present in Cx43-deficient animals, indicating that either Cx30 is generally responsible for oligodendrocyte-to-astrocyte coupling or that it is up-regulated in Cx43-deficient animals (Nakase et al. 2004; Theis et al. 2003) and therefore substitutes for the loss of Cx43.

5.6 Cx43 influences oligodendrocyte precursors coupling

To my knowledge, coupling of oligodendrocyte precursors has been poorly investigated. Two recent studies, performed at early postnatal age, reported that biocytin injection into single oligodendrocyte precursors identified by their expression of the specific marker NG2 did not reveal intercellular coupling in gray matter regions (Houades et al. 2008; Muller et al. 2009). The oligodendrocytic Cx32 has, however, been detected in subset of NG2-positive oligodendrocyte progenitors of the adult dentate gyrus (Melanson-Drapeau et al. 2003). Here I found that in the white matter oligodendrocytes couple to a cell population which is CNPase- and GFAP-negative. By immunostaining for NG2 and Olig2 and by examining coupling in NG2-EYFP knockin mice I found that this population at least in part expressed NG2 and also the transcription factor Olig2, identifying these cells as oligodendrocyte precursors. Thus, oligodendrocytes not only couple to astrocytes, but also to immature cells of the oligodendrocyte lineage.

I observed that conditional deletion of the astrocytic Cx43 leads to the loss of the subpopulation of oligodendrocyte progenitors coupled within the syncytium. There could be two explanations: (1) either coupling to these precursors is impaired or (2) the population of progenitor cells is affected. Indeed there is evidence for the impact of Cx43 expression on glial precursor cells proliferation and differentiation (Cheng et al. 2004; Kunze et al. 2009; Melanson-Drapeau et al. 2003). Ablation of both astrocytic Cx43 and Cx30 in radial glia like cells decreases proliferation and neurogenesis in the adult dentate gyrus (Kunze et al. 2009). In Cx43-deficient mice disorganized ventricular and subventricular zones have been described, probably arising from altered glial and neuronal proliferation (Wiencken-Barger et al. 2007). Indeed, according to this study, Cx43-deficient mice display a significant reduction in the number of neural precursor cells at postnatal day 2, not observed at p10

(Wiencken-Barger et al. 2007). Thus it is likely that the expression of the astrocytic Cx43 affects the oligodendrocyte precursor population in the juvenile corpus callosum.

5.7 Cx47M282T mutants cause a simple loss of function

Recessive mutations in the *CX47* gene GJA12/GJC2 cause the human leukodystrohy Pelizaeus-Merzbacher-like disease. Patients displaying different genotypes –homozygous P128frameshift, M283T, G233S, or L278frameshift mutations, compound heterozygotes for P87S/P327frameshift or Y269D/R237stop mutations – present similar phenotype, implying that all these mutations cause loss of function or a gain of function in cell toxicity (Uhlenberg et al. 2004; Bugiani et al. 2006). Electrophysiological and scrape-loading studies performed on transfected HeLa or Neuro2A cells showed that P87S, Y269D, and M283T mutants fail to form functional homotypic gap junction channels. All the three mutated proteins were found partially accumulated in the endoplasmic reticulum, possibly contributing to their inhability to form functional channels. The mutated connexins had no impact on increased apoptosis via unfolded protein response pathways, implying that endoplasmic reticulum retention of Cx47 mutants does not result into a gain of function in oligodendrocyte toxicity (Orthmann-Murphy et al. 2007a).

Mouse mutants expressing the orthologous Cx47M282T mutation homozygously are viable and show an only mild phenotype, comparable to Cx47-deficient mice. Heterozygous Cx47M282T mice also display a delayed myelin development but perform less efficiently in the open field behavioural test in comparison to homozygous animals. Although in p10 and p16 old $Cx47^{M282T/M282T}$ and $Cx47^{M282T/WT}$ mice a reduction in myelin proteins expression was detected by immunoblot analyses, in three monthes old mice no significant difference was observed.

Accordingly, adult Cx47M282T expressing animals did not exhibit motor coordination deficits in the rotarod assay (Tress et al., unpublished).

The experiments described here are the first demonstration that mutated Cx47M282T causes a loss of function *in vivo*, since inter-oligodendrocytic as well as oligodendrocyte-to-astrocyte coupling is impaired in homozygous $Cx47^{M282T/M282T}$ mice, similarly to the reduction of gap junctional communication in Cx47-deficient mice. If Cx47M282T mutants would have exerted a transdominant effect on Cx32 proper functionality, one would have expected the complete abolishment of oligodendrocytic coupling, as seen in this study for Cx47- and Cx32-double-deficient mice. Therefore, these findings indicate that the mutant Cx47M282T has no significant transdominant effect on inter-oligodendrocytic coupling mediated by Cx32. According to immunocytochemical and electrophysiological assays in transfected cells, Cx47M282T mutants partially colocalize with Cx43 at the plasma membrane but fail to form functional heterotypic channels (Orthmann-Murphy et al. 2007b). The reduced coupling of oligodendrocytes to astrocytes observed in homozygous $Cx47^{M282T/M282T}$, althought not significant, support these studies. In these mutant mice heterotypic Cx32/Cx30 gap junctions can possibly compensate for the loss of functional Cx47/Cx43 channels. This compensation was not observed in Cx47-deficient mice, in which oligodendrocyte-to-astrocyte coupling was completely abolished, most likely due to the loss of Cx30 at oligodendrocyte-to-astrocyte gap junction plaques after cx47 gene deletion reported by Li et al. (2008).

Additionally, in heterozygous $Cx47^{M282T/WT}$ animals the number of injected oligodendrocytes forming networks was reduced by 68% in comparison to wildtype, while in homozygous $Cx47^{M282T/M282T}$ and in Cx47-decifient mice by 20% and 22% respectively. In contrast to the decrease observed in homozygous $Cx47^{M282T/M282T}$ and Cx47-deficient animals, the stronger reduction in the number of injected

oligodendrocytes forming a network in heterozygous Cx47$^{M282T/WT}$ mice could result from a compensatory upregulation of Cx32 in Cx47-deficient and homozygous Cx47$^{M282T/M282T}$ mice, which may not take place in heterozygous Cx47$^{M282T/WT}$ mice. However, in the few networks observed heterozygous Cx47M282T mutants did not affect inter-oligodendrocytic and oligodendrocyte-to-astrocyte coupling, indicating that Cx47M282T mutants do not exert a negative effect on functional heterotypic channels formed by wildtype Cx47 colocalized with Cx43.

Mice expressing homozygous Cx47M282T mutations do not show the severe CNS pathological phenotype seen in Cx47/Cx32-double-deficient mice. However, Cx47$^{M282T/M282T}$/Cx32-deficient animals are characterized by severe motor impairment, myelin defects and die during early adulthood (Tress et al., unpublished). These findings furthermore support the possibility of a compensatory effect on Cx47M282T mutants via Cx32 expression.

Altogether, Cx47$^{M282T/M282T}$ mice display a delayed CNS myelin development but in contrast to the typical Pelizaeus-Merzbacher-like-disease phenotype in human, the hypomyelination can be compensated in mice, most likely by upregulation of Cx32 expression.

5.8 Gap junctional coupling is a prerequisite for proper oligodendrocytic functions

The importance of the oligodendrocytic connexins for myelination became evident in Cx47- and Cx32-double-deficient mice which display conspicuous vacuolization in the central nervous system, develop an action tremor and die around day 51 (Menichella et al. 2003; Odermatt et al. 2003). Furthermore the human leucodystrophy, Pelizaeus-Merzbacher-like disease and Hereditary Spastic Paraplasia (HSP, Orthmann-Murphy et al. 2009) are caused by Cx47 mutations

(Bugiani et al. 2006; Uhlenberg et al. 2004). Cx32 mutations lead to Charcot-Marie-Tooth type X (Bergoffen et al. 1993) and are sometimes associated with brain abnormalities (Halbrich et al. 2008; Mazzeo et al. 2008).

The pertinence of astrocytic Cx43 expression regarding remyelination has recently been discussed (Cronin et al. 2008; Roscoe et al. 2007). In an experimental allergic encephalomyelitis model (EAE) Cx43 expression was considerably increased in remyelinating lesions following treatments (Roscoe et al. 2007). Furthermore, Lutz et al. (2009) demonstrated that Cx30-deficient mice with astrocyte-targeted deletion of Cx43 display white matter pathology, characterized by vacuolated oligodendrocytes, intramyelinic edema and reduced myelin basic protein expression.

The possible biological function of oligodendrocytic coupling could be to provide pathways for controlling the homeostasis of K^+ during axonal activity, as originally proposed in the model of K^+ spatial buffering by Orkand et al. 1966 (Newman 1986; Orkand et al. 1966; Orthmann-Murphy et al. 2008). Observations that mice lacking Cx32 and Cx47 display a much more severe phenotype than mice deficient for both Cx30 and Cx43 suggest that homotypic oligodendrocytic coupling is more important than coupling of oligodendrocytes to astrocytes (Lutz et al. 2009; Wallraff et al. 2006). According to the study performed in the hippocampal gray matter by Wallraff et al. (2006), ablation of Cx30 and Cx43 in astrocytes modestly diminished K^+ buffering. These authors did not address whether white matter regions in Cx43- and Cx30-double-deficient mice were similarly affected. Recently Menichella et al. (2006) provided the first physiological evidence that neuronal activity correlates with the onset of myelin-associated vacuolization in the CNS of Cx47- and Cx32-double-deficient mice, thus consolidating the notion that oligodendrocytes play a critical role in buffering K^+ ions released during neuronal activity.

In line with these findings, my results demonstrate that oligodendrocyte-to-oligodendrocytic coupling is still present in Cx43- and Cx30-double-deficient mice, despite the loss of oligodendrocyte-to-astrocytes coupling. Therefore inter-oligodendrocytic coupling could play a specific functional role regarding distribution of metabolites in the developing brain particularly during myelin formation.

Few studies tried to identify the endogenous transjunctional substances which permeate gap junctions in order to elucidate the specific roles that different connexin channels play in development, physiology and pathology (for review see Harris et al. 2007).

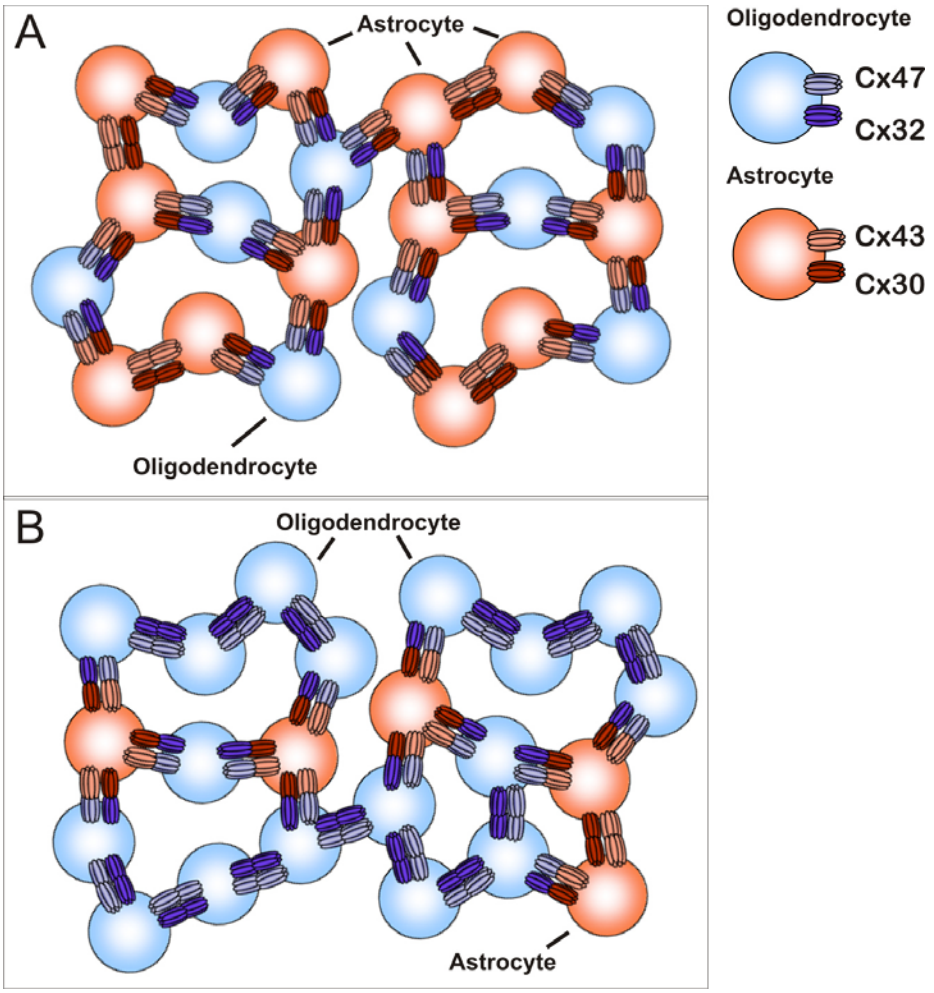

Figure 5.1: The panglia syncytium: gap junction network of astrocytes and oligodendrocytes. Proposed model for oligodendrocytic functional coupling in the CNS white matter. (A) Schematic representation of the model describing the gap junctional communication between astrocyte and oligodendrocytes as proposed recently by Orthmann-Murphy et al. (2008). Oligodendrocytes do not directly couple to other oligodendrocytes, but only to astrocytes through heterotypic Cx47/Cx43 and Cx32/Cx30 channels. Therefore astrocytes are intermediaries that distribute metabolites through oligodendrocytes. (B) Diagram representing the proposed model of oligodendrocytic coupling in the

juvenile corpus callosum. Oligodendrocytes directly couple to each other through homotypic Cx47 and Cx32 gap junctions, thus forming intercellular units which may be the prerequisite for redistributing K+ and metabolites for proper myelination and axonal function. However, oligodendrocyte-to-astrocyte coupling mediated by heterotypic Cx47/Cx43 and Cx32/Cx30 gap junctions is necessary to extend the size of the oligodendrocytic network, since lack of Cx47 and both the astrocytic Cx43 and Cx30 resulted in a significant reduction in the number of coupled cells within the syncytium. The disruption of oligodendrocyte gap junctional coupling by ablation of Cx47 and Cx32 result in a severe myelin disorder, while double deficiency of Cx43 and Cx30 cause a milder phenotype since inter-oligodendrocytic coupling is not completely lost. Blue connexons, Cx32; lilac connexons, Cx47; red connexons, Cx43; orange connexons Cx30.

Homotypic Cx32 channels were found to display a high gap junctional permeability to inositol 1,4,5 triphosphate (IP3; Niessen et al. 2000) and a 12 fold higher permeability to adenosine then homotypic channels formed by Cx43 *in vitro*. In contrast, Cx43 gap junctions were more permeable to glucose and glutamate, as well as to ATP, which permeate 300 fold better than in homotypic Cx32 channels (Goldberg et al. 2002). Therefore distinct permeability and gating properties of homotypic Cx47 and Cx32 channels versus heterotypic Cx47/Cx43 and Cx32/Cx30 could account for a selective transfer of specific metabolites between oligodendrocytes.

However, in Cx47- and Cx32-double-deficient mice myelin formation is hindered but not completely abolished. This indicates that other mechanisms apart from gap junctional coupling are involved in distribution of metabolites for proper myelination.

Altogether my results suggest a new model for the complex communication within the panglial syncytium in the corpus callosum, in which oligodendrocytes directly communicate to each other (fig. 5.1), thus forming intercellular units which may be the prerequisite for redistributing K^+ and thus maintaining proper axonal function.

6 Summary

Cx32 and Cx47 are the major gap junction proteins expressed by oligodendrocytes, the myelinating cells in the CNS. In addition to their role in cell communication, the expression of these proteins is essential for the formation and maintenance of myelin since mutations results in severe myelin related disorders. According to previously published ultra structural studies, oligodendrocytes in white matter exhibit gap junctions with astrocytes, but not among each other, while in cell culture experiments oligodendrocytes form functional gap junctions. In order to understand the basis of the myelin related diseases caused by mutations in oligodendrocytic connexins is necessary to determine which connexin form functional gap junction channels in the CNS white matter. Therefore functional coupling among oligodendrocytes and astrocytes in the corpus callosum from wildtype and different connexin-deficient mouse lines has been investigated. In addition, the impact of Cx47 mutants associated to the human leukodistrophy Paelizeus-Merzbacher-like-disease (PMLD) was studied using mice carrying the Cx47M282T point mutation ($Cx47^{M282T/M282T}$). Using the patch-clamp technique the gap-junction-permeable tracer biocytin was injected into single oligodendrocytes in acute slices of corpus callosum (postnatal day 10-15). The coupled cells in the network were identified combining biocytin labeling with immunostaining for specific glial cell markers. On average 61 cells were positive for the tracer detected by biocytin labeling with fluorochrome-conjugated streptavidin. The majority of coupled cells were positive for the oligodendrocyte marker CNPase, while only 9% expressed the astrocyte marker GFAP. A small population of cells within the network expressed NG2 and Olig2, markers for oligodendrocyte precursors. Oligodendrocytes are known to express Cx47, Cx32 and Cx29, astrocytes Cx43 and Cx30. In Cx47-deficient mice, the number of coupled cells was reduced by 80%. Deletion of Cx32 or Cx29 alone did not significantly reduce the number of coupled cells, but coupling was completely absent in Cx47/Cx32-double-deficient mice. Cx47-ablation completely abolished coupling of oligodendrocytes to astrocytes. Lack of the astrocytic Cx43 resulted in a reduction of the oligodendocytic network and in the complete loss of oligodendrocyte precursors coupling, althought astrocytic coupling was still present. Animals double-deficient for the astrocytic Cx43 and Cx30 showed a significant reduction in the number of coupled cells accompanied by loss of oligodendrocyte-to-astrocyte coupling. Also in

this strain coupling to oligodendrocyte precursors was never observed. Additionally uncoupled oligodendrocytes could be distinguished from the coupled one by their higher input resistance.

Dye transfer experiments in mice Cx47$^{M282T/M282T}$ revealed that the mutated Cx47M282T causes a loss of function *in situ*, since inter-oligodendrocytic as well as oligodendrocytic-astrocytic coupling is significantly diminished, similarly to the reduction of gap junctional communication observed in Cx47-deficient mice. In addition homozygous Cx47M282T do not affect Cx32 proper function. With these approaches the present work clearly demonstrates that oligodendrocytes in white matter directly couple to each other depending on Cx47 and Cx32 expression. In contrast, oligodendrocyte-to-astrocyte coupling is minor, but necessary to extend the oligodendrocytic syncytium. In addition a smaller population of glial precursor cells belongs to the network. Altogether this study shows for the first time that oligodendrocytes form a syncytium among each other in situ indicating that the establishment of this network has an impact on myelination.

7 Zusammenfassung

In Oligodendrozyten, den Myelin bildenden Gliazellen des ZNS, stellen Cx32 und Cx47 die wichtigsten Vertreter der Connexine dar. Connexine besitzen als molekulare Einheit der Gap Junctions neben ihrer Bedeutung für Zell-Zell-Kommunikation eine essenzielle Rolle für die Ausbildung und Erhaltung der Myelinscheide, denn Mutationen in Connexin Genen beim Menschen führen zu schwerwiegenden Myelin assoziierten Krankheiten.. Elektronenmikroskopische Untersuchungen haben gezeigt, dass Oligodendrozyten der weissen Substanz Gap Junctions nur mit Astrozyten ausbilden, nicht aber mit anderen Oligodendrozyten. Oligodendrozyten in Kultur hingegen bilden untereinander Gap Junctions aus. Für ein besseres molekulares Verständnis der auf Connexin-Mutationen beruhenden Krankheiten ist es von Bedeutung zu wissen, welche Connexin Typen innerhalb der weißen Substanz funktionelle Gap Junctions ausbilden können.

In dieser Arbeit wurde daher die funktionelle Kopplung zwischen Oligodendrozyten und Astrozyten im Corpus Callosum verschiedener Connexin-defizienter Mauslinien bzw. deren Wildtypen untersucht. Desweiteren soll die Bedeutung der Cx47M282T Punktmutation auf die Ausbildung funktioneller Netzwerke zwischen Oligodendrozyten erforscht werden. Die Mauslinie $Cx47^{M282T/M282T}$ stellt ein Modell zur Untersuchung der beim Menschen auftretenden Leukodystrophie Paelizeus-Merzbacher-like-disease (PMLD) dar. Mithilfe der Patch-Clamp Technik wurden Oligodendrozyten in akuten Hirnschnittpräparaten des Corpus Callosums 10-15 Tage alter Mäuse mit dem Gap-Junction permeablen Indikatorfarbstoff Biocytin gefüllt. Zur Darstellung der gekoppelten Zellen wurde eine immunhistochemische Färbung des Indikatorfarbstoffes Biocytin mit Fluorchrom-konjugierten Streptavidin mit spezifischen Färbungen für Gliazellen kombiniert (CNPase zur Darstellung von Oligodendrozyten, GFAP zur Darstellung von Astrozyten). Die durch Biocytin markierten Netzwerke bestanden im Mittel aus 61 gekoppelten Zellen, wovon 77% den Oligodendrozytenmarker CNPase exprimierten, 9% GFAP-positiv waren und 14% weder CNPase noch GFAP exprimierten. Ca. 50 % der Zellen aus der zuletzt genannten Gruppe exprimierten Olig2, einige wenige waren positiv für NG2, beides Marker für Oligodendrozyten-Vorläufer. Es ist bekannt, dass Oligodendrozyten Cx47, Cx32 und Cx29, Astrozyten hingegen die Connexine Cx43 undCx30 exprimieren In Cx47-defizienten Mäusen war die Anzahl der gekoppelten Zellen um 80% reduziert.

Während die Deletion von Cx32 oder Cx29 nicht zu einer messbaren Reduktion der gekoppelten Zellen führte, war die Kopplung der Zellen in Cx47/Cx32-doppelt defizienten Mäusen vollständig aufgehoben. In Cx47-defizienten Tieren war die Kopplung zwischen Astrozyten und Oligodendrozyten komplett aufgehoben. Das Fehlen des astrozytären Cx43 führte zu einer Reduktion der Oligodendrozyten-Kopplung und zu einem kompletten Verlust der Kopplung innerhalb der Oligodendrozyten-Vorläuferzellen, wogegen die Kopplung der Astrozyten nicht beeinträchtigt war. In Tieren, denen sowohl astrozytäres Cx43 und Cx30 fehlte, war die Anzahl der gekoppelten Zellen deutlich reduziert und die Kopplung zwischen Oligodendrozyten und Astrozyten komplett aufgehoben. In dieser Mauslinie wurde auch niemals eine Kopplung zwischen Oligodendrozyten-Vorläuferzellen beobachtet. Desweiteren ließen sich (bei dieser Mauslinie) ungekoppelte von gekoppelten Oligodendrozyen anhand ihres höheren elektrischen Eingangswiderstandes unterscheiden.

Mithilfe von Dye-Transfer Experimenten an $Cx47^{M282T/M282T}$ Mäusen konnte gezeigt werden, dass die CxM282T Mutation zu einem Funktionsverlust *in situ* führt, denn in diesem Modell war sowohl die Kopplung zwischen Oligodendrozyten als auch zwischen Oligodendrozyten und Astrozyten deutlich verringert, und somit vergleichbar mit den an den Cx47-defizienten Mäusen gefunden Ergebnissen. Die Ergebnisse dieser Arbeit zeigen, dass Oligodendrozyten der weißen Substanz direkt untereinander gekoppelt sind, und diese Kopplung von der Expression des Cx47 und Cx32 abhängt. Im Gegensatz dazu ist die Kopplung zwischen Astrozyten und Oligodendrozyten wesentlich schwächer ausgeprägt, aber wiederum notwendig für die Ausbildung des Syncytiums aus Oligodendrozyten. Desweiteren konnte gezeigt werden, dass auch eine kleinere Population von Vorläuferzellen ist in das Netzwerk eingebunden ist. Die Ergebnisse dieser Arbeit zeigen zum ersten mal, dass die Olgodendrozyten untereinander ein funktionelles Netzwerk ausbilden können und dass dieses von Bedeutung für die Myelinisierung ist.

8 References

Aboitiz F, Scheibel AB, Fisher RS, Zaidel E. 1992. Fiber composition of the human corpus callosum. Brain Res 598(1-2):143-53.

Ahn M, Lee J, Gustafsson A, Enriquez A, Lancaster E, Sul JY, Haydon PG, Paul DL, Huang Y, Abrams CK, Scherer SS. 2008. Cx29 and Cx32, two connexins expressed by myelinating glia, do not interact and are functionally distinct. J Neurosci Res 86(5):992-1006.

Altevogt BM, Kleopa KA, Postma FR, Scherer SS, Paul DL. 2002. Connexin29 is uniquely distributed within myelinating glial cells of the central and peripheral nervous systems. J Neurosci 22(15):6458-70.

Altevogt BM, Paul DL. 2004. Four classes of intercellular channels between glial cells in the CNS. J Neurosci 24(18):4313-23.

Anzini P, Neuberg DH, Schachner M, Nelles E, Willecke K, Zielasek J, Toyka KV, Suter U, Martini R. 1997. Structural abnormalities and deficient maintenance of peripheral nerve myelin in mice lacking the gap junction protein connexin 32. J Neurosci 17(12):4545-51.

Araque A, Parpura V, Sanzgiri RP, Haydon PG. 1999. Tripartite synapses: glia, the unacknowledged partner. Trends Neurosci 22(5):208-15.

Bakiri Y, Burzomato V, Frugier G, Hamilton NB, Karadottir R, Attwell D. 2009. Glutamatergic signaling in the brain's white matter. Neuroscience 158(1):266-74.

Balda MS, Matter K. 2000. The tight junction protein ZO-1 and an interacting transcription factor regulate ErbB-2 expression. EMBO J 19(9):2024-33.

Bansal R, Stefansson K, Pfeiffer SE. 1992. Proligodendroblast antigen (POA), a developmental antigen expressed by A007/O4-positive oligodendrocyte progenitors prior to the appearance of sulfatide and galactocerebroside. J Neurochem 58(6):2221-9.

Barres BA. 2008. The mystery and magic of glia: a perspective on their roles in health and disease. Neuron 60(3):430-40.

Barres BA, Chun LL, Corey DP. 1988. Ion channel expression by white matter glia: I. Type 2 astrocytes and oligodendrocytes. Glia 1(1):10-30.

Baumann N, Pham-Dinh D. 2001. Biology of oligodendrocyte and myelin in the mammalian central nervous system. Physiol Rev 81(2):871-927.

Bedner P, Niessen H, Odermatt B, Kretz M, Willecke K, Harz H. 2006. Selective permeability of different connexin channels to the second messenger cyclic AMP. J Biol Chem 281(10):6673-81.

Behar T, McMorris FA, Novotny EA, Barker JL, Dubois-Dalcq M. 1988. Growth and differentiation properties of O-2A progenitors purified from rat cerebral hemispheres. J Neurosci Res 21(2-4):168-80.

Ben-Hur T, Rogister B, Murray K, Rougon G, Dubois-Dalcq M. 1998. Growth and fate of PSA-NCAM+ precursors of the postnatal brain. J Neurosci 18(15):5777-88.

Bennett MV, Contreras JE, Bukauskas FF, Saez JC. 2003. New roles for astrocytes: gap junction hemichannels have something to communicate. Trends Neurosci 26(11):610-7.

Bennett MV, Zukin RS. 2004. Electrical coupling and neuronal synchronization in the Mammalian brain. Neuron 41(4):495-511.

Berger T, Muller T, Kettenmann H. 1995. Developmental regulation of ion channels and receptors on glial cells. Perspect Dev Neurobiol 2(4):347-56.

Berger T, Schnitzer J, Kettenmann H. 1991. Developmental changes in the membrane current pattern, K+ buffer capacity, and morphology of glial cells in the corpus callosum slice. J Neurosci 11(10):3008-24.

Bergles DE, Roberts JD, Somogyi P, Jahr CE. 2000. Glutamatergic synapses on oligodendrocyte precursor cells in the hippocampus. Nature 405(6783):187-91.

Bergoffen J, Scherer SS, Wang S, Scott MO, Bone LJ, Paul DL, Chen K, Lensch MW, Chance PF, Fischbeck KH. 1993. Connexin mutations in X-linked Charcot-Marie-Tooth disease. Science 262(5142):2039-42.

Blankenfeld Gv GV, Verkhratsky AN, Kettenmann H. 1992. Ca2+ Channel Expression in the Oligodendrocyte Lineage. Eur J Neurosci 4(11):1035-1048.

Blomstrand F, Venance L, Siren AL, Ezan P, Hanse E, Glowinski J, Ehrenreich H, Giaume C. 2004. Endothelins regulate astrocyte gap junctions in rat hippocampal slices. Eur J Neurosci 19(4):1005-15.

Bruzzone R, White TW, Paul DL. 1996. Connections with connexins: the molecular basis of direct intercellular signaling. Eur J Biochem 238(1):1-27.

Bugiani M, Al Shahwan S, Lamantea E, Bizzi A, Bakhsh E, Moroni I, Balestrini MR, Uziel G, Zeviani M. 2006. GJA12 mutations in children with recessive hypomyelinating leukoencephalopathy. Neurology 67(2):273-9.

Butt AM, Hamilton N, Hubbard P, Pugh M, Ibrahim M. 2005. Synantocytes: the fifth element. J Anat 207(6):695-706.

Butt AM, Ransom BR. 1989. Visualization of oligodendrocytes and astrocytes in the intact rat optic nerve by intracellular injection of lucifer yellow and horseradish peroxidase. Glia 2(6):470-5.

Butt AM, Ransom BR. 1993. Morphology of astrocytes and oligodendrocytes during development in the intact rat optic nerve. J Comp Neurol 338(1):141-58.

Chang A, Nishiyama A, Peterson J, Prineas J, Trapp BD. 2000. NG2-positive oligodendrocyte progenitor cells in adult human brain and multiple sclerosis lesions. J Neurosci 20(17):6404-12.

Cheng A, Tang H, Cai J, Zhu M, Zhang X, Rao M, Mattson MP. 2004. Gap junctional communication is required to maintain mouse cortical neural progenitor cells in a proliferative state. Dev Biol 272:203–216.

Chvatal A, Anderova M, Ziak D, Sykova E. 1999. Glial depolarization evokes a larger potassium accumulation around oligodendrocytes than around astrocytes in gray matter of rat spinal cord slices. J Neurosci Res 56(5):493-505.

Cronin M, Anderson PN, Cook JE, Green CR, Becker DL. 2008. Blocking connexin43 expression reduces inflammation and improves functional recovery after spinal cord injury. Mol Cell Neurosci 39(2):152-60.

D'Ambrosio R, Wenzel J, Schwartzkroin PA, McKhann GM II, Janigro D. 1998. Functional specialization and topographic segregation of hippocampal astrocytes. J Neurosci 18(12):4425-38.

Dahl E, Winterhager E, Reuss B, Traub O, Butterweck A, Willecke K. 1996. Expression of the gap junction proteins connexin31 and connexin43 correlates with communication compartments in extraembryonic tissues and in the gastrulating mouse embryo, respectively. J Cell Sci 109 (Pt 1):191-7.

de Roos AD, van Zoelen EJ, Theuvenet AP. 1996. Determination of gap junctional intercellular communication by capacitance measurements. Pflugers Arch 431(4):556-63.

Deber CM, Reynolds SJ. 1991. Central nervous system myelin: structure, function, and pathology. Clin Biochem 24(2):113-34.

Dermietzel R, Traub O, Hwang TK, Beyer E, Bennett MV, Spray DC, Willecke K. 1989. Differential expression of three gap junction proteins in developing and mature brain tissues. Proc Natl Acad Sci U S A 86(24):10148-52.

Eiberger J, Kibschull M, Strenzke N, Schober A, Bussow H, Wessig C, Djahed S, Reucher H, Koch DA, Lautermann J, Moser T, Winterhager E, Willecke K. 2006. Expression pattern and functional characterization of connexin29 in transgenic mice. Glia 53(6):601-11.

Elfgang C, Eckert R, Lichtenberg-Frate H, Butterweck A, Traub O, Klein RA, Hulser DF, Willecke K. 1995. Specific permeability and selective formation of gap junction channels in connexin-transfected HeLa cells. J Cell Biol 129(3):805-17.

Evans WH, De Vuyst E, Leybaert L. 2006. The gap junction cellular internet: connexin hemichannels enter the signalling limelight. Biochem J 397(1):1-14.

Filbin MT. 1996. The muddle with MAG. Mol Cell Neurosci 8(2-3):84-92.

Filippov MA, Hormuzdi SG, Fuchs EC, Monyer H. 2003. A reporter allele for investigating connexin 26 gene expression in the mouse brain. Eur J Neurosci 18(12):3183-92.

Finkelstein A. 1994. Gap junctions and intercellular communications. Science 265(5175):1017-8; author reply 1019-20.

Fredman P, Magnani JL, Nirenberg M, Ginsburg V. 1984. Monoclonal antibody A2B5 reacts with many gangliosides in neuronal tissue. Arch Biochem Biophys 233(2):661-6.

Gaietta G, Deerinck TJ, Adams SR, Bouwer J, Tour O, Laird DW, Sosinsky GE, Tsien RY, Ellisman MH. 2002. Multicolor and electron microscopic imaging of connexin trafficking. Science 296(5567):503-7.

Garbern J, Cambi F, Shy M, Kamholz J. 1999. The molecular pathogenesis of Pelizaeus-Merzbacher disease. Arch Neurol 56(10):1210-4.

Garbern JY, Yool DA, Moore GJ, Wilds IB, Faulk MW, Klugmann M, Nave KA, Sistermans EA, van der Knaap MS, Bird TD, Shy ME, Kamholz JA, Griffiths IR. 2002. Patients lacking the major CNS myelin protein, proteolipid protein 1,

develop length-dependent axonal degeneration in the absence of demyelination and inflammation. Brain 125(Pt 3):551-61.

Gard AL, Pfeiffer SE. 1990. Two proliferative stages of the oligodendrocyte lineage (A2B5+O4- and O4+GalC-) under different mitogenic control. Neuron 5(5):615-25.

Goldberg GS, Moreno AP, Lampe PD. 2002. Gap junctions between cells expressing connexin 43 or 32 show inverse permselectivity to adenosine and ATP. J Biol Chem 277(39):36725-30.

Gravel M, Peterson J, Yong VW, Kottis V, Trapp B, Braun PE. 1996. Overexpression of 2',3'-cyclic nucleotide 3'-phosphodiesterase in transgenic mice alters oligodendrocyte development and produces aberrant myelination. Mol Cell Neurosci 7(6):453-66.

Griffiths I, Klugmann M, Anderson T, Yool D, Thomson C, Schwab MH, Schneider A, Zimmermann F, McCulloch M, Nadon N, Nave KA. 1998. Axonal swellings and degeneration in mice lacking the major proteolipid of myelin. Science 280(5369):1610-3.

Grinspan JB, Coulalaglou M, Beesley JS, Carpio DF, Scherer SS. 1998. Maturation-dependent apoptotic cell death of oligodendrocytes in myelin-deficient rats. J Neurosci Res 54(5):623-34.

Grinspan JB, Franceschini B. 1995. Platelet-derived growth factor is a survival factor for PSA-NCAM+ oligodendrocyte pre-progenitor cells. J Neurosci Res 41(4):540-51.

Grosche J, Kettenmann H, Reichenbach A. 2002. Bergmann glial cells form distinct morphological structures to interact with cerebellar neurons. J Neurosci Res 68(2):138-49.

Grosche J, Matyash V, Moller T, Verkhratsky A, Reichenbach A, Kettenmann H. 1999. Microdomains for neuron-glia interaction: parallel fiber signaling to Bergmann glial cells. Nat Neurosci 2(2):139-43.

Gu S, Yu XS, Yin X, Jiang JX. 2003. Stimulation of lens cell differentiation by gap junction protein connexin 45.6. Invest Ophthalmol Vis Sci 44(5):2103-11.

Haas B, Schipke CG, Peters O, Sohl G, Willecke K, Kettenmann H. 2006. Activity-dependent ATP-waves in the mouse neocortex are independent from astrocytic calcium waves. Cereb Cortex 16(2):237-46.

Haas S, Brockhaus J, Verkhratsky A, Kettenmann H. 1996. ATP-induced membrane currents in ameboid microglia acutely isolated from mouse brain slices. Neuroscience 75(1):257-61.

Hahn AF, Ainsworth PJ, Naus CC, Mao J, Bolton CF. 2000. Clinical and pathological observations in men lacking the gap junction protein connexin 32. Muscle Nerve Suppl 9:S39-48.

Halbrich M, Barnes J, Bunge M, Joshi C. 2008. A V139M mutation also causes the reversible CNS phenotype in CMTX. Can J Neurol Sci 35(3):372-4.

Hamill OP, Marty A, Neher E, Sakmann B, Sigworth FJ. 1981. Improved patch-clamp techniques for high-resolution current recording from cells and cell-free membrane patches. Pflugers Arch 391(2):85-100.

Hampson EC, Robinson SR. 1995. Heterogeneous morphology and tracer coupling patterns of retinal oligodendrocytes. Philos Trans R Soc Lond B Biol Sci 349(1330):353-64.

Hanemann CO, Bergmann C, Senderek J, Zerres K, Sperfeld AD. 2003. Transient, recurrent, white matter lesions in X-linked Charcot-Marie-Tooth disease with novel connexin 32 mutation. Arch Neurol 60(4):605-9.

Hardy R, Reynolds R. 1993. Neuron-oligodendroglial interactions during central nervous system development. J Neurosci Res 36(2):121-6.

Harks EG, de Roos AD, Peters PH, de Haan LH, Brouwer A, Ypey DL, van Zoelen EJ, Theuvenet AP. 2001. Fenamates: a novel class of reversible gap junction blockers. J Pharmacol Exp Ther 298(3):1033-41.

Harris AL. 2001. Emerging issues of connexin channels: biophysics fills the gap. Q Rev Biophys 34(3):325-472.

Harris AL. 2007. Connexin channel permeability to cytoplasmic molecules. Prog Biophys Mol Biol 94(1-2):120-43.

Hart IK, Richardson WD, Bolsover SR, Raff MC. 1989. PDGF and intracellular signaling in the timing of oligodendrocyte differentiation. J Cell Biol 109(6 Pt 2):3411-7.

Hildebrand C, Remahl S, Persson H, Bjartmar C. 1993. Myelinated nerve fibres in the CNS. Prog Neurobiol 40(3):319-84.

Hildebrand JG, Christensen TA, Harrow ID, Homberg U, Matsumoto SG, Waldrop BR. 1992. The roles of local interneurons in the processing of olfactory information in the antennal lobes of the moth Manduca sexta. Acta Biol Hung 43(1-4):167-74.

Hockfield S, McKay RD. 1985. Identification of major cell classes in the developing mammalian nervous system. J Neurosci 5(12):3310-28.

Houades V, Koulakoff A, Ezan P, Seif I, Giaume C. 2008. Gap junction-mediated astrocytic networks in the mouse barrel cortex. J Neurosci 28(20):5207-17.

Kamasawa N, Sik A, Morita M, Yasumura T, Davidson KG, Nagy JI, Rash JE. 2005. Connexin-47 and connexin-32 in gap junctions of oligodendrocyte somata, myelin sheaths, paranodal loops and Schmidt-Lanterman incisures: implications for ionic homeostasis and potassium siphoning. Neuroscience 136(1):65-86.

Karadottir R, Cavelier P, Bergersen LH, Attwell D. 2005. NMDA receptors are expressed in oligodendrocytes and activated in ischaemia. Nature 438(7071):1162-6.

Karram K, Chatterjee N, Trotter J. 2005. NG2-expressing cells in the nervous system: role of the proteoglycan in migration and glial-neuron interaction. J Anat 207(6):735-44.

Karram K, Goebbels S, Schwab M, Jennissen K, Seifert G, Steinhauser C, Nave KA, Trotter J. 2008. NG2-expressing cells in the nervous system revealed by the NG2-EYFP-knockin mouse. Genesis 46(12):743-57.

Kettenmann H. 1999. Physiology of glial cells. Adv Neurol 79:565-71.

Kettenmann H, Orkand RK, Schachner M. 1983. Coupling among identified cells in mammalian nervous system cultures. J Neurosci 3(3):506-16.

Kettenmann H, Sonnhof U, Camerer H, Kuhlmann S, Orkand RK, Schachner M. 1984. Electrical properties of oligodendrocytes in culture. Pflugers Arch 401(4):324-32.

Kettenmann H, Verkhratsky A. 2008. Neuroglia: the 150 years after. Trends Neurosci 31(12):653-9.

Kim JY, Sun Q, Oglesbee M, Yoon SO. 2003. The role of ErbB2 signaling in the onset of terminal differentiation of oligodendrocytes in vivo. J Neurosci 23(13):5561-71.

Kleopa KA, Orthmann JL, Enriquez A, Paul DL, Scherer SS. 2004. Unique distributions of the gap junction proteins connexin29, connexin32, and connexin47 in oligodendrocytes. Glia 47(4):346-57.

Kleopa KA, Scherer SS. 2002. Inherited neuropathies. Neurol Clin 20(3):679-709.

Kressin K, Kuprijanova E, Jabs R, Seifert G, Steinhauser C. 1995. Developmental regulation of Na+ and K+ conductances in glial cells of mouse hippocampal brain slices. Glia 15(2):173-87.

Kunze A, Congreso MR, Hartmann C, Wallraff-Beck A, Huttmann K, Bedner P, Requardt R, Seifert G, Redecker C, Willecke K, Hofmann A, Pfeifer A, Theis M, Steinhauser C. 2009. Connexin expression by radial glia-like cells is required for neurogenesis in the adult dentate gyrus. Proc Natl Acad Sci U S A 106(27):11336-41.

Lendahl U, Zimmerman LB, McKay RD. 1990. CNS stem cells express a new class of intermediate filament protein. Cell 60(4):585-95.

Levison SW, Goldman JE. 1993. Both oligodendrocytes and astrocytes develop from progenitors in the subventricular zone of postnatal rat forebrain. Neuron 10(2):201-12.

Li J, Hertzberg EL, Nagy JI. 1997. Connexin32 in oligodendrocytes and association with myelinated fibers in mouse and rat brain. J Comp Neurol 379(4):571-91.

Li X, Ionescu AV, Lynn BD, Lu S, Kamasawa N, Morita M, Davidson KG, Yasumura T, Rash JE, Nagy JI. 2004. Connexin47, connexin29 and connexin32 co-expression in oligodendrocytes and Cx47 association with zonula occludens-1 (ZO-1) in mouse brain. Neuroscience 126(3):611-30.

Li X, Penes M, Odermatt B, Willecke K, Nagy JI. 2008. Ablation of Cx47 in transgenic mice leads to the loss of MUPP1, ZONAB and multiple connexins at oligodendrocyte-astrocyte gap junctions. Eur J Neurosci 28(8):1503-17.

Ligon KL, Fancy SP, Franklin RJ, Rowitch DH. 2006. Olig gene function in CNS development and disease. Glia 54(1):1-10.

Lu QR, Sun T, Zhu Z, Ma N, Garcia M, Stiles CD, Rowitch DH. 2002. Common developmental requirement for Olig function indicates a motor neuron/oligodendrocyte connection. Cell 109(1):75-86.

Lu QR, Yuk D, Alberta JA, Zhu Z, Pawlitzky I, Chan J, McMahon AP, Stiles CD, Rowitch DH. 2000. Sonic hedgehog--regulated oligodendrocyte lineage genes encoding bHLH proteins in the mammalian central nervous system. Neuron 25(2):317-29.

Lutz SE, Zhao Y, Gulinello M, Lee SC, Raine CS, Brosnan CF. 2009. Deletion of astrocyte connexins 43 and 30 leads to a dysmyelinating phenotype and hippocampal CA1 vacuolation. J Neurosci 29(24):7743-52.

Magistretti PJ. 2006. Neuron-glia metabolic coupling and plasticity. J Exp Biol 209(Pt 12):2304-11.

Massa PT, Mugnaini E. 1982. Cell junctions and intramembrane particles of astrocytes and oligodendrocytes: a freeze-fracture study. Neuroscience 7(2):523-38.

Massa PT, Mugnaini E. 1985. Cell-cell junctional interactions and characteristic plasma membrane features of cultured rat glial cells. Neuroscience 14(2):695-709.

Mazzeo A, Di Leo R, Toscano A, Muglia M, Patitucci A, Messina C, Vita G. 2008. Charcot-Marie-Tooth type X: unusual phenotype of a novel CX32 mutation. Eur J Neurol 15(10):1140-2.

Melanson-Drapeau L, Beyko S, Dave S, Hebb AL, Franks DJ, Sellitto C, Paul DL, Bennett SA. 2003. Oligodendrocyte progenitor enrichment in the connexin32 null-mutant mouse. J Neurosci 23(5):1759-68.

Meme W, Vandecasteele M, Giaume C, Venance L. 2009. Electrical coupling between hippocampal astrocytes in rat brain slices. Neurosci Res 63(4):236-43.

Menichella DM, Goodenough DA, Sirkowski E, Scherer SS, Paul DL. 2003. Connexins are critical for normal myelination in the CNS. J Neurosci 23(13):5963-73.

Menichella DM, Majdan M, Awatramani R, Goodenough DA, Sirkowski E, Scherer SS, Paul DL. 2006. Genetic and physiological evidence that oligodendrocyte gap junctions contribute to spatial buffering of potassium released during neuronal activity. J Neurosci 26(43):10984-91.

Mercier F, Hatton GI. 2001. Connexin 26 and basic fibroblast growth factor are expressed primarily in the subpial and subependymal layers in adult brain parenchyma: roles in stem cell proliferation and morphological plasticity? J Comp Neurol 431(1):88-104.

Morell P. 1984. A correlative synopsis of the leukodystrophies. Neuropediatrics 15 Suppl:62-5.

Morell P, Ousley AH. 1994. Metabolic turnover of myelin glycerophospholipids. Neurochem Res 19(8):967-74.

Muller J, Reyes-Haro D, Pivneva T, Nolte C, Schaette R, Lubke J, Kettenmann H. 2009. The principal neurons of the medial nucleus of the trapezoid body and NG2(+) glial cells receive coordinated excitatory synaptic input. J Gen Physiol 134(2):115-27.

Mulligan SJ, MacVicar BA. 2004. Calcium transients in astrocyte endfeet cause cerebrovascular constrictions. Nature 431(7005):195-9.

Nadarajah B, Jones AM, Evans WH, Parnavelas JG. 1997. Differential expression of connexins during neocortical development and neuronal circuit formation. J Neurosci 17(9):3096-111.

Nagy JI, Ionescu AV, Lynn BD, Rash JE. 2003a. Connexin29 and connexin32 at oligodendrocyte and astrocyte gap junctions and in myelin of the mouse central nervous system. J Comp Neurol 464(3):356-70.

Nagy JI, Ionescu AV, Lynn BD, Rash JE. 2003b. Coupling of astrocyte connexins Cx26, Cx30, Cx43 to oligodendrocyte Cx29, Cx32, Cx47: Implications from normal and connexin32 knockout mice. Glia 44(3):205-18.

Nagy JI, Li X, Rempel J, Stelmack G, Patel D, Staines WA, Yasumura T, Rash JE. 2001. Connexin26 in adult rodent central nervous system: demonstration at astrocytic gap junctions and colocalization with connexin30 and connexin43. J Comp Neurol 441(4):302-23.

Nagy JI, Rash JE. 2000. Connexins and gap junctions of astrocytes and oligodendrocytes in the CNS. Brain Res Brain Res Rev 32(1):29-44.

Nakase T, Sohl G, Theis M, Willecke K, Naus CC. 2004. Increased apoptosis and inflammation after focal brain ischemia in mice lacking connexin43 in astrocytes. Am J Pathol 164(6):2067-75.

Neijssen J, Herberts C, Drijfhout JW, Reits E, Janssen L, Neefjes J. 2005. Cross-presentation by intercellular peptide transfer through gap junctions. Nature 434(7029):83-8.

Nelles E, Butzler C, Jung D, Temme A, Gabriel HD, Dahl U, Traub O, Stumpel F, Jungermann K, Zielasek J, Toyka KV, Dermietzel R, Willecke K. 1996. Defective propagation of signals generated by sympathetic nerve stimulation in the liver of connexin32-deficient mice. Proc Natl Acad Sci U S A 93(18):9565-70.

Newman EA. 1986. High potassium conductance in astrocyte endfeet. Science 233(4762):453-4.

Niessen H, Harz H, Bedner P, Kramer K, Willecke K. 2000. Selective permeability of different connexin channels to the second messenger inositol 1,4,5-trisphosphate. J Cell Sci 113 (Pt 8):1365-72.

Nishiyama A. 2007. Polydendrocytes: NG2 cells with many roles in development and repair of the CNS. Neuroscientist 13(1):62-76.

Nishiyama A, Chang A, Trapp BD. 1999. NG2+ glial cells: a novel glial cell population in the adult brain. J Neuropathol Exp Neurol 58(11):1113-24.

Nishiyama A, Komitova M, Suzuki R, Zhu X. 2009. Polydendrocytes (NG2 cells): multifunctional cells with lineage plasticity. Nat Rev Neurosci 10(1):9-22.

Nishiyama A, Lin XH, Giese N, Heldin CH, Stallcup WB. 1996. Interaction between NG2 proteoglycan and PDGF alpha-receptor on O2A progenitor cells is required for optimal response to PDGF. J Neurosci Res 43(3):315-30.

Odermatt B, Wellershaus K, Wallraff A, Seifert G, Degen J, Euwens C, Fuss B, Bussow H, Schilling K, Steinhauser C, Willecke K. 2003. Connexin 47 (Cx47)-deficient mice with enhanced green fluorescent protein reporter gene reveal predominant oligodendrocytic expression of Cx47 and display vacuolized myelin in the CNS. J Neurosci 23(11):4549-59.

Olsen ML, Sontheimer H. 2008. Functional implications for Kir4.1 channels in glial biology: from K+ buffering to cell differentiation. J Neurochem 107(3):589-601.

Orkand RK, Nicholls JG, Kuffler SW. 1966. Effect of nerve impulses on the membrane potential of glial cells in the central nervous system of amphibia. J Neurophysiol 29(4):788-806.

Orthmann-Murphy JL, Abrams CK, Scherer SS. 2008. Gap junctions couple astrocytes and oligodendrocytes. J Mol Neurosci 35(1):101-16.

Orthmann-Murphy JL, Enriquez AD, Abrams CK, Scherer SS. 2007a. Loss-of-function GJA12/Connexin47 mutations cause Pelizaeus-Merzbacher-like disease. Mol Cell Neurosci 34(4):629-41.

Orthmann-Murphy JL, Freidin M, Fischer E, Scherer SS, Abrams CK. 2007b. Two distinct heterotypic channels mediate gap junction coupling between astrocyte and oligodendrocyte connexins. J Neurosci 27(51):13949-57.

Orthmann-Murphy JL, Salsano E, Abrams CK, Bizzi A, Uziel G, Freidin MM, Lamantea E, Zeviani M, Scherer SS, Pareyson D. 2009. Hereditary spastic paraplegia is a novel phenotype for GJA12/GJC2 mutations. Brain 132(Pt 2):426-38.

Pastor A, Kremer M, Moller T, Kettenmann H, Dermietzel R. 1998. Dye coupling between spinal cord oligodendrocytes: differences in coupling efficiency between gray and white matter. Glia 24(1):108-20.

Penes MC, Li X, Nagy JI. 2005. Expression of zonula occludens-1 (ZO-1) and the transcription factor ZO-1-associated nucleic acid-binding protein (ZONAB)-MsY3 in glial cells and colocalization at oligodendrocyte and astrocyte gap junctions in mouse brain. Eur J Neurosci 22(2):404-18.

Peters A. 2004. A fourth type of neuroglial cell in the adult central nervous system. J Neurocytol 33(3):345-57.

Peters A, Josephson K, Vincent SL. 1991. Effects of aging on the neuroglial cells and pericytes within area 17 of the rhesus monkey cerebral cortex. Anat Rec 229(3):384-98.

Peters O, Schipke CG, Philipps A, Haas B, Pannasch U, Wang LP, Benedetti B, Kingston AE, Kettenmann H. 2009. Astrocyte function is modified by Alzheimer's disease-like pathology in aged mice. J Alzheimers Dis 18(1):177-89.

Pfeiffer SE, Warrington AE, Bansal R. 1993. The oligodendrocyte and its many cellular processes. Trends Cell Biol 3(6):191-7.

Pfrieger FW, Barres BA. 1995. What the fly's glia tell the fly's brain. Cell 83(5):671-4.

Poliak S, Peles E. 2003. The local differentiation of myelinated axons at nodes of Ranvier. Nat Rev Neurosci 4(12):968-80.

Postma FR, Hengeveld T, Alblas J, Giepmans BN, Zondag GC, Jalink K, Moolenaar WH. 1998. Acute loss of cell-cell communication caused by G protein-coupled receptors: a critical role for c-Src. J Cell Biol 140(5):1199-209.

Prime G, Horn G, Sutor B. 2000. Time-related changes in connexin mRNA abundance in the rat neocortex during postnatal development. Brain Res Dev Brain Res 119(1):111-25.

Purves D, Augustine GJ, Fitzpatrick D, Hall WC, LaMantia AS, McNamara JO, White LE. 2001. Increased Conduction Velocity as a Result of Myelination. Neuroscience 2nd edition, Sinauer Associate Inc.

Raff MC, Abney ER, Fok-Seang J. 1985. Reconstitution of a developmental clock in vitro: a critical role for astrocytes in the timing of oligodendrocyte differentiation. Cell 42(1):61-9.

Raff MC, Miller RH, Noble M. 1983a. Glial cell lineages in the rat optic nerve. Cold Spring Harb Symp Quant Biol 48 Pt 2:569-72.

Raff MC, Miller RH, Noble M. 1983b. A glial progenitor cell that develops in vitro into an astrocyte or an oligodendrocyte depending on culture medium. Nature 303(5916):390-6.

Raff MC, Mirsky R, Fields KL, Lisak RP, Dorfman SH, Silberberg DH, Gregson NA, Leibowitz S, Kennedy MC. 1978. Galactocerebroside is a specific cell-surface antigenic marker for oligodendrocytes in culture. Nature 274(5673):813-6.

Raff MC, Williams BP, Miller RH. 1984. The in vitro differentiation of a bipotential glial progenitor cell. EMBO J 3(8):1857-64.

Ransom BR, Kettenmann H. 1990. Electrical coupling, without dye coupling, between mammalian astrocytes and oligodendrocytes in cell culture. Glia 3(4):258-66.

Requardt RP, Kaczmarczyk L, Dublin P, Wallraff-Beck A, Mikeska T, Degen J, Waha A, Steinhauser C, Willecke K, Theis M. 2009. Quality control of astrocyte-directed Cre transgenic mice: The benefits of a direct link between loss of gene expression and reporter activation. Glia 57(6):680-92.

Reynolds R, Wilkin GP. 1988. Development of macroglial cells in rat cerebellum. II. An in situ immunohistochemical study of oligodendroglial lineage from precursor to mature myelinating cell. Development 102(2):409-25.

Robinson SR, Hampson EC, Munro MN, Vaney DI. 1993. Unidirectional coupling of gap junctions between neuroglia. Science 262(5136):1072-4.

Rorig B, Klausa G, Sutor B. 1996. Intracellular acidification reduced gap junction coupling between immature rat neocortical pyramidal neurones. J Physiol 490 (Pt 1):31-49.

Roscoe WA, Messersmith E, Meyer-Franke A, Wipke B, Karlik SJ. 2007. Connexin 43 gap junction proteins are up-regulated in remyelinating spinal cord. J Neurosci Res 85(5):945-53.

Rouach N, Koulakoff A, Abudara V, Willecke K, Giaume C. 2008. Astroglial metabolic networks sustain hippocampal synaptic transmission. Science 322(5907):1551-5.

Salviati L, Trevisson E, Baldoin MC, Toldo I, Sartori S, Calderone M, Tenconi R, Laverda A. 2007. A novel deletion in the GJA12 gene causes Pelizaeus-Merzbacher-like disease. Neurogenetics 8(1):57-60.

Scherer SS, Deschenes SM, Xu YT, Grinspan JB, Fischbeck KH, Paul DL. 1995. Connexin32 is a myelin-related protein in the PNS and CNS. J Neurosci 15(12):8281-94.

Scherer SS, Wrabetz L. 2008. Molecular mechanisms of inherited demyelinating neuropathies. Glia 56(14):1578-89.

Schiffmann R, Boespflug-Tanguy O. 2001. An update on the leukodsytrophies. Curr Opin Neurol 14(6):789-94.

Schneider A, Montague P, Griffiths I, Fanarraga M, Kennedy P, Brophy P, Nave KA. 1992. Uncoupling of hypomyelination and glial cell death by a mutation in the proteolipid protein gene. Nature 358(6389):758-61.

Sohl G, Maxeiner S, Willecke K. 2005. Expression and functions of neuronal gap junctions. Nat Rev Neurosci 6(3):191-200.

Sohl G, Odermatt B, Maxeiner S, Degen J, Willecke K. 2004. New insights into the expression and function of neural connexins with transgenic mouse mutants. Brain Res Brain Res Rev 47(1-3):245-59.

Sommer I, Schachner M. 1981. Monoclonal antibodies (O1 to O4) to oligodendrocyte cell surfaces: an immunocytological study in the central nervous system. Dev Biol 83(2):311-27.

Sontheimer H, Trotter J, Schachner M, Kettenmann H. 1989. Channel expression correlates with differentiation stage during the development of oligodendrocytes from their precursor cells in culture. Neuron 2(2):1135-45.

Sontheimer H, Waxman SG. 1993. Expression of voltage-activated ion channels by astrocytes and oligodendrocytes in the hippocampal slice. J Neurophysiol 70(5):1863-73.

Spray DC, Ye ZC, Ransom BR. 2006. Functional connexin "hemichannels": a critical appraisal. Glia 54(7):758-73.

Teubner B, Michel V, Pesch J, Lautermann J, Cohen-Salmon M, Sohl G, Jahnke K, Winterhager E, Herberhold C, Hardelin JP, Petit C, Willecke K. 2003. Connexin30 (Gjb6)-deficiency causes severe hearing impairment and lack of endocochlear potential. Hum Mol Genet 12(1):13-21.

Teubner B, Odermatt B, Guldenagel M, Sohl G, Degen J, Bukauskas F, Kronengold J, Verselis VK, Jung YT, Kozak CA, Schilling K, Willecke K. Functional expression of the new gap junction gene connexin47 transcribed in mouse brain and spinal cord neurons. J Neurosci 21(4):1117-26.

Theis M, de Wit C, Schlaeger TM, Eckardt D, Kruger O, Doring B, Risau W, Deutsch U, Pohl U, Willecke K. 2001. Endothelium-specific replacement of the connexin43 coding region by a lacZ reporter gene. Genesis 29(1):1-13.

Theis M, Jauch R, Zhuo L, Speidel D, Wallraff A, Doring B, Frisch C, Sohl G, Teubner B, Euwens C, Huston J, Steinhauser C, Messing A, Heinemann U, Willecke K. 2003. Accelerated hippocampal spreading depression and enhanced locomotory activity in mice with astrocyte-directed inactivation of connexin43. J Neurosci 23(3):766-76.

Uhlenberg B, Schuelke M, Ruschendorf F, Ruf N, Kaindl AM, Henneke M, Thiele H, Stoltenburg-Didinger G, Aksu F, Topaloglu H, Nurnberg P, Hubner C, Weschke B, Gartner J. 2004. Mutations in the gene encoding gap junction protein alpha 12 (connexin 46.6) cause Pelizaeus-Merzbacher-like disease. Am J Hum Genet 75(2):251-60.

Verkhratsky A, Orkand RK, Kettenmann H. 1998. Glial calcium: homeostasis and signaling function. Physiol Rev 78(1):99-141.

Volterra A, Meldolesi J. 2005. Astrocytes, from brain glue to communication elements: the revolution continues. Nat Rev Neurosci 6(8):626-40.

Wagner C. 2008. Function of connexins in the renal circulation. Kidney Int 73(5):547-55.

Wallraff A, Kohling R, Heinemann U, Theis M, Willecke K, Steinhauser C. 2006. The impact of astrocytic gap junctional coupling on potassium buffering in the hippocampus. J Neurosci 26(20):5438-47.

Wang C, Rougon G, Kiss JZ. 1994. Requirement of polysialic acid for the migration of the O-2A glial progenitor cell from neurohypophyseal explants. J Neurosci 14(7):4446-57.

Wang LP, Cheung G, Kronenberg G, Gertz K, Ji S, Kempermann G, Endres M, Kettenmann H. 2008. Mild brain ischemia induces unique physiological properties in striatal astrocytes. Glia 56(9):925-34.

Waxman SG, Black JA, Sontheimer H, Kocsis JD. 1994. Glial cells and axo-glial interactions: implications for demyelinating disorders. Clin Neurosci 2(3-4):202-10.

Wiencken-Barger AE, Djukic B, Casper KB, McCarthy KD. 2007. A role for Connexin43 during neurodevelopment. Glia 55(7):675-86.

Wolf NI, Cundall M, Rutland P, Rosser E, Surtees R, Benton S, Chong WK, Malcolm S, Ebinger F, Bitner-Glindzicz M, Woodward KJ. 2007. Frameshift mutation in GJA12 leading to nystagmus, spastic ataxia and CNS dys-/demyelination. Neurogenetics 8(1):39-44.

Yeager M, Harris AL. 2007. Gap junction channel structure in the early 21st century: facts and fantasies. Curr Opin Cell Biol 19(5):521-8.

Yeager M, Unger VM, Falk MM. 1998. Synthesis, assembly and structure of gap junction intercellular channels. Curr Opin Struct Biol 8(4):517-24.

Zhang H, Vutskits L, Calaora V, Durbec P, Kiss JZ. 2004. A role for the polysialic acid-neural cell adhesion molecule in PDGF-induced chemotaxis of oligodendrocyte precursor cells. J Cell Sci 117(Pt 1):93-103.

Zhou M, Schools GP, Kimelberg HK. 2006. Development of GLAST(+) astrocytes and NG2(+) glia in rat hippocampus CA1: mature astrocytes are electrophysiologically passive. J Neurophysiol 95(1):134-43.

Zhou Q, Wang S, Anderson DJ. 2000. Identification of a novel family of oligodendrocyte lineage-specific basic helix-loop-helix transcription factors. Neuron 25(2):331-43.

Curriculum Vitae

Mein Lebenslauf wird aus datenschutzrechtlichen Gründen in der elektronischen Version meiner Arbeit nicht veröffentlicht.

Publications

Maglione M, Tress O, Haas B, Willecke K, Kettenmann H,

Gap junctional coupling in oligodendrocytes dependent from connexin47 and connexin32 expression (accepted, Glia 2010)

Tress O, **Maglione M**, Degen J, Kettenmann H, Willecke K,

A transgenic mouse model for the inherited Pelizaeus-Merzbacher-like disease (submitted)

Maglione M*, Tress O*, Pivneva T, Seyfarth J, May D, Dere E, Zlomuzica A, Willecke K+, Kettenmann H + (*,+ equal contribution).

Ablation of Connexin47 and Connexin30 leads to loss of oligodendrocyte-to-astrocyte coupling and hypomyelination in CNS white matter (in preparation)

Meetings and Presentations

Talks

M.Maglione, O. Tress, B. Haas, Karram K, Trotter J, K. Willecke, H. Kettenmann.

Oligodendrocytes communicate to each other via gap junction channels formed by Cx47 and Cx32. Berlin Brain Days 2009, December 09th-11th, Berlin, Germany

M.Maglione, O. Tress, B. Haas, Karram K, Trotter J, K. Willecke, H. Kettenmann

Oligodendrocytes in mouse corpus callosum are coupled via gap junction channels formed by Connexin47 and Connexin32. Invited by Dr. C. Abrams, November 05th 2009, Down State University, New York, USA

M.Maglione, O. Tress, B. Haas, Karram K, Trotter J, K. Willecke, H. Kettenmann

Oligodendrocytes in mouse corpus callosum are coupled via gap junction channels formed by Cx47 and Cx32. Invited by Dr. C. Giaume, September 09th 2009, INSERM U840, Collège de France, Paris

M. Maglione, B. Uhlenberg, K. Willecke, H. Kettenmann.

The role of connexin47 in CNS myelination. Berlin Brain Days 2006, October 29th-30th, Berlin, Germany

Posters

M. Maglione1*, O. Tress*, T. Pivneva, J. Seyfarth, D. May, E. Dere, A. Zlomuzica, K. Willecke+, H. Kettenmann+. *, + authors contributed equally.

Myelination in the mouse cerebellar white matter depends on oligodendrocyte to astrocyte coupling mediated by Connexin47 and Connexin30. Abstract submitted-Berlin Neuroscience Forum 2010, June 10th-12th, Liebenwalde, Germany

M. Maglione*, O. Tress*, T. Pivneva, J. Seyfarth, D. May, E. Dere, A. Zlomuzica, K. Willecke+, H. Kettenmann+. *, + authors contributed equally.

Loss of oligodendrocyte-to-astrocyte coupling in mice double deficient for Connexin47 and Connexin30 leads to hypomyelination in cerebellar white matter. Abstract submitted-FENS 2010, July 3rd-7th, Amsterdam, The Nederlands

M.Maglione, O. Tress, B. Haas, K. Willecke, H. Kettenmann

Gap junction coupling among oligodendrocytes in mouse corpus callosum is largely promoted by Connexin47. Max-Delbrueck-Center for Molecular Medicine Neuro Retreat 2009, September 30th-October 1st, Hubertusstock, Joachimsthal, Germany

M.Maglione, O. Tress, B. Haas, K. Willecke, H. Kettenmann

Gap junction coupling among oligodendrocytes in mouse corpus callosum is largely promoted by Connexin47. Euroglia 2009, September 8th-12th, Paris, France

M. Maglione, O. Tress, B. Haas, K. Willecke, H. Kettenmann

Oligodendrocytes form coupled networks in mouse corpus callosum largely promoted by Connexin47. Berlin Brain Days 2008; December 10th-12th, Berlin, Germany

M. Maglione, O. Tress, B. Haas, K. Willecke, H. Kettenmann

Oligodendrocytic coupling in corpus callosum is mediated by connexin47. FMP and MDC PhD Retreat, September 18th- 20th 2008, Hotel Döllnsee, Schorfheide, Germany

M. Maglione, O. Tress, B. Haas, K. Willecke, H. Kettenmann

Oligodendrocytes form coupled networks in mouse corpus callosum largely promoted by Connexin47. Society for Neuroscience 2008; November 15th-19th, Washington, DC, USA

M. Maglione, O. Tress, K. Willecke, H. Kettenmann

Oligodendrocytic coupling in corpus callosum is mediated by connexin47. Berlin Neuroscience Forum 2008; June 5th-7th, Liebenwalde, Germany

M. Maglione, K. Willecke and H. Kettenmann

Gap junctional coupling in oligodendrocytes from the mouse corpus callosum. Berlin Brain Days 2007, November 26th-29th, Berlin, Germany

M. Maglione, B. Uhlenberg, K. Willecke, H. Kettenmann

The role of gap junction protein connexin47 in CNS myelination. SFB 665: Developmental Disturbances in the Nervous System International Symposium 2007, November 15th - 17th, Hermannswerderinsel-Potsdam, Germany

Erklärung

„Ich, Marta Maglione, erkläre, dass ich die vorgelegte Dissertation mit dem Thema: *Role of the oligodendrocytic connexin47 in CNS myelination* selbst verfasst und keine anderen als die angegebenen Quellen und Hilfsmittel benutzt, ohne die (unzulässige) Hilfe Dritter verfasst und auch in Teilen keine Kopien anderer Arbeiten dargestellt habe.“

Berlin, den 08.04.2010 Marta Maglione……..